SSME SEAL TEST PROGRAM: TEST RESULTS FOR SMOOTH, HOLE-PATTERN, AND HELICALLY-GROOVED STATORS

INTERIM PROGRESS REPORT
NASA CONTRACT NAS8-35824

Prepared by

DARA W. CHILDS, PH.D., P.E.
PROFESSOR OF MECHANICAL ENGINEERING

Texas A&M University
College Station, Texas 77843

Prepared for

GEORGE C. MARSHALL SPACE FLIGHT CENTER
MARSHALL SPACE FLIGHT CENTER, ALABAMA 35812

April 1987

TRC-Seal-7-87

TABLE OF CONTENTS

List of Figures iii

List of Tables v

Appendix A. Static Test Conditions for Tested Seals vi

Appendix B. Dynamic Test Data vii

Abstract viii

I. Introduction 1

II. Hirs' Coefficient Calculations from Static Test Data for Damper and Smooth Seals 4

2.1 Introduction 4

2.2 Hirs' Turbulent Lubrication Model 5

2.3 Empirical Turbulence Coefficients 7

2.4 Friction Factor and Empirical-Coefficient Results for Smooth, Centered Seals 11

III. Static and Dynamic Test Results for Nominally Smooth Seals with Three Different Radial Clearances 13

3.1 Introduction 13

3.2 Friction-Factor Data 13

3.3 Leakage Data 13

3.4 Dynamic Test Data 15

3.5 Conclusions 21

IV. Test Results for Round-Hole Pattern Damper Seals at Reduced Clearance 25

4.1 Introduction 25

4.2 Friction-Factor Data 26

4.3 Leakage Data 26

4.4 Dynamic Test Data 26

4.5 Conclusions 34

V. Test Results for Helically-Grooved Stators 46

5.1 Introduction 46

5.2 Friction-Factor Data 46

5.3 Leakage Data 46

5.4 Dynamic Test Data 46

5.5 Conclusions 63

VI. Test Results for a 30°-Helically-Grooved Stator in an Air-Seal Test Facility 66

6.1 Introduction 66

6.2 Test Facility 67

6.3 Test Results 67

6.4 Conclusions 73
VII. Summary and Conclusions 74
7.1 Summary and Conclusions 74
7.2 Comments on Friction Factors 74
References 77
Appendix A. Static Test Conditions for Tested Seals 78
Appendix B. Dynamic Test Data 96

List of Figures

1. Hole-pattern stator.
2. High-Reynolds-Number seal test section.
3. Differential fluid element for Hirs' bulk-flow model.
4. Flowchart for the solution of the empirical coefficients for equal rotor and stator roughnesses. The subscript i denotes the ith data point.
5. Flowchart for the solution of stator empirical turbulence coefficients ms, ns from test data and known rotor coefficients. The subscript i denotes the ith data point.
6. Measured and theoretical values for σ versus Reynolds number and running speed for a centered smooth seal, $C_r = 0.312mm, 0.375mm, 0.446mm, 0.508mm$.
7. Measured and theoretical values for σ versus Reynolds number and running speed for seals with a smooth stator and a smooth eccentric rotor; $C_r = 0.254, 0.381, 0.508mm$.
8. $C_d^{-1/2}$ and C_L for smooth seals; $C_r = 0.254, 0.381$, and $0.508mm$.
9. Measured and theoretical [2] results for F_r/A and F_θ/A; smooth seal, $C_r = 0.254mm$.
10. Measured and theoretical [2] results for F_r/A and F_θ/A; smooth seal, $C_r = 0.381mm$.
11. Measured and theoretical [2] results for F_r/A and F_θ/A; smooth seal, $C_r = 0.508mm$.
12. K_{ef} and $\overline{K}_{ef}$ versus ΔP for smooth seals at three different clearances.
13. C_{ef} versus ΔP for smooth seals at three different clearances.
14. $\overline{C}_{ef}$ and $\hat{C}_e f$ versus ΔP for smooth seals at three different clearances.
15. Round-hole-pattern stator configurations, detail A.
16. Combined sigma data for damper seals with hole-pattern-stators 1 and 2.
17. Combined sigma data for damper seals with hole-pattern-stators 3 and 4.
18. Combined sigma data for damper seals with hole-pattern-stators 5 and 6.
19. Stator sigma data for hole-pattern-stators 1 and 2.
20. Stator sigma data for hole-pattern-stators 3 and 4.
21. Stator sigma data for hole-pattern-stators 5 and 6.
22. $C_d^{-1/2}$ for hole-pattern-stator seals.
23. Measured and theoretical [2] results for F_r/A and F_θ/A; hole-pattern stator 1.
24. Measured and theoretical [2] results for F_r/A and F_θ/A; hole-pattern stator 2.
25. Measured and theoretical [2] results for F_r/A and F_θ/A; hole-pattern stator 3.
26. Measured and theoretical [2] results for F_r/A and F_θ/A; hole-pattern stator 4.
27. Measured and theoretical [2] results for F_r/A and F_θ/A; hole-pattern stator 5
28. Measured and theoretical [2] results for F_r/A and F_θ/A; hole-pattern stator 6.
29. K_{ef} for hole-pattern stators 1 through 6.
30. $\overline{K}_{ef}$ for hole-pattern stators 1 through 6.
31. C_{ef} for hole-pattern stators 1 through 6.
32. $\overline{C}_{ef}$ for hole-pattern stators 1 through 6.
33. Helically-grooved stator, detail A.
34. Combined-sigma, σ_c, data for helically-grooved-stators 1 and 2 versus R_a and ω.
35. Combined-sigma, σ_c, data for helically-grooved-stators 3 and 4 versus R_a and ω.

36. Combined-sigma, σ_c, data for helically-grooved-stators 5 and 6 versus R_a and ω.
37. Combined-sigma, σ_c, data for helically-grooved-stators 7 and 8 versus R_a and ω.
38. Combined-sigma data, σ_c, for helix-angles 0° through 70° at 7200 rpm, versus R_a.
39. $C_d^{-1/2}$ versus ΔP for helically-grooved-stator seals.
40. F_r/A and F_θ/A for helically-grooved-stator seal 1, $\alpha = 0°$.
41. F_r/A and F_θ/A for helically-grooved-stator seal 2, $\alpha = 15°$.
42. F_r/A and F_θ/A for helically-grooved-stator seal 3, $\alpha = 30°$.
43. F_r/A and F_θ/A for helically-grooved-stator seal 4, $\alpha = 30°$ with end lands.
44. F_r/A and F_θ/A for helically-grooved-stator seal 5, $\alpha = 40°$.
45. F_r/A and F_θ/A for helically-grooved-stator seal 6, $\alpha = 50°$.
46. F_r/A and F_θ/A for helically-grooved-stator seal 7, $\alpha = 60°$.
47. F_r/A and F_θ/A for helically-grooved-stator seal 8, $\alpha = 70°$.
48. $\overline{K}_{sf}$ versus ΔP for the helically-grooved stator seals.
49. $\overline{C}_{sf}$ versus ΔP for the helically-grooved stator seals.
50. Helically-grooved air seal.
51. Test-apparatus, isometric view.
52. Components used for static and dynamic displacement of seal rotor.
53. Inlet guide vane detail.
54(a). K_{xx} and K_{xy} versus u_{ϕ_o} for smooth (1), honeycomb (2), and helix (3) stators at 3,000 CPM.
54(b). C_{xx} and $K_{xy}/\omega C_{xx}$ versus u_{ϕ_o} for smooth (1), honeycomb (2), and helix (3) stators at 3,000 CPM.
55(a). K_{xx} and K_{xy} versus u_{ϕ_o} for smooth (1), honeycomb (2), and helix (3) stators at 16,000 CPM.
55(b). C_{xx} and $K_{xy}/\omega C_{xx}$ versus u_{ϕ_o} for smooth (1), honeycomb (2), and helix (3) stators at 16,000 CPM.
56(a). Test results for K_{xx} and K_{xy} versus running speed for smooth (1), honeycomb (2), and helix (3) stators versus running speed for maximum inlet-flow prerotation in the direction of shaft rotation.
56(b). Test results for C_{xx} and $K_{xy}/\omega C_{xx}$ versus running speed for smooth (1), honeycomb (2), and helix (3) stators versus running speed for maximum inlet-flow prerotation in the direction of shaft rotation.
57. Measured friction-factor data plotted on a Moody diagram.

LIST OF TABLES

1. Hirs coefficients for 0.81μm roughness, mm diameter seals with a concentric rotor and stator.
2. Hirs coefficients for 0.81μm roughness seals with an eccentric rotor; $A = 0.089mm$.
3. Measured values for K_{sf}, C_{sf}, and M_{sf}; comparison of theory and experiment for smooth seals at three different clearances.
4. Hirs coefficients for hole-pattern stators as calculated using the solution approach of figure 5.
5. Measured values for K_{sf}, C_{sf}, and M_{sf}; comparison of theory and experiments for hole-pattern stators.
6. Measured values for K_{sf}, C_{sf}, and M_{sf} for helically-grooved-stator seals.

LIST OF TABLES
APPENDIX A. STATIC TEST CONDITIONS FOR TESTED SEALS

A.1. Operating conditions and parameters, smooth stator; $C_r = 0.254mm$.
A.2. Operating conditions and parameters, smooth stator; $C_r = 0.381mm$.
A.3. Operating conditions and parameters, smooth stator; $C_r = 0.508mm$.
A.4. Operating conditions and parameters, hole-pattern stator 1.
A.5. Operating conditions and parameters, hole-pattern stator 2.
A.6. Operating conditions and parameters, hole-pattern stator 3.
A.7. Operating conditions and parameters, hole-pattern stator 4.
A.8. Operating conditions and parameters, hole-pattern stator 5.
A.9. Operating conditions and parameters, hole-pattern stator 6.
A.10. Operating conditions and parameters, helically-grooved stator 1, $\alpha = 0°$.
A.11. Operating conditions and parameters, helically-grooved stator 2, $\alpha = 15°$.
A.12. Operating conditions and parameters, helically-grooved stator 3, $\alpha = 30°$.
A.13. Operating conditions and parameters, helically-grooved stator 4, $\alpha = 30°$. End lands are used on this seal.
A.14. Operating conditions and parameters, helically-grooved stator 5, $\alpha = 40°$.
A.15. Operating conditions and parameters, helically-grooved stator 6, $\alpha = 50°$.
A.16. Operating conditions and parameters, helically-grooved stator 7, $\alpha = 60°$.
A.17. Operating conditions and parameters, helically-grooved stator 8, $\alpha = 70°$.

LIST OF TABLES
APPENDIX B. DYNAMIC TEST DATA

B.1 Force coefficients (average and standard deviations) and average force magnitudes for a smooth stator; $C_r = 0.254mm$.

B.2 Force coefficients (average and standard deviations) and average force magnitudes for a smooth stator; $C_r = 0.381mm$.

B.3 Force coefficients (average and standard deviations) and average force magnitudes for a smooth stator; $C_r = 0.508mm$.

B.4 Force coefficients (average and standard deviations) and average force coefficients for hole-pattern stator 1.

B.5 Force coefficients (average and standard deviations) and average force coefficients for hole-pattern stator 2.

B.6 Force coefficients (average and standard deviations) and average force coefficients for hole-pattern stator 3.

B.7 Force coefficients (average and standard deviations) and average force coefficients for hole-pattern stator 4.

B.8 Force coefficients (average and standard deviations) and average force coefficients for hole-pattern stator 5.

B.9 Force coefficients (average and standard deviations) and average force coefficients for hole-pattern stator 6.

B.10 Operating conditions and parameters, helically-grooved stator 1, $\alpha = 0°$.

B.11 Operating conditions and parameters, helically-grooved stator 2, $\alpha = 15°$.

B.12 Operating conditions and parameters, helically-grooved stator 3, $\alpha = 30°$.

B.13 Operating conditions and parameters, helically-grooved stator 4, $\alpha = 30°$. End lands are used on this seal.

B.14 Operating conditions and parameters, helically-grooved stator 5, $\alpha = 40°$.

B.15 Operating conditions and parameters, helically-grooved stator 6, $\alpha = 50°$.

B.16 Operating conditions and parameters, helically-grooved stator 7, $\alpha = 60°$.

B.17 Operating conditions and parameters, helically-grooved stator 8, $\alpha = 70°$.

ABSTRACT

Test results are presented for the following seals:

(a) smooth, concentric seals at four clearances (static-test-data only),
(b) smooth seals at three clearances,
(c) hole-pattern-damper seals, six configurations, and
(d) helically-grooved-stator seals, seven helix angles

All of the above seals are tested in a liquid Halon test facility at high Reynolds numbers. In addition, a helically-grooved-stator seal was tested in an air-seal test facility.

An analysis of the test results with comparisons to theoretical predictions supports the following conclusions:

(a) For small seals, the Hirs' friction-factor model is more restricted than had been through previously. Experimentally-derived-Hirs empirical coefficients apply for a reasonable Reynolds number range but are clearly a function of clearance. Further, there are significant differences between measured σ values with centered concentric seals and a seal with the rotor orbiting. Fortunately, the difference between concentric and orbiting-rotor friction factor data is reduced as the radial clearance is reduced.
(b) For smooth seals, predictions of stiffness and damping improve markedly as the radial clearance is reduced.
(c) Friction-factor data for hole-pattern-seal stators frequently deviates from the Hirs model.
(d) Predictions of stiffness and damping coefficients for hole-pattern-stator seals is generally reasonable.
(e) Test for the hole-pattern stators at reduced clearances (0.30 mm versus 0.51 mm) show no clear optimum for hole-pattern seals with respect to either hole-area ratio or hole depth to minimum-clearance ratios.
(f) Tests of these hole-pattern stators show no significant advantage in net damping over smooth seals; however, the seals leak about 30% less than smooth seals.
(g) Tests of helically-grooved seal stators in Halon show reasonable agreement between theory and prediction for leakage and direct stiffness but poor agreement for the net damping coefficient.
(h) Tests of a helically-grooved stator in the air seal facility shows superior stability characteristics at high speeds (16,000 rpm) as compared of a honeycomb seal.

Chapter I
INTRODUCTION

The test and analysis results which are reported here were obtained under NASA Contract NAS8-35824. The present work continues research activity which began in January of 1980 under NASA Contract NAS8-33716. Earlier contract reports [3-7] provide detailed information covering the following points:

(a) test-section and facility description,
(b) test-objectives and procedures, and
(c) data acquisition, analysis, and procedures.

Most of this information is not repeated here, and interested readers are referred to earlier reports.

From a rotordynamics viewpoint, seal analysis has the objective of predicting the coefficients for the following motion/reaction-force model

$$-\begin{Bmatrix} F_X \\ F_Y \end{Bmatrix} = \begin{bmatrix} K & k \\ -k & K \end{bmatrix} \begin{Bmatrix} X \\ Y \end{Bmatrix} + \begin{bmatrix} C & c \\ -c & C \end{bmatrix} \begin{Bmatrix} \dot{X} \\ \dot{Y} \end{Bmatrix} + M \begin{Bmatrix} \ddot{X} \\ \ddot{Y} \end{Bmatrix} \tag{1}$$

where X, Y are components of the seal-rotor displacement relative to its stator and F_X, F_Y are components of the reaction force. The diagonal and off-diagonal stiffness and damping coefficients are referred to, respectively, as "direct" and "cross-coupled". The cross-coupled coefficients arise due to fluid rotation within the seal. The coefficient M accounts for the seal's added mass.

If a circular orbit of the form

$$X = A\cos\omega t, \quad Y = A\sin\omega t \tag{2}$$

is assumed, Eq. (1) yields the following definition of force coefficients which are, respectively, parallel and perpendicular to the rotating displacement vector

$$\begin{aligned} F_r/A &= -K - c\omega + M\omega^2 \\ F_\theta/A &= k - C\omega \end{aligned} \tag{3}$$

Observe that the cross-coupled-stiffness coefficient k yields a "driving" tangential contribution in the direction of rotation, while the direct damping coefficient develops a drag force opposing the tangential velocity.

Recent test activities in this project have concerned "damper seal" configurations, which were largely inspired by von Pragenau's work [1]. Von Pragenau's analysis predicts that a smooth-rotor/rough-stator combination will yield a reduced asymptotic fluid tangential velocity within the seal, which will, in turn, yield a reduction in the cross-coupled stiffness coefficient. A reduced cross-coupled stiffness coefficient reduces the destabilising

tangential driving force on the rotor, yields an increased net damping force, and generally enhances rotor stability and response. A subsequent and more comprehensive analysis by Childs and Kim [2] yields the same sort of encouraging predictions.

Reference [6] includes results for five new damper seal configurations including a round-hole-pattern stator similar to that illustrated in figure 1. The results for this seal configurations were encouraging, and a lengthy test series [7] was carried out which varied the following parameters:

(a) Hole-area density. This parameter is defined by

$$\gamma = \frac{hole\ density}{total\ area} \tag{4}$$

(b) Hole depth to minimum-clearance ratio, h/C_r.

The test results of reference [7] showed that an optimum value for net damping could be obtained for $\gamma \cong 0.34$ and $h/C_r \cong 3$. All of the tests in references [6] and [7] were carried out with $C_r = 0.51mm$ (.020 in), which corresponds to $C_r/R = 0.01$. By comparison, the interstage seals of the HPFTP operate at $C_r/R = .0035$. To examine the influence of a reduction in clearance, six additional hole-pattern stators were tested in the current program with $C_r = 0.38mm$ (0.15 in).

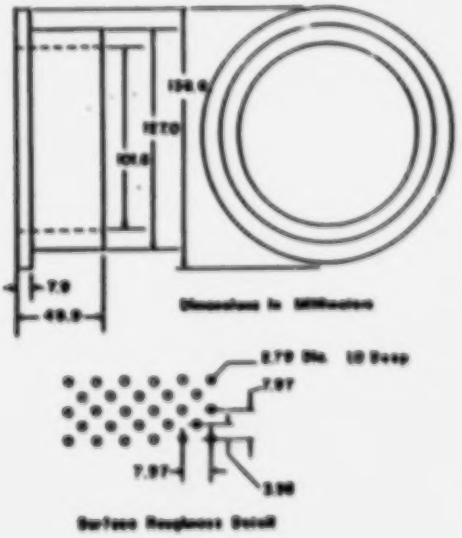

Figure 1. Hole-pattern stator.

Kim and Childs [8] completed an analysis for helically-grooved seals during 1985 which indicated some distinct advantages, from a rotordynamic stability viewpoint, for properly-designed, helically-grooved seals versus smooth or hole-pattern damper stators. Tests were carried out on eight (8) helically-grooved stators in the present study to examine the correctness of these predictions.

The test apparatus used in this program does not control the inlet tangential velocity to the seal and provides no intentional fluid prerotation. Recent tests of honeycomb stators in an airseal test facility at TAMU has shown that honeycomb stators are clearly superior to smooth stators when the inlet air is prerotated in the direction of rotation, but are no better than smooth stators in the absence of fluid prerotation. Hence, one helically-grooved stator was manufactured and tested in the air-seal test facility.

The Hirs-based theory for damper seals [2] characterizes the shear stress at the rotor and stator in terms of empirical parameters which must be obtained from test data. The test data obtained from our test operations and used to calculate these parameters consists of the leakage rate, running speed, and axial pressure gradient. The procedure which has been used in this program to calculate the empirical coefficients has yielded erratic results. Hence, a new procedure is used to calculate the empirical coefficients for both hole-pattern stators and a smooth-stator/smooth-rotor seal at three different clearances.

In summary, the contents of this report cover the following topics:

(a) analysis procedures for calculating Hirs' coefficients for rotor and stator surfaces with test results for four, smooth, centered seals,
(b) static and dynamic test data for six additional hole-pattern stators,
(c) static and dynamic test data for eight helically-grooved stators tested in the Halon test facility, and
(d) static and dynamic test data for a smooth-rotor/smooth-stator seal at three different clearances.

CHAPTER II
HIRS' COEFFICIENT CALCULATIONS FROM STATIC TEST DATA FOR DAMPER AND SMOOTH SEALS

2.1 Introduction

Figure 2 illustrates the liquid-seal test rig used in this study. Dynamic force coefficients represent the principal output of the apparatus; however, static test data are obtained during testing and consist of the following parameters:

(a) leakage rate,
(b) static pressure measurements near the entrance and exit and along the seal, and
(c) running speed.

The balance of this chapter explains how these data are used to calculate the empirical coefficients used in Hirs' turbulent lubrication model [9].

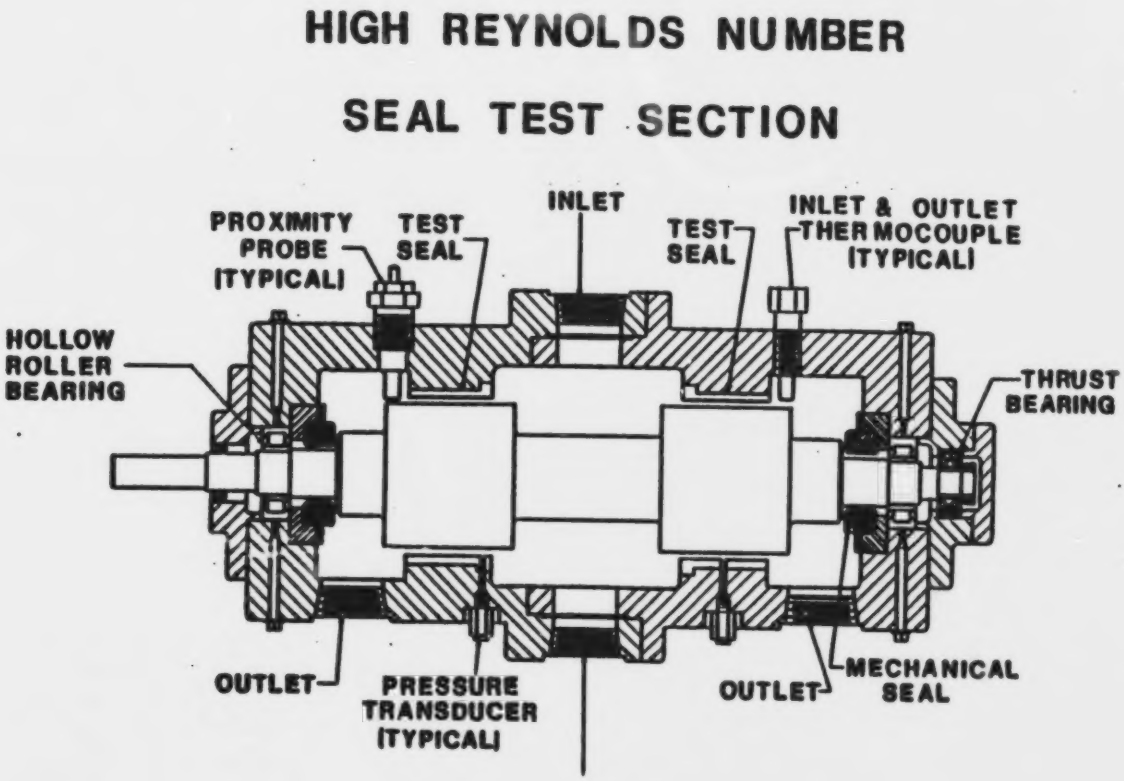

Figure 2. High-Reynolds-Number Seal Test Section.

2.2 Hirs' Turbulent Lubrication Model

A differential fluid element, with upper and lower surfaces corresponding to the rotor and stator surfaces respectively, is shown in Figure 3.

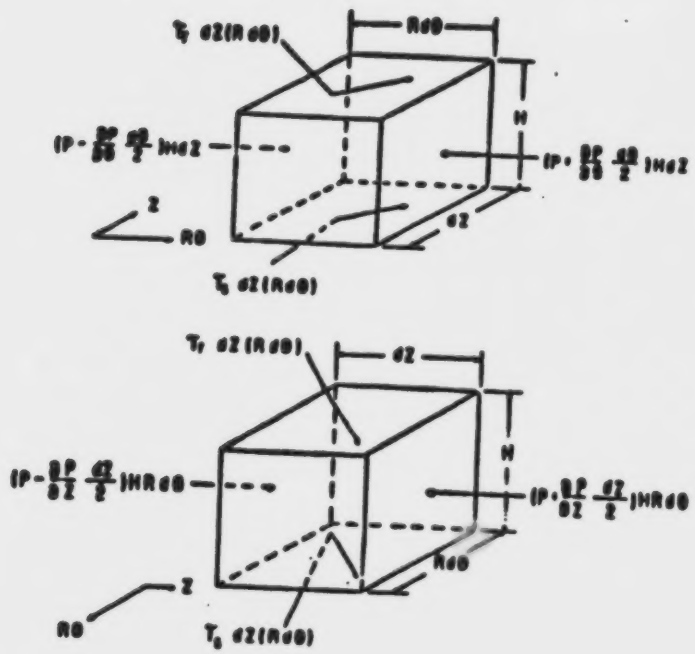

Figure 3. Differential fluid element for Hirs' bulk-flow model.

The bulk fluid velocities, which are averages across the film height $H(\theta, z)$ of the axial and circumferential fluid velocities, are U_z and U_θ. Hirs' turbulence formulation is based on an empirical function for the wall shear stress, τ_w, of the form

$$\tau_w = \rho \frac{V_w^2}{2} n_o R^{mo}$$

where R is the Reynolds number defined by

$$R = \frac{2\rho V_w H}{\mu}$$

and V_w is the average bulk-flow velocity relative to the wall. For the same surface roughness on the stator and rotor surface, the empirical coefficients m_o and n_o apply to both surfaces. For different surface roughnesses on the rotor and stator, the wall shear stresses are respectively

$$\tau_r = \rho \frac{V_r^2}{2} n_r \left(\frac{2\rho V_r H}{\mu} \right)^{m_r}$$

$$\tau_s = \rho \frac{V_s^2}{2} n_s \left(\frac{2\rho V_s H}{\mu} \right)^{m_s} \tag{5}$$

V_r and V_s are the bulk flow velocities relative to the rotor and stator walls defined by

$$V_r = (U_\theta - R\omega)\epsilon_\theta + U_z \epsilon_z$$

$$V_s = U_\theta \epsilon_\theta + U_z \epsilon_z$$

Using the above definitions for the shear-stress, governing equations consisting of axial and circumferential momentum equations are developed. The bulk flow continuity equation completes the governing equations.

The governing equations define the bulk-flow velocity components and the pressure as functions of the spatial variables, $R\theta$ and Z, and the time. Using a perturbation technique the nondimensional variables of these equations (u_z, u_θ, p and h) are expanded into zeroth-order and first-order equations. The zeroth-order equations can be solved for steady-state leakage, velocity fields, and the pressure field. The first-order equations define the rotordynamic coefficients.

For a constant clearance seal, the nondimensional zeroth-order equations are

$$\frac{dp_o}{dz} = -(a_{os}\sigma + a_{or}\sigma_r)/2 \tag{6}$$

$$\frac{du_{\theta o}}{dz} = [a_{os}\sigma_s u_{\theta o} + a_{or}\sigma_r (u_{\theta o} - 1)]$$

where

$$a_{os} = \left[\frac{1+(u_{\theta o}/bu_{ss})^2}{1+(1/4b^2)} \right]^{\frac{m_s+1}{2}}$$

$$a_{or} = \left[\frac{1+(u_{\theta o}-1)/bu_{sr})^2}{1+(1/4b^2)} \right]^{\frac{m_r+1}{2}}$$

Since the zeroth-order equations are coupled and nonlinear their solution is iterative. The initial conditions for these two nonlinear equations are

$$p(0) = \Delta P / \rho V^2 \tag{7}$$

$$u_{\theta o}(0) = U_{\theta o}(0)/R\omega$$

2.3 Empirical Turbulence Coefficients.

The analysis of Childs and Kim [2] characterizes the surface roughness of the stator and rotor in terms of empirical coefficients (n_o, m_o, n_r, m_r). These are the same coefficients that appear in Eq. 5, and they must be determined from static test data before the theoretical predictions can be made for F_r/A and F_θ/A. The coefficients can be calculated in the following manner.

The steady-state axial pressure gradient can be stated as

$$\frac{dP_o}{dz} = -\sigma\rho V^2$$

Leakage is measured in the test apparatus, and the static pressure is measured at five axial locations. Averages of the measured upstream and downstream temperature and pressure are used to define the density. Hence, the parameter σ can be determined from known values for the density, axial velocity, and the measured pressure gradient. The pressure gradient is determined from a curve fit of the three middle pressure locations so entrance and exit effects do not significantly influence the calculation. The three locations are at approximately 20, 50, and 80 percent of the seal length. For a rough-stator/smooth-rotor combination this value is σ_o, which is related to the stator, σ_s, and rotor, σ_r, by

$$\sigma_o = \frac{\sigma_r + \sigma_s}{2} \tag{8}$$

The σ parameters are related to the friction factor, λ, by

$$\sigma_r = \lambda_r \frac{L}{C_r}\ , \sigma_s = \lambda_s \frac{L}{C_r}\ , \tag{9}$$

and the friction factor is related to the empirical coefficients through the following friction-factor formulas

$$\lambda_r = n_r R_a^{mr} [1 + ((u_{\phi o-1})/b)^2]^{\frac{mr-1}{2}} \tag{10}$$

$$\lambda_s = n_s R_a^{ms} [1 + (u_{\phi o}/b)^2]^{\frac{ms-1}{2}} \tag{11}$$

where

$$R_a = \frac{VC\rho}{\mu}\ ,\ b = V/R\omega$$

This leads to the following problem which must be resolved: given measured data sets $(R_{ai}, \omega_i, \lambda_i)$, determine the values for m_r, n_r, m_s, and n_s from Eqs. (10) and (11).

The tangential velocity component, u_ϕ, of Eqs. (10) and (11) is generally a function of the axial position z. In previous analyses, u_ϕ has been set equal to one half, the asymptotic value for seals with equal rotor and stator roughnesses. For the present analysis, u_ϕ is set equal to the average nondimensional circumferential velocity

$$\bar{u}_{\phi_o} = \int_0^1 u_{\phi_o}(z)dz \tag{12}$$

where $u_{\phi_o}(z)$ is the solution of the zeroth-order equations. Hence Eqs. (10) and (11) become

$$\lambda_r = n_r R_a^{m_r} [1 + ((\bar{u}_{\phi_o} - 1)/b)^2]^{\frac{m_r+1}{2}} \tag{13}$$

$$\lambda_s = n_s R_a^{m_s} [1 + (\bar{u}_{\phi_o}/b)^2]^{\frac{m_s+1}{2}} \tag{14}$$

Since the solution of the zeroth-order equations for u_{ϕ_o} and p_o depend on m_r, n_r, m_s, and n_s, the solution is iterative. A value must be assumed for $u_{\phi_o}(0)$ to begin the iterative solution procedure. Once this value is assumed, first approximations for m_r, n_r, m_s, and n_s can be calculated from Eqs. (13) and (14). Experience shows that for the present apparatus, $u_{\phi_o}(0) = 0.1$ is an adequate approximation.

For a smooth stator and smooth rotor the same coefficients apply for both rotor and stator; hence, $m_s = m_r$, and $n_s = m_s$, so n_r and n_r can be found from the smooth-rotor/smooth-stator data. The parameter-identification procedure is slightly different when both surfaces have the same roughness, as apposed to the smooth rotor/rough stator combination, and a more detailed explanation of this problem is provided below.

From Eq. (8)

$$\sigma_o = \frac{L}{2C_r}(\lambda_r + \lambda_s) \tag{15}$$

For the same roughness on both surfaces, the empirical coefficients $n = nr = ns, m = mr = ms$, and Eq. (15) can be stated

$$2\sigma_o \frac{C_r}{L} = 2\lambda_o = n(C_1 X^m + C_2 Y^m) \tag{16}$$

where

$$C_1 = [1 + ((u_{\phi_o} - 1)/b)^2]^{1/2}$$

$$C_2 = [1 + (u_{\phi_o}/b)^2]^{1/2} \tag{17}$$

$$X = R_a C_1 \ , Y = R_a C_2 \ ,$$

This form of the governing equations isolates the unknown coefficients m and n.

If the circumferential velocity u_{ϕ_o} is assumed to be the asymptotic value, $1/2, C_1 = C_2, X = Y$, and a linear curve fit of the log form of Eq.(16) yields ln(n) and m. However,

if $u_{\phi_o} \neq 1/2, C_1 \neq C_2$, and performing the logarithm of Eq. (16) is not helpful in reducing the problem.

In the following procedure, u_{ϕ_o} is set equal to $\bar{u}_{\phi_o}$ in Eq. (17). The parameters m and n are defined by minimising the following objective function

$$E = \sum_{i=1}^{k} (2\lambda_{ci} - 2\hat{\lambda}_{ci})^2 = \sum_{i=1}^{k} [n(C_{1i} X_i^m + C_{2i} Y_i^m) - 2\hat{\lambda}_{2i}]^2 \tag{18}$$

which is the summation over the k data points of the squared difference between the predicted, λ_{ci}, and the measured, $\hat{\lambda}_{ci}$, friction factors. Minimisation of E with respect to m and n yields the following equations

$$f = \frac{\partial E}{\partial n} = \sum_{i=1}^{k} [n(C_{1i} X_i^m + C_{2i} Y_i^m) - 2\hat{\lambda}_{ci}](C_{1i} X_i^m + C_{2i} Y_i^m) = 0 \tag{19}$$

$$g = \frac{\partial E}{\partial m} = \sum_{i=1}^{k} [n(C_{1i} X_i^m + C_{2i} Y_i^m) - 2\hat{\lambda}_{ci}] n(C_{1i} X_i^m 1nX_i + C_{2i} Y_i^m 1nY_i) m = 0$$

These nonlinear equations are solved for n and m using a Newton-Raphson procedure. Figure 4 provides a flowchart for the solution algorithm used to obtain n and m for equal rotor and stator roughnesses. An iterative solution is required since the differential equations (6) include the unknown parameters n and m, and Eq. (19) contains C_1 and C_2 which depend on $\bar{u}_{\phi_o}$.

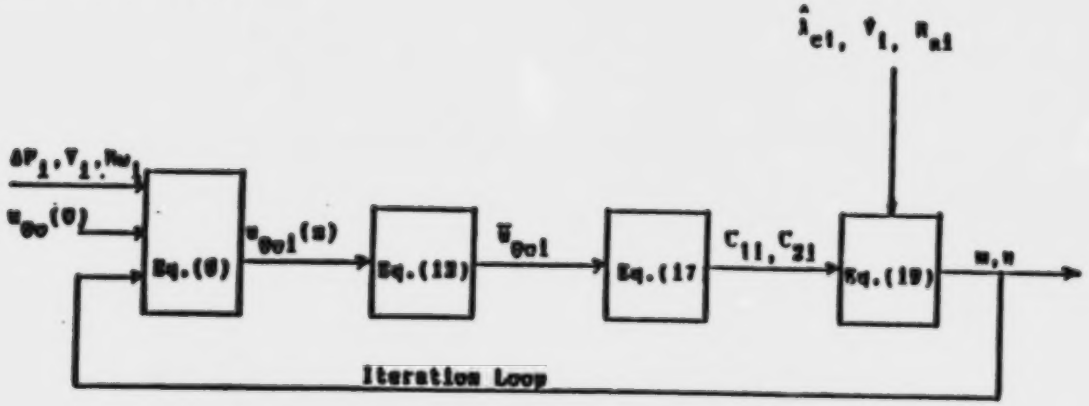

Figure 4. Flowchart for the solution of the empirical coefficients for equal rotor and stator surface roughnesses. The subscript i denotes the ith data point.

In the present investigation, the empirical coefficients *ms* and *ns* are to be calculated for various surface roughened stators assuming that values for *mr* and *nr* are known for the rotor. The values for *mr* and *nr* are obtained from Eq. (19) from tests of seals with

smooth rotors and stators. The flowchart of figure 5 illustrates the solution procedure for this problem. The upper portion of this figure shows the calculation of λ_{ri} from Eq. (13). Eq. (15) is then used to subtract λ_{ri} from the measured combined seal friction factor λ_{ci} to obtain a value for λ_{si}. For a given data point, Eq. (14) can be restated as

$$Z_i = \ln(n_s) + m_s X_i$$

where

$$Z_i = \ln\left(\frac{\lambda_{si}}{[1+(\bar{u}_{\theta oi}/b_i)^2]^{1/2}}\right)$$

$$X_i = \ln(R_m[1 + (\bar{u}_{\theta oi}/b_i)^2]^{1/2})$$

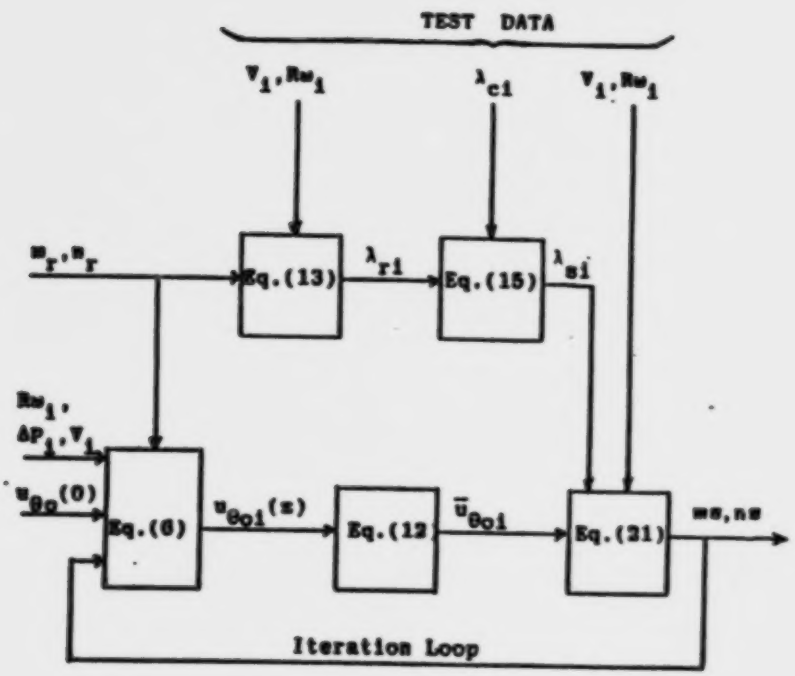

Figure 5. Flowchart for the solution of stator empirical turbulence coefficients ms, ns from test data and known rotor coefficients. The subscript i denotes the ith data point

The objective function to be minimized with respect to $\ln(n_s)$ and m_s is

$$E = \sum_{i=1}^{k} (Z_i - \hat{Z}_i)^2$$

where Z_i and $\hat{Z}_i$ are the measured and predicted values for Z_i respectively. A least-square curve fit of this relationship yields the following equations

$$\begin{bmatrix} k & \sum_{i=1}^{k} X_i \\ \sum_{i=1}^{k} X_i & \sum_{i=1}^{k} X_i^2 \end{bmatrix} \begin{Bmatrix} \ln(n_o) \\ m_o \end{Bmatrix} = \begin{Bmatrix} \sum_{i=1}^{k} \hat{Z}_i \\ \sum_{i=1}^{k} X_i \hat{Z}_i \end{Bmatrix} \tag{20}$$

2.4 Friction Factor and Empirical-Coefficient Results for Smooth, Centered Seals.

Four smooth stators were manufactured and tested in the apparatus of figure 2 solely to obtain friction-factor versus leakage data. The test rotor was run at speeds from 1000 to 7200 rpm; however, the seal elements of the rotor had no eccentricity, unlike the dynamic tests with eccentric rotors which are reported in subsequent chapters. The stators all had measured surface roughnesses of approximately $0.81\mu m$. The seals were tested at the following clearances: (a) .312 mm, (b) .375 mm, (c) .446 mm, and (d) .500 mm. Figure 6 illustrates test and theoretical results for σ as a function of running speed and Reynolds number. The theoretical results of figure 6 are based on calculated m, n values which were obtained from the solution procedure of figure 4. An inspection of these figures shows a generally good agreement between experiment and theory. A summary of the m, n results is provided in Table 1.

$C_r(mm)$	$D(mm)$	m	n	$R_a(max)$
0.312	101.00	-.208	.168	250,000
0.375	100.85	-.055	.0169	360,000
0.446	100.71	-.142	.0736	360,000
0.508	100.58	-.111	.0351	475,000

Table 1. Hirs Coefficients for $0.81\mu m$ roughness.

These data indicate that the empirical parameters m, n can only characterise the friction-factor properties of the stator for the same clearance, roughness, and Reynolds-number range. The data can also be interpreted in terms of changes in relative roughness, $\epsilon = e/2C_r$, where e the absolute roughness. As the clearance is reduced e remains fixed; however, ϵ increases. These results support the use of a Moody friction-factor characterization as proposed by Nelson and Nguyen [9] rather than a Hirs-based analysis.

ORIGINAL PAGE IS
OF POOR QUALITY

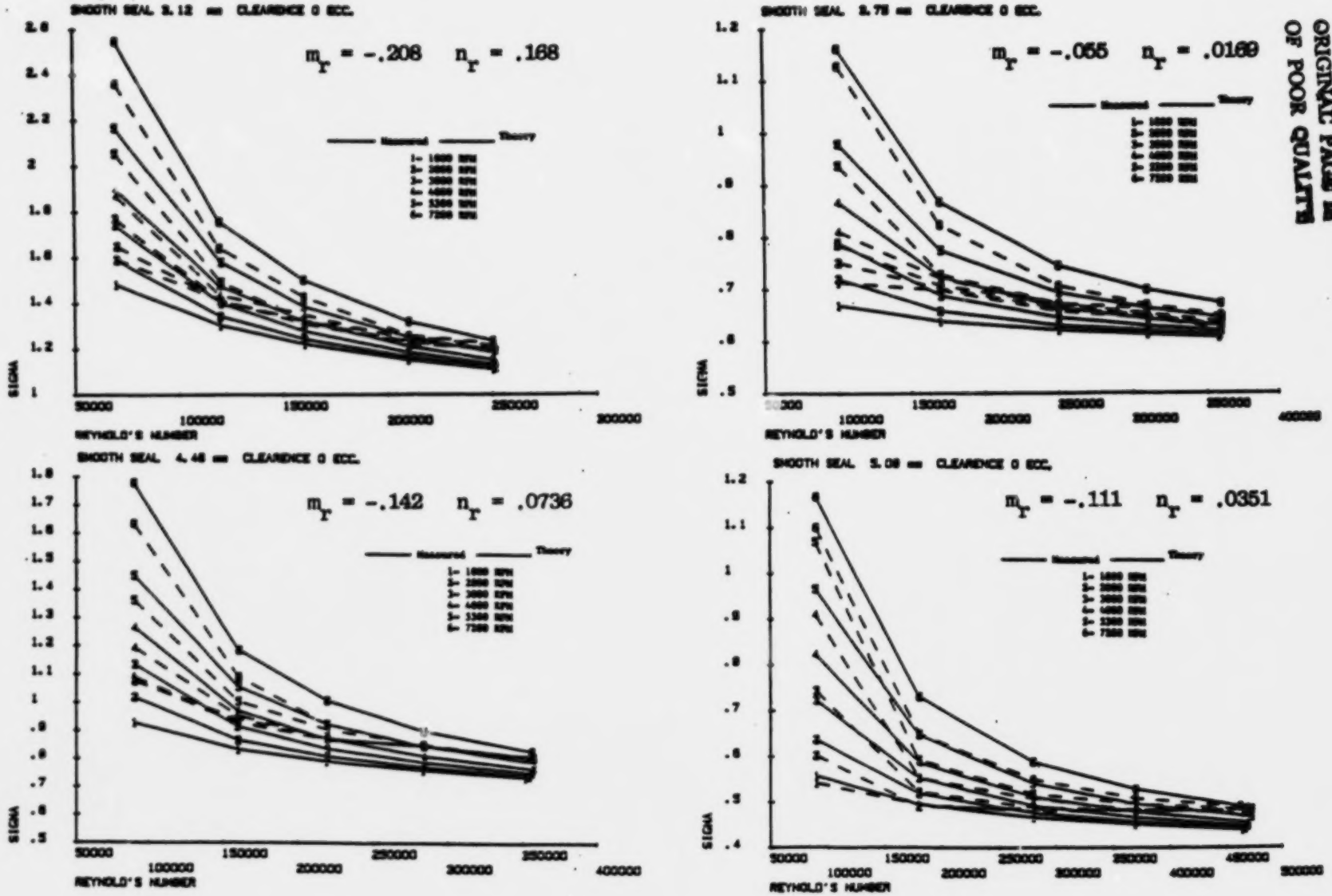
SMOOTH SEAL 3.12 mm CLEARENCE 0 ECC.
m_r = -.208 n_r = .168
SMOOTH SEAL 3.78 mm CLEARENCE 0 ECC.
m_r = -.055 n_r = .0169
SMOOTH SEAL 4.48 mm CLEARENCE 0 ECC.
m_r = -.142 n_r = .0736
SMOOTH SEAL 5.08 mm CLEARENCE 0 ECC.
m_r = -.111 n_r = .0351
Measured
Theory
SIGMA
REYNOLD'S NUMBER

Figure 6. Measured and theoretical values for σ versus Reynolds number and running speed for a centered smooth seal, $C_r = 0.312mm, 0.375mm, 0.446mm, 0.508mm$.

CHAPTER III
STATIC AND DYNAMIC TEST RESULTS FOR NOMINALLY SMOOTH SEALS WITH THREE DIFFERENT RADIAL CLEARANCES

3.1 Introduction

As noted previously, a substantial portion of this study involved testing hole-pattern damper seals at reduced radial clearances. As will be discussed in the following chapter, these tests showed some unexpected results; hence, the decision was made to test a nominally smooth seal ($0.81\mu m$) at the following three radial clearances: 0.254, 0.381, and 0.508 mm. For all tests, the radial eccentricity was set at $89\mu m$. Test results for these seals are presented below.

3.2 Friction-Factor Data

Figure 7 illustrates σ versus R_a and running speed for the seal at three different clearances. Observe that σ decreases monotonically with R_a and increases with running speed. The Hirs' coefficients for these three seal clearances are provided in Table 2.

$C_r(mm)$	m	n	$R_a(max)$
0.254	-0.258	0.293	190,000
0.381	-0.098	0.031	350,000
0.508	-0.059	0.028	450,000

Table 2. Hirs coefficients for $0.81\mu m$ roughness seals with an eccentric rotor; seal diameter $101.6mm$

The data of table 2 agree "reasonably" well with the data of table 1 for which the rotor is concentric.

3.3 Leakage Data

Leakage data are presented in terms of the discharge coefficient definition

$$\Delta P = C_d \frac{\rho V^2}{2}$$

which yields

$$\dot{Q} = 2\pi R C_r V = \left(\frac{C_r}{R}\right) C_d^{-1/2} \bullet 2\pi R^2 \sqrt{\frac{2\Delta P}{\rho}} = C_L \bullet 2\pi R^2 \sqrt{\frac{2\Delta P}{\rho}} \qquad (21)$$

Hence,

$$C_L = \left(\frac{C_r}{R}\right) C_d^{-1/2} = \dot{Q} / \left(2\pi R^2 \sqrt{\frac{2\Delta P}{\rho}}\right) \qquad (22)$$

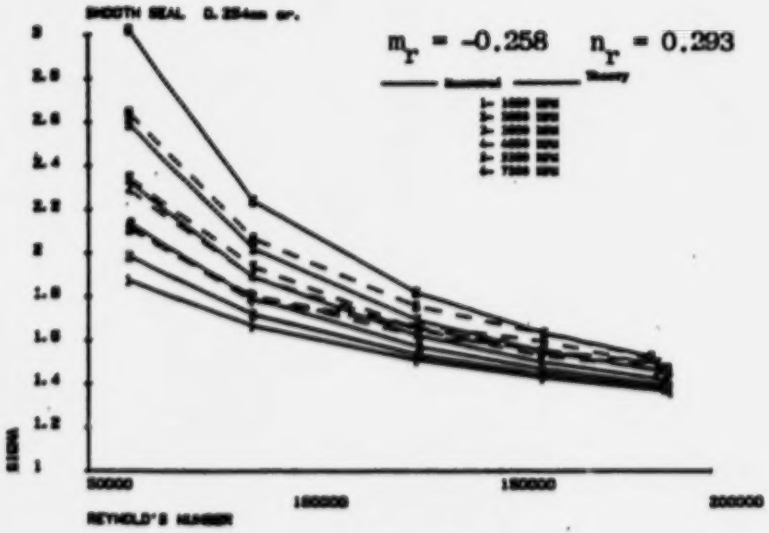

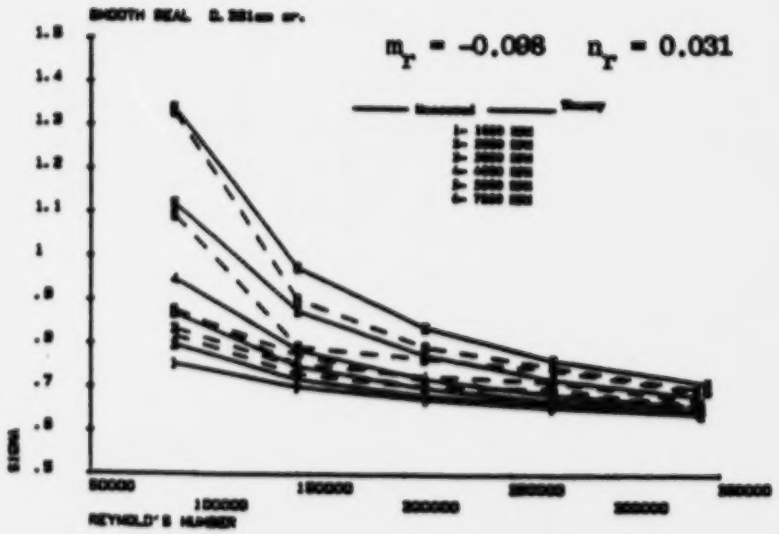

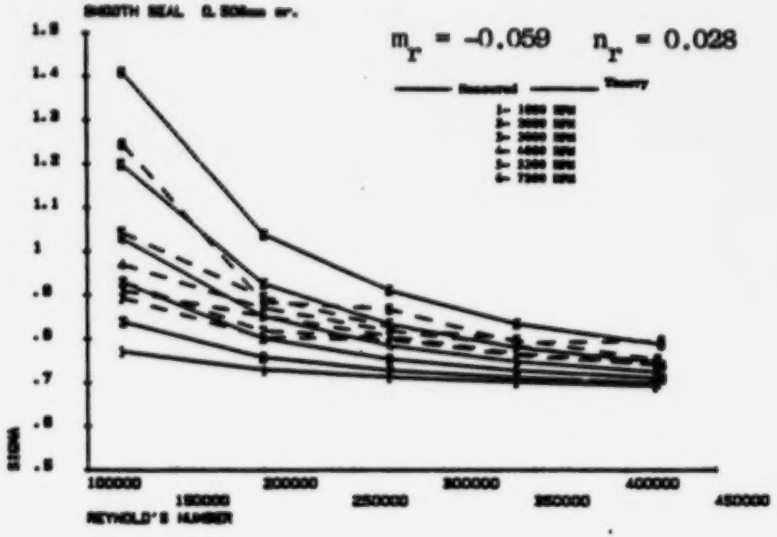

Figure 7. Measured and theoretical values for σ versus Reynolds number and running speed for seals with a smooth stator and a smooth eccentric rotor; $C_r = 0.254, 0.381, 0.508mm$.

ORIGINAL PAGE IS
OF POOR QUALITY

Seal-leakage data may be presented in terms of either $C_d^{-1/2}$ or C_L. Figure 8 illustrates both these parameters as a function of ΔP. Observe that C_L increases linearly with increasing C_r; however, $C_d^{1/2}$ first increases and then decreases as C_r increases.

3.4 Dynamic Test Data

Figure 9 illustrates measured and theoretical results for F_r/A and F_θ/A versus R_a and ω for the 0.254*mm* radial-clearance seal. The measured results are taken from Table b.1, while the theoretical results are calculated using the analysis of [2] with the empirical parameters of Table 2. An inspection of these results demonstrates a "reasonable" agreement between theory and experiment with respect to the tangential force but larger measured radial-force-coefficients magnitudes at low speeds than predicted. Further, the magnitude of F_r/A decreases more rapidly with increasing running speed than predicted. Figures 10 and 11 illustrate measured and theoretical predictions for the two remaining smooth seals.

Eq. (3) provides the basis for a quantitative comparison of theory and experiment. At first glance these equations suggest that sufficient independent equations could be obtained to calculate all the rotordynamic coefficients by simply testing at three running speeds. However, the fact that the coefficients depend on ω precludes this approach. While K, C, and M are weak functions of ω through their dependence on σ, the "cross-coupled" coefficients k and c are linear functions of ω. In fact, if the fluid is prerotated prior to entering the seal such that the inlet tangential velocity is $U_\theta o = R\omega/2$, then theory predicts that $k = C\omega/2, c = -C\omega/2, c = M\omega$, and

$$F_r/A = -K, F_\theta/A = -C\omega/2 \tag{23}$$

The present test apparatus provides no intentional prerotation, and the expected result is of the form

$$k = b_1 C\omega/2, b_1 < 1 \tag{24}$$

$$c = b_2 M\omega, b_2 < 1$$

$$F_\theta/A \cong -C_{sf}\omega = -C(1 - b_1/2)\omega \tag{25}$$

$$F_r/A \cong K_{sf} + M_{sf}\omega^2 = -K + M(1 - b_2)\omega^2$$

The term C_{sf} denotes the "net damping coefficient" resulting from the drag force $C\omega A$ and the forward whirl excitation force kA. A direct comparison between theory and experiment is obtained by curvefitting the theoretical and experimental results for the F_r/A and F_θ/A data to obtain predictions for K_{sf}, C_{sf}, and M_{sf}. Note that the procedure of curvefitting the data with respect to ω eliminates the running-speed dependency. Further, K_{sf} is the zero-running speed intercept of the F_r/A versus ω curve, and C_{sf} is the slope of the F_θ/A versus ω curve.

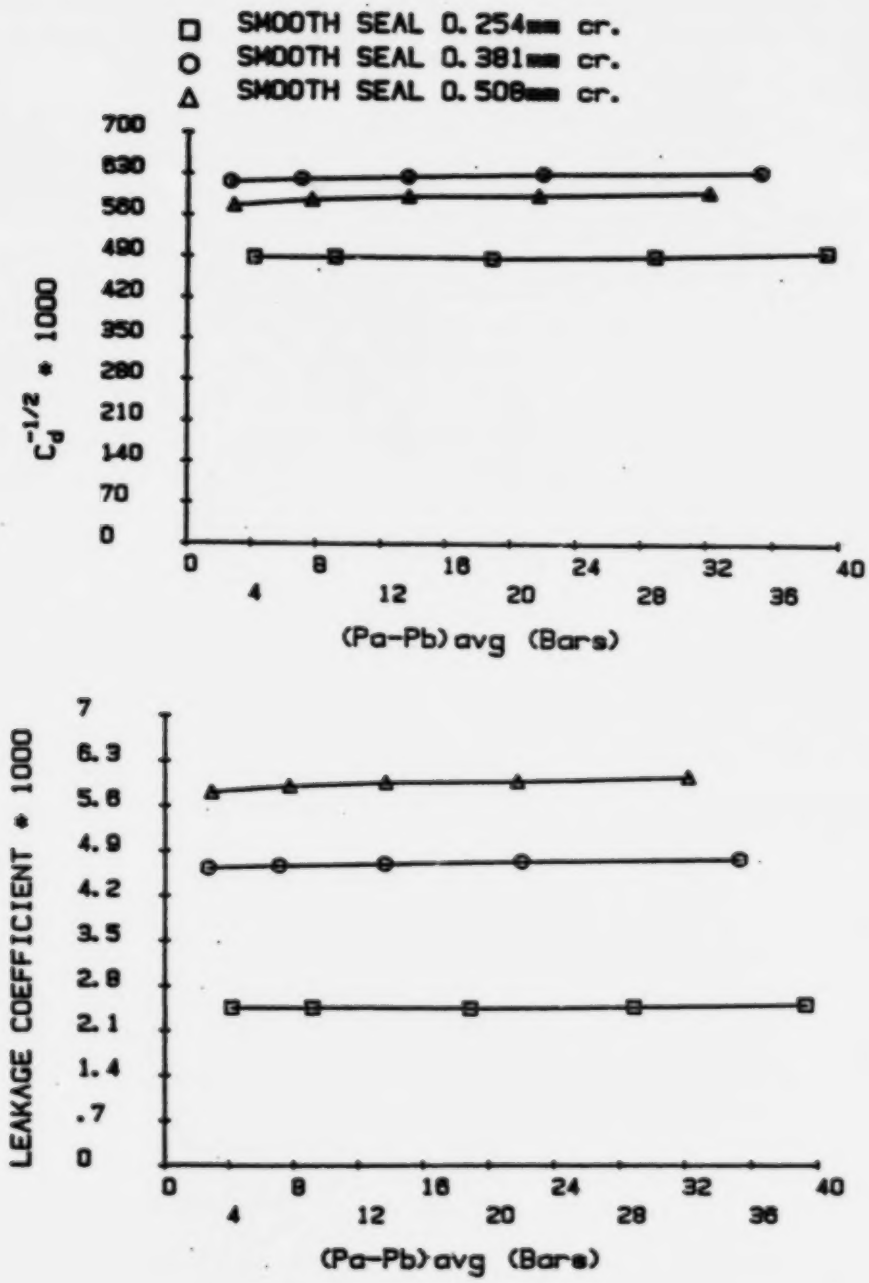

Figure 8. $C_d^{-1/2}$ and C_L for smooth seals;
$C_r = 0.254, 0.381$, and $0.508mm$.

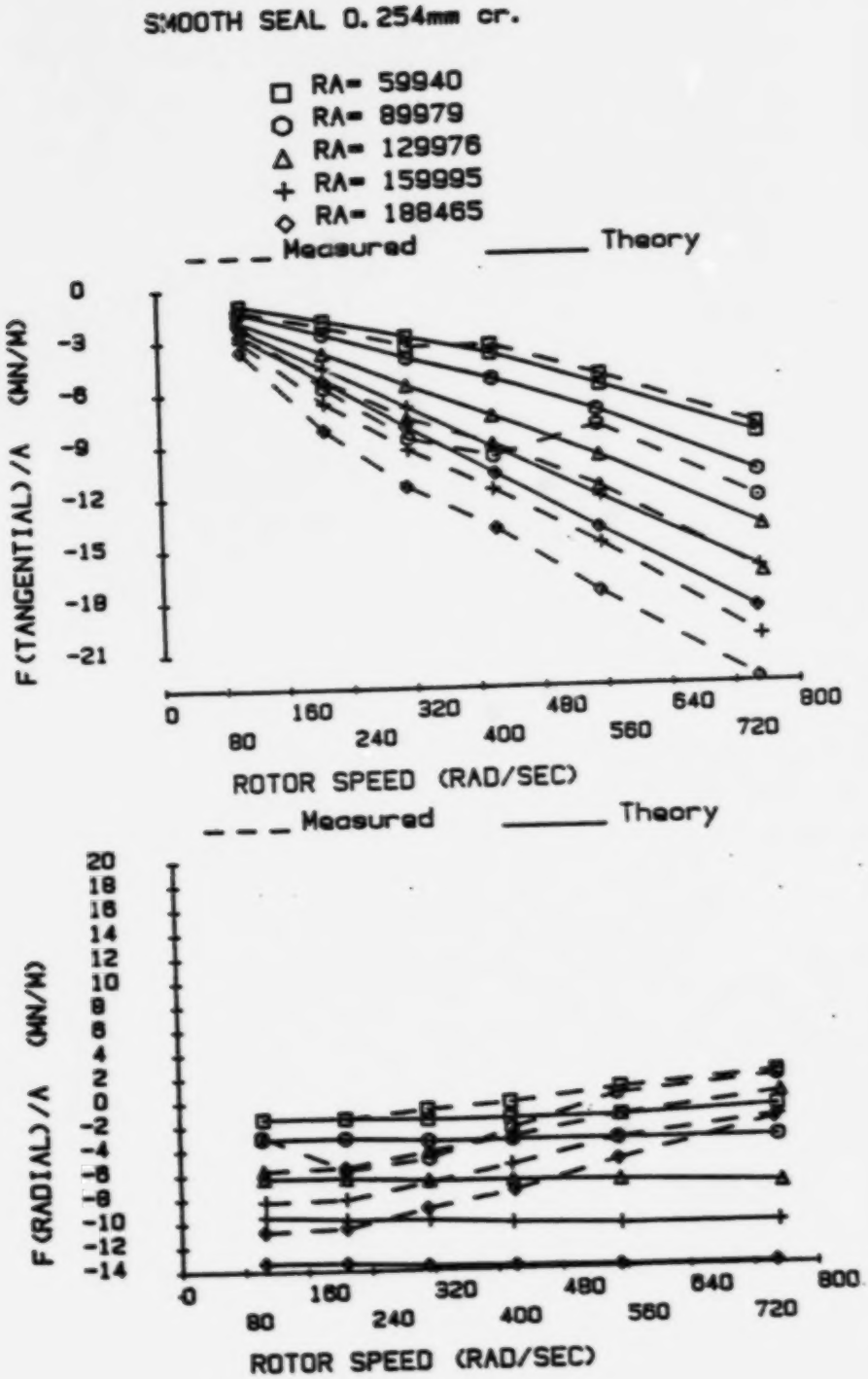

Figure 9. Measured and theoretical [2] results for F_r/A and F_θ/A; smooth seal, $C_r = 0.254mm$.

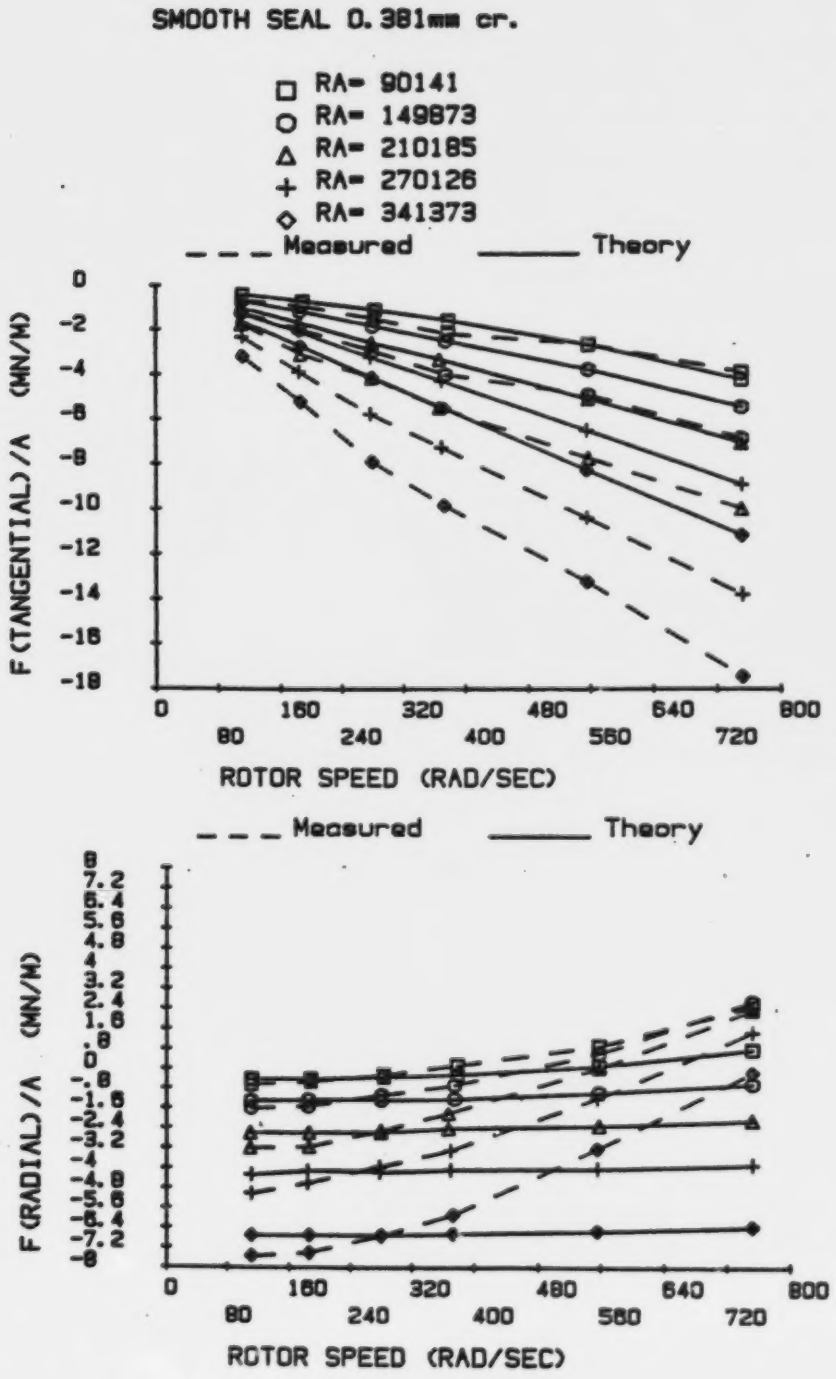

Figure 10. Measured and theoretical [2] results for F_r/A and F_θ/A; smooth seal, $C_r = 0.381mm$.

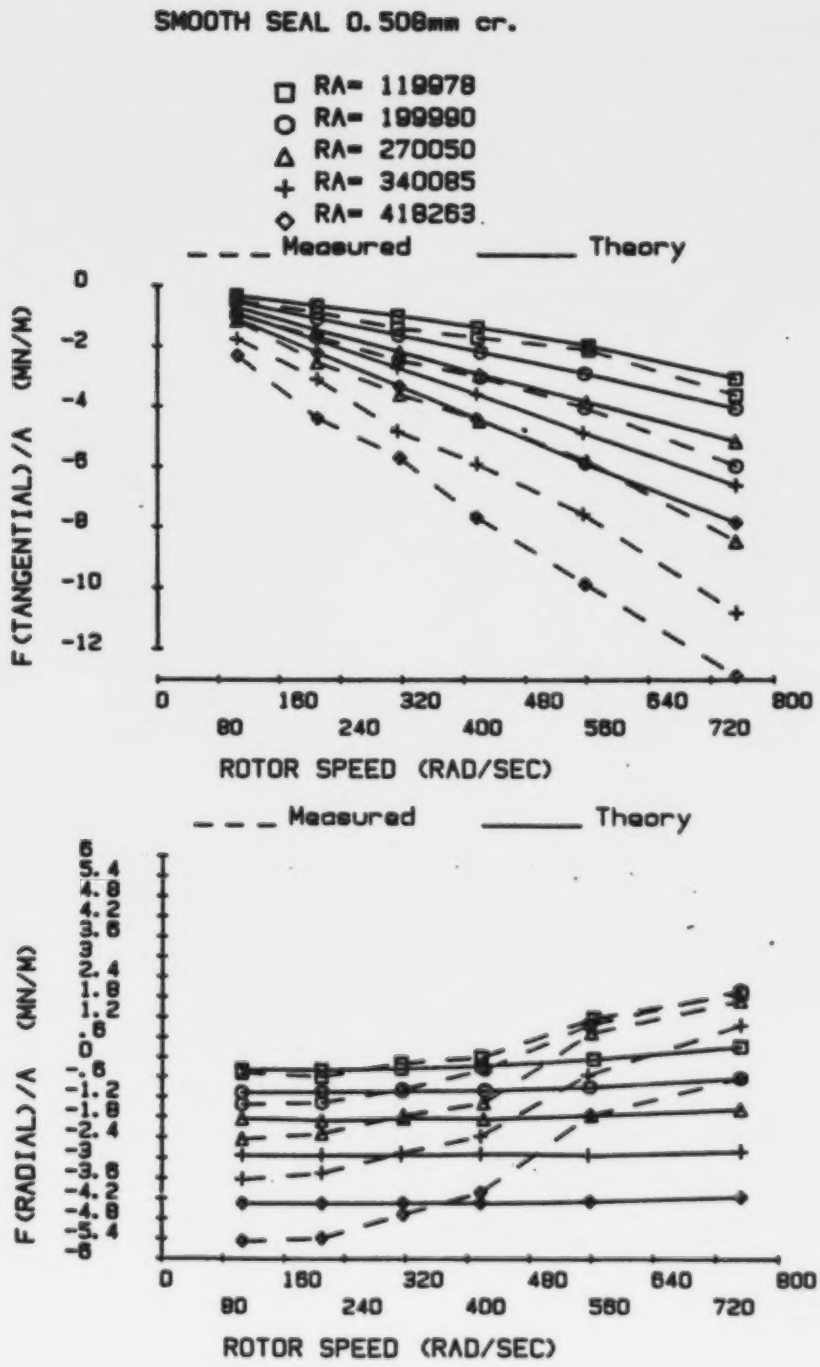

Figure 11. Measured and theoretical [2] results for F_r/A and F_θ/A; smooth seal, $C_r = 0.508mm$.

Experimentally-determined values are presented in table 3 for K_{ef}, C_{ef}, and M_{ef}. A comparison of theoretical and experimental results is also presented in these tables. Observe that the seals are generally stiffer than predicted, but that the correlation improves with increasing R_e and decreasing C_r. The correlation for C_{ef} worsens as R_e increases, but rapidly approaches an asymptote. The "correlation" for M_{ef} is too erratic to comment on except to note that measured M_{ef} values are generally much larger than predictions.

S.I. Units	K_{ef} (EXP)	C_{ef} (EXP)	M_{ef} (EXP)	K_{ef} (EXP/TH)	C_{ef} (EXP/TH)	M_{ef} (EXP/TH)
SMOOTH SEAL 0.254mm cr.						
R_e=59940	1944000	10250	3.082	1.755	0.8549	0.7611
R_e=89980	3876000	13440	17.42	1.341	0.9268	14.22
R_e=130000	6825000	20830	1.886	1.099	1.131	-2.824
R_e=160000	9667000	25980	1.834	1.053	1.189	0.9135
R_e=188500	11790000	28900	9.239	0.9056	1.157	4.57
SMOOTH SEAL 0.381mm cr.						
R_e=90140	668500	4971	5.921	1.810	0.8402	1.868
R_e=149900	1668000	8507	8.196	1.347	1.157	4.057
R_e=210200	3617000	12670	8.112	1.367	1.351	12.32
R_e=270100	5420000	17620	8.285	1.272	1.480	73.17
R_e=341400	7981000	21740	1.96	1.189	1.460	15.62
SMOOTH SEAL 0.508mm cr.						
R_e=120000	679000	4554	4.581	2.003	1.095	2.269
R_e=200000	1800000	7534	4.733	1.777	1.395	3.573
R_e=270100	2901000	10830	5.520	1.594	1.580	5.017
R_e=340100	4027000	13720	6.561	1.386	1.553	18.23
R_e=418300	6183000	16240	5.351	1.435	1.554	6.817

Table 3. Measured values for K_{ef}, C_{ef}, and M_{ef}; comparison of theory and experiment for smooth seals at three difference clearances.

The parameter K_{ef} can be normalized as follows

$$\overline{K}_{ef} = K_{ef}\left(\frac{C_r}{DL\Delta P}\right), \tag{26}$$

while C_{ef} can be similarly mormalized as

$$\overline{C}_{ef} = C_{ef}\left(\frac{C_r}{DL\Delta P}\right), \tag{27}$$

or nondimensionalized as

$$\hat{C}_{ef} = C_{ef}\left(\frac{C_r T}{DL\Delta P}\right), \tag{28}$$

where T = L/V is the transit time for flow through the seal.

Figure 12 illustrates K_{ef} and $\overline{K}_{ef}$ versus ΔP. Observe that K_{ef} increases monotonically as C_r is reduced, and that the nondimensionalised parameter $\overline{K}_{ef}$ generally collapses the test data into a narrow band. Hence the nondimensionalisation is effective.

Figure 13 illustrates C_{ef} versus ΔP for three different clearances. Observe that C_{ef} increases monotonically as ΔP increases and C_r increases. The objective of a nondimensionalisation for C_{ef} would be to reduce the three curves of figure 13 into a straight line, independent of both C_r and ΔP. Figure 14 illustrates both the normalised parameter $\overline{C}_{ef}$ and nondimensionalised parameter $\hat{C}_{ef}$. Observe that the normalisation which yields $\overline{C}_{ef}$ pulls the three curves into a tight band, largely eliminating the clearance dependency; however, $\overline{C}_{ef}$ is now a decreasing function of ΔP. The nondimensionalisation which yields $\hat{C}_{ef}$ eliminates the pressure dependency but leaves a dependency on C_r; i.e., the $C_r = 0.254mm$ curve is significantly displaced from the remaining two curves.

3.5 Conclusions

The test results presented here support the following conclusions:

(a) The friction-factor data demonstrate that the Hirs' wall-friction model is considerably more restricted than had previously been thought. The empirical coefficients only characterise the seal surfaces at a fixed clearance and over a restricted Reynolds number range. The "Moody" approach of von Pragenau and Nelson and Nguyen needs to be examined to see whether it yields broader ranges of applicability.

(b) The agreement between theory and experiment for K_{ef} and C_{ef} is reasonable for all cases and improves as R_a increases and C_r decreases. Hence, the validity of predictions for SSME turbopumps should be acceptable.

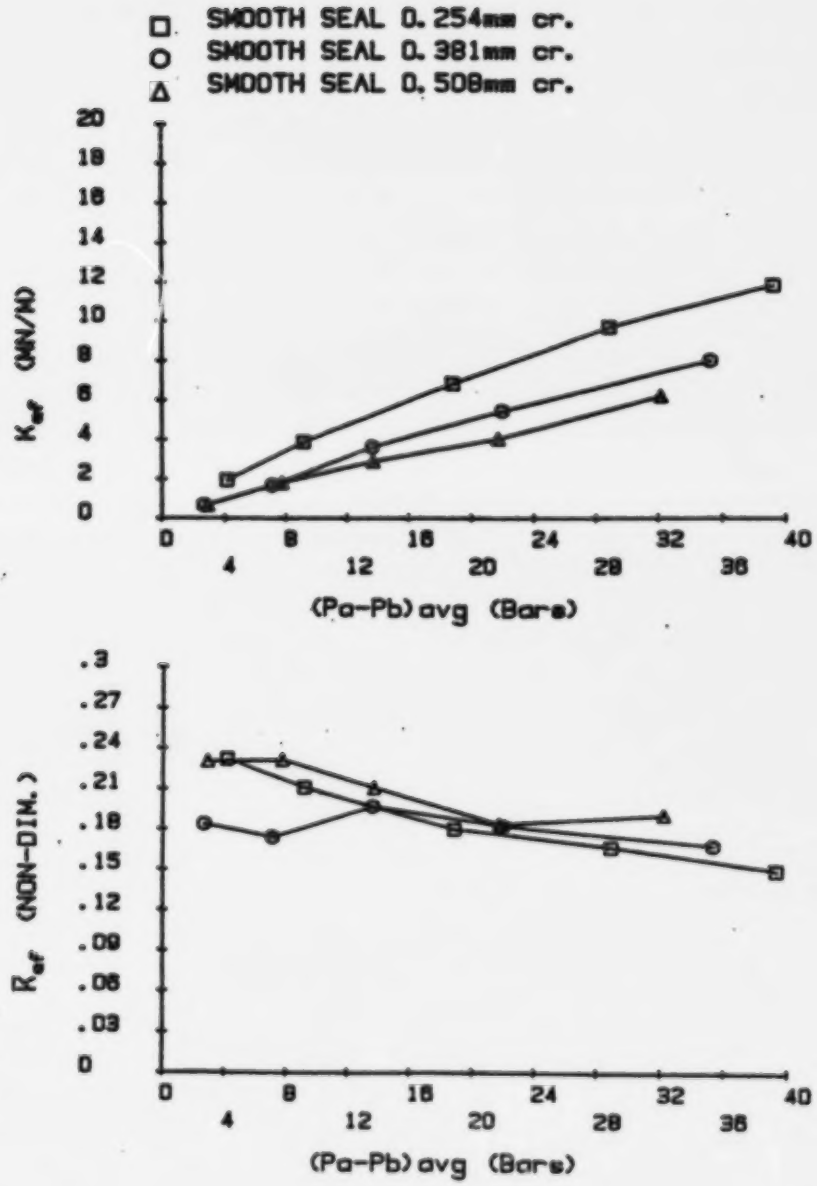

Figure 12. K_{ef} and $\overline{K}_{ef}$ versus ΔP
for smooth seals at three different clearances.

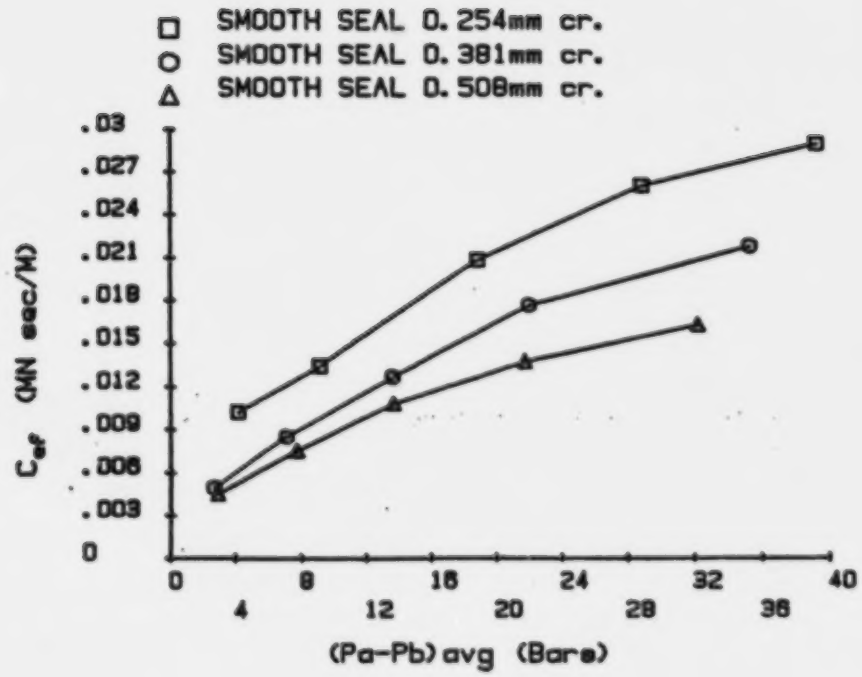

Figure 13. C_{ef} **versus** ΔP **for smooth seals at three different clearances.**

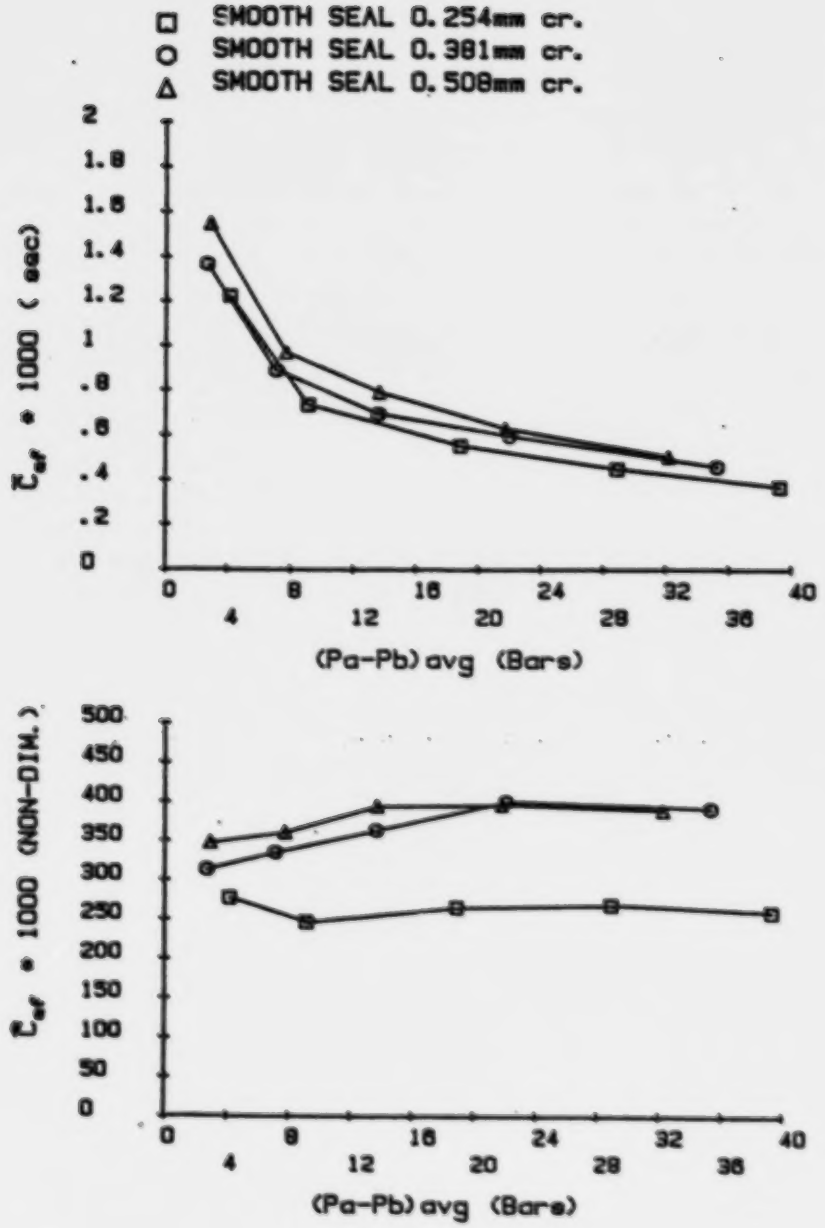

Figure 14. $\overline{C}_{ef}$ and $\hat{C}_{ef}$ versus ΔP for smooth seals at three different clearances.

CHAPTER IV
TEST RESULTS FOR ROUND-HOLE PATTERN DAMPER SEALS AT REDUCED CLEARANCE

4.1 Introduction

Figure 15 illustrates the round-hole-pattern stator configurations which were tested in this contract phase. All seals were tested at 0.381*mm* radial clearances versus earlier tests at 0.51*mm*. The first four stators have $\gamma = 0.34$, which proved to be optimum in earlier test results, with a variation in h/C_r from 1.00 to 4.03. These tests include $h/C_r = 2.92$, which was the optimum result in our earlier tests. The parameter h/C_r is held constant for seals 5 and 6 while γ is changed to 0.27 and 0.42, respectively.

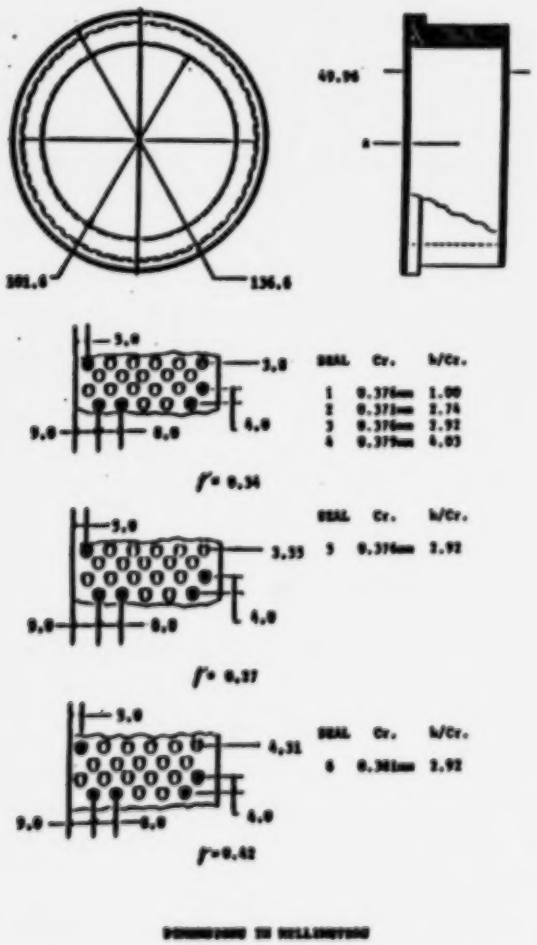

Figure 15. Round-hole-pattern and stator configuration detail A.

4.2 Friction-Factor Data

Figures 16 through 18 present measurements and predictions of σ_o versus R_a and ω for test seals with the six hole-pattern stators. Recall from Eq. (18) that the σ_o values are obtained from measured, axial-pressure gradients and are assumed to be the average of σ_r (rotor) and σ_s (stator). The curves in these figures are generally similar to those obtained earlier for smooth seals. As expected, σ_o values are consistently higher for the rougher, round-hole-pattern stators. Note that the test results for $\gamma = 0.42$ are markedly different from the remaining test data, with much greater speed sensitivity. Also note for this figure that at low speeds σ_o increases with R_a. At higher values of R_a, σ_o decreases with increasing ω.

Except for the $\gamma = 0.42$ results, there is generally good agreement between σ_o measured and σ_o predicted in figures 16 through 18; however, this masks a significantly greater discrepancy between predictions and measurements for σ_s. Recall from chapter II that "experimental data" for σ_s are derived from measured values for σ_o and predicted values for σ_r. The predicted values for σ_r are based on values of mr, nr which are obtained from separate pressure-gradient measurements in seals with the same smooth rotor and stator surfaces. Figures 19 through 21 compare "derived" and predicted values for σ_s. Note that the correlation between theory and derived data are generally not very good. Test results show much greater sensitivity to speed than the derived data. Also the derived data show σ_s decreasing with increasing speed at higher values for R_a, while the theory shows the opposite trend. Several of the lower-speed data curves show σ_s increasing with R_a instead of decreasing.

Table 4 presents calculated values for ms and ns for the six hole-pattern stators.

Stator	ms	ns	$R_a(max)$
1	-0.0547	0.059	242,120
2	-0.0926	0.103	233,560
3	0.0103	0.0279	236,570
4	-0.0433	0.056	240,140
5	-0.0360	0.048	260,600
6	0.0680	0.019	253,980

Table 4. Hirs coefficients for hole-pattern stators as calculated using the solution approach of figure 5.

4.3 Leakage Data

Figure 22 presents $C_d^{-\frac{1}{2}}$ for the six hole-pattern stators. Observe that there is very little difference in the leakage performance of the seals using these stators. Minimum leakage results are obtained for $(h/C_r = 1.0, \gamma = 0.34)$ and $(h/C_r = 2.92, \gamma = 0.42)$.

4.4 Dynamic Test Data

Figures 23 through 28 provide comparisons between measured and theoretical values for F_r/A and F_θ/A versus R_a and ω. As with smooth seals, the prediction for F_θ/A is generally better than F_r/A.

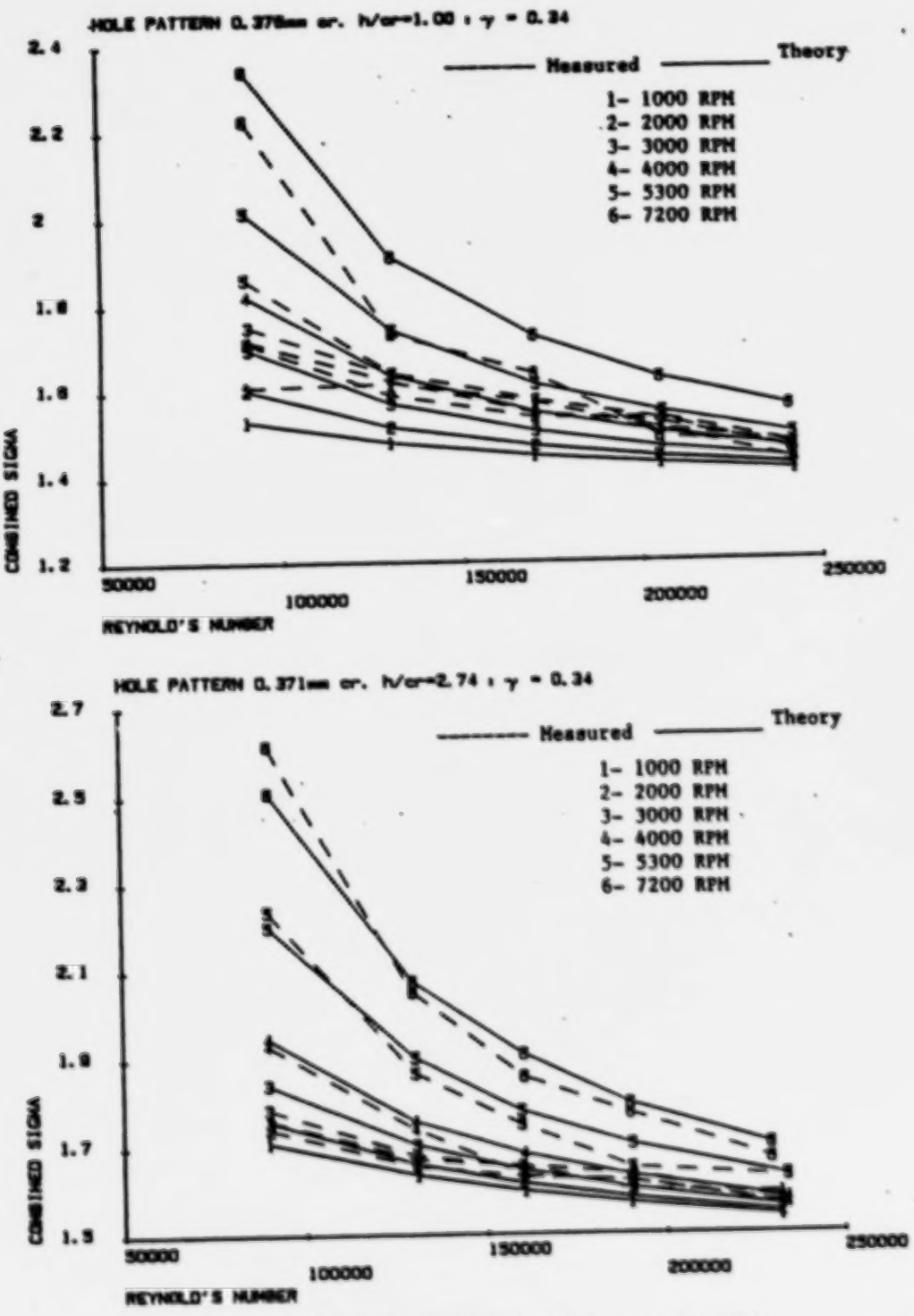

Figure 16. Combined sigma data for damper seals with hole-pattern-stators 1 and 2.

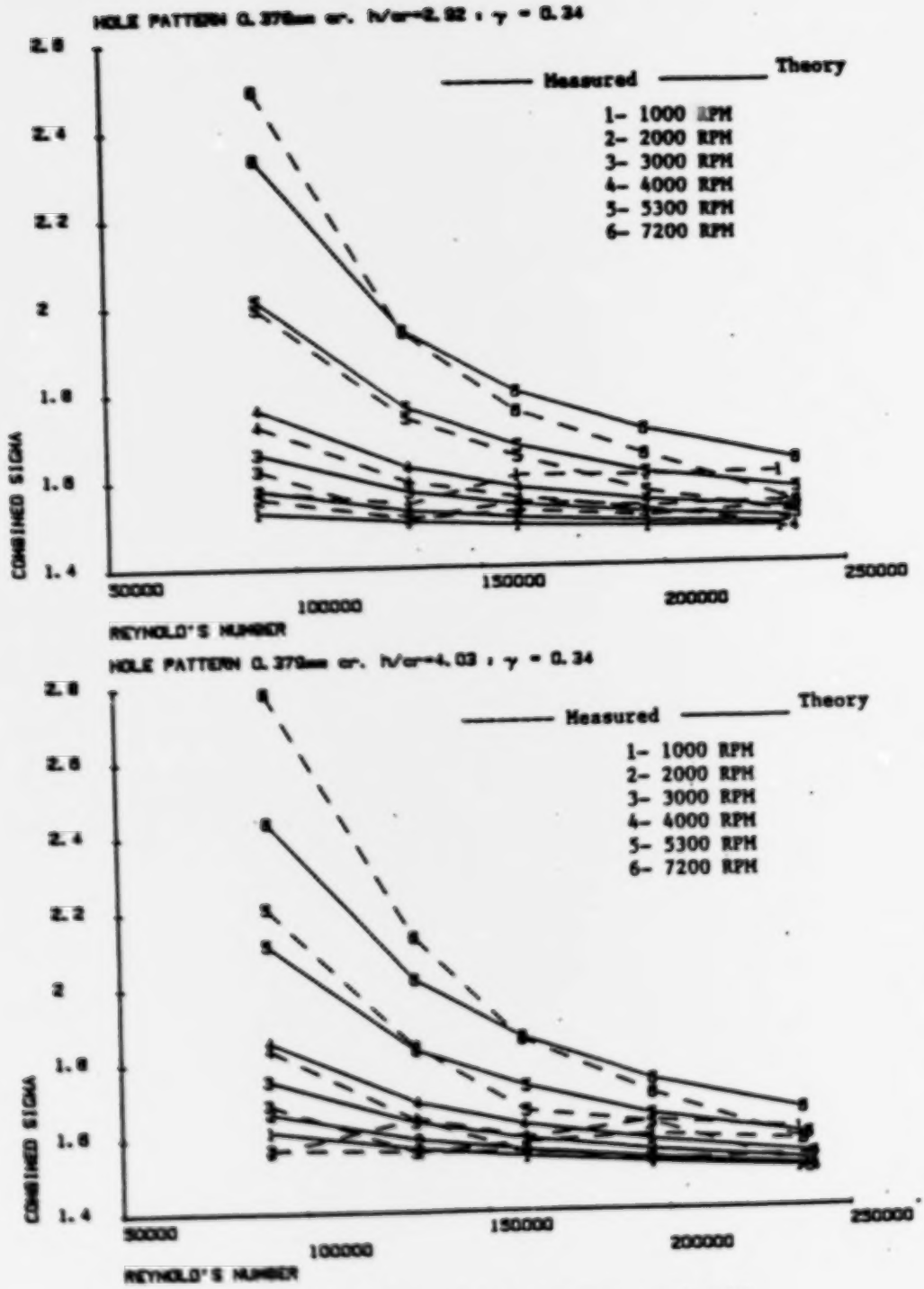

Figure 17. Combined sigma data for damper seals with hole-pattern-stators 3 and 4.

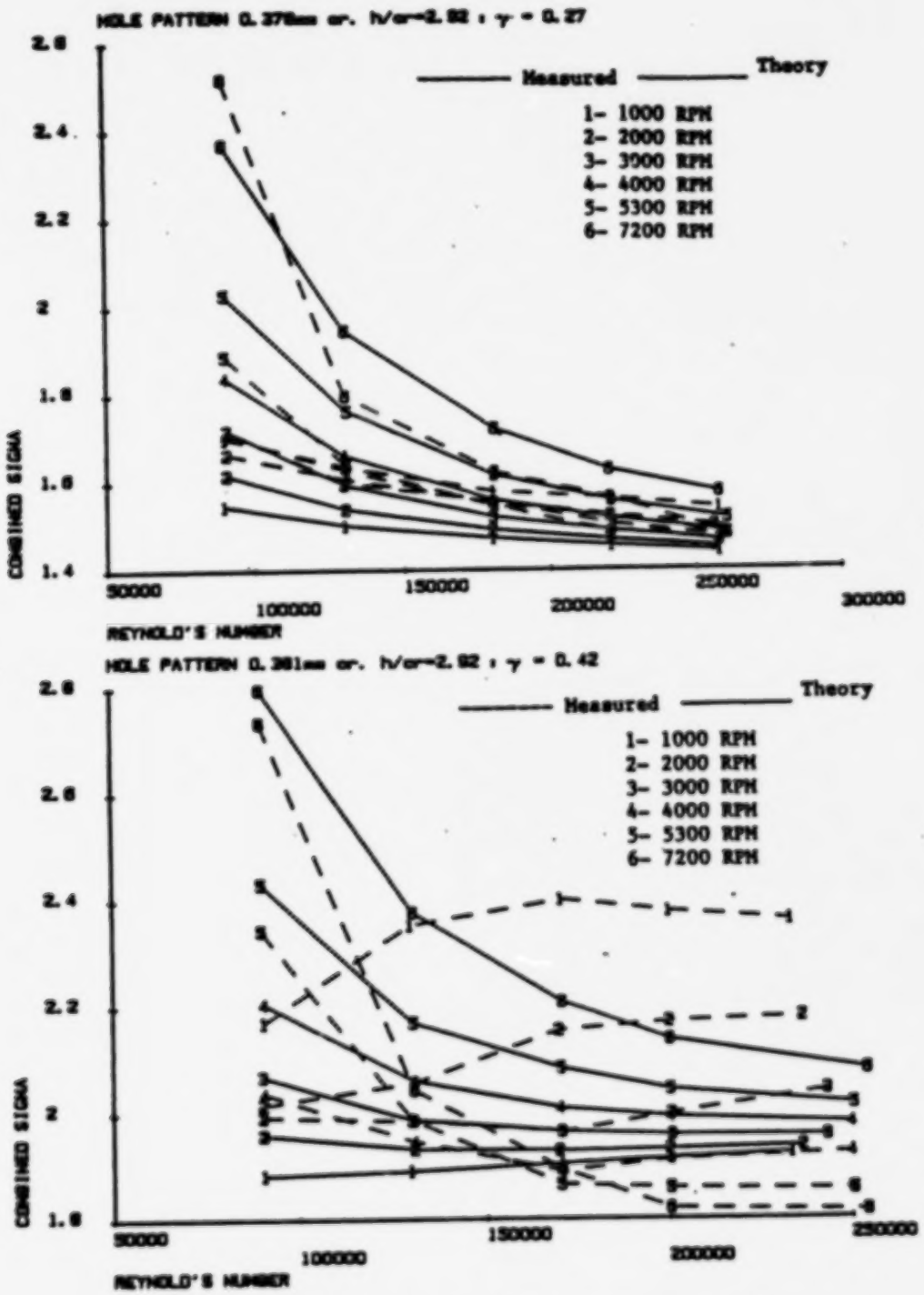

Figure 18. Combined sigma data for damper seals with hole-pattern-stators 5 and 6.

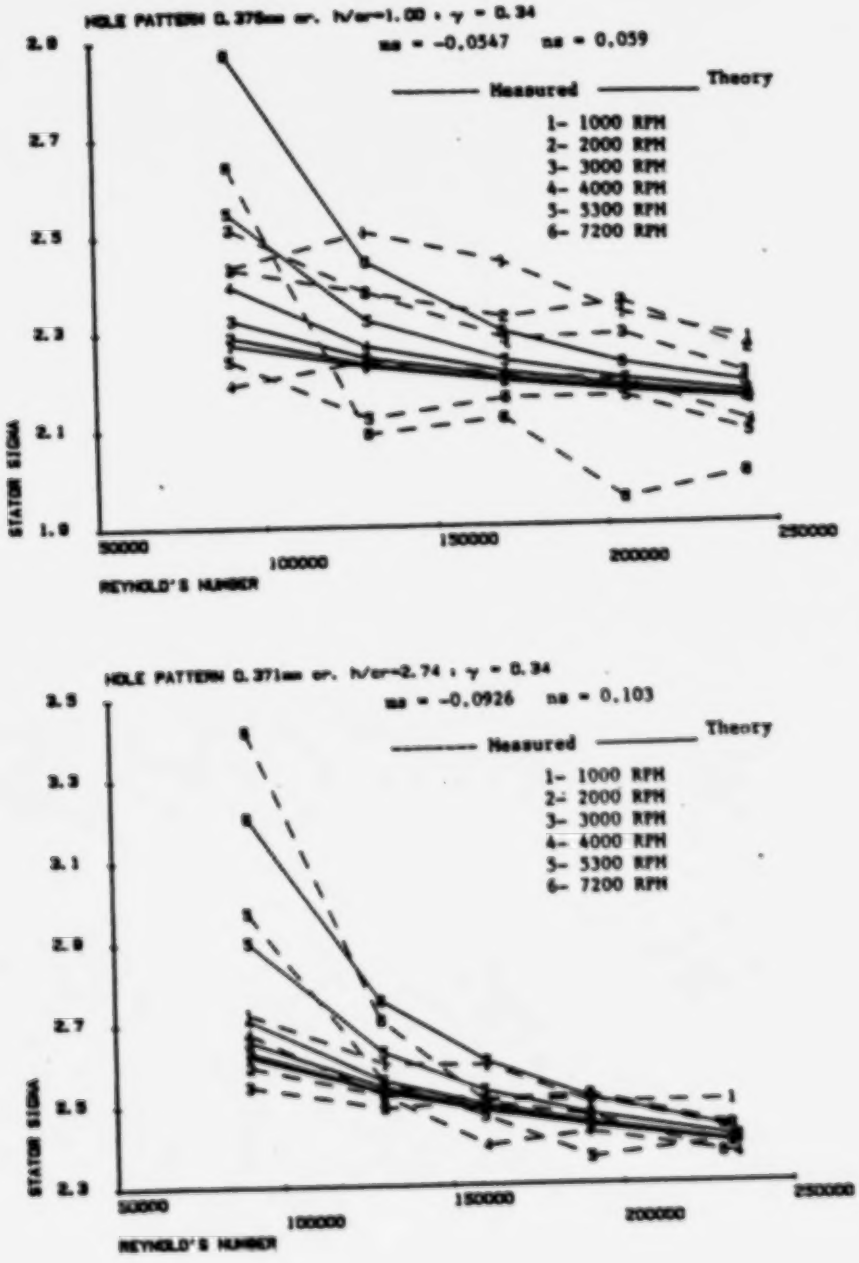

Figure 19. Stator sigma data for hole-pattern-stators 1 and 2.

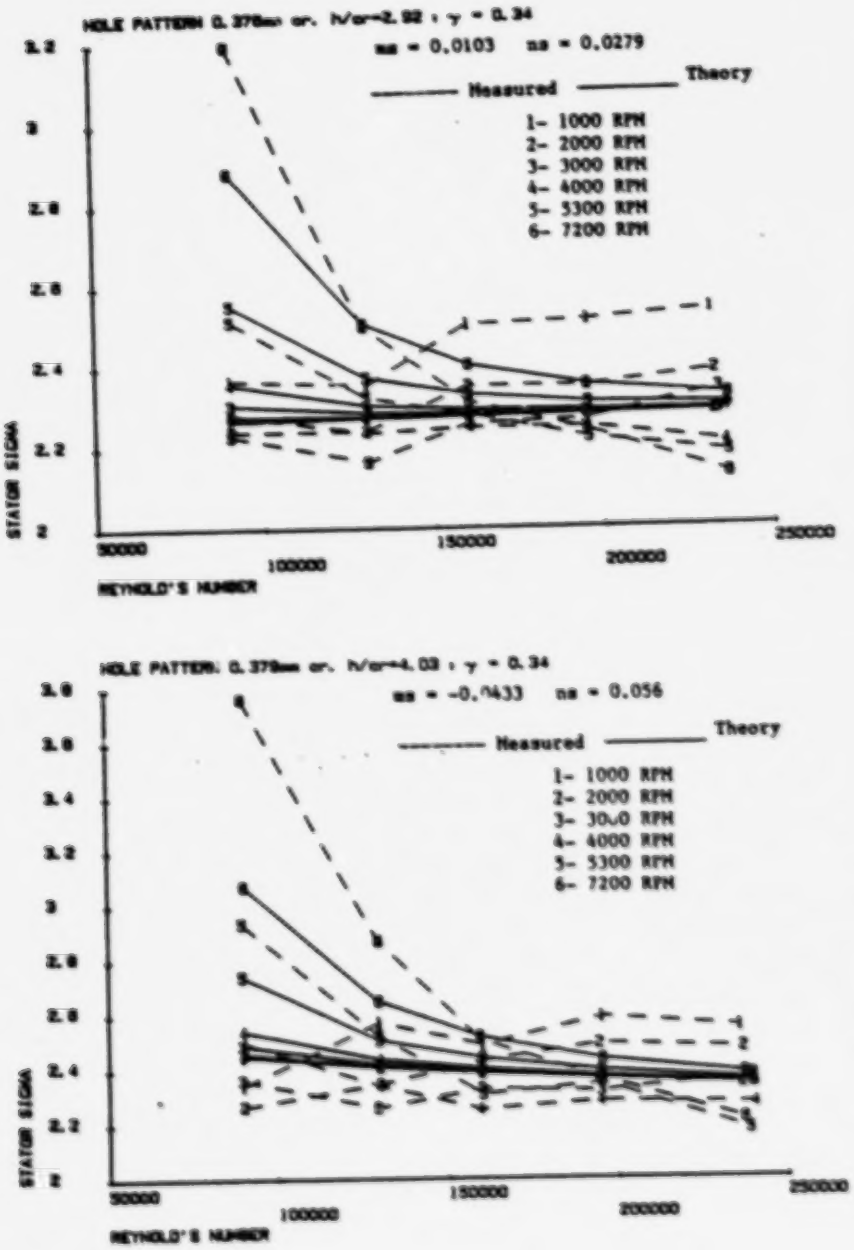

Figure 20. Stator sigma data for hole-pattern-stators 3 and 4.

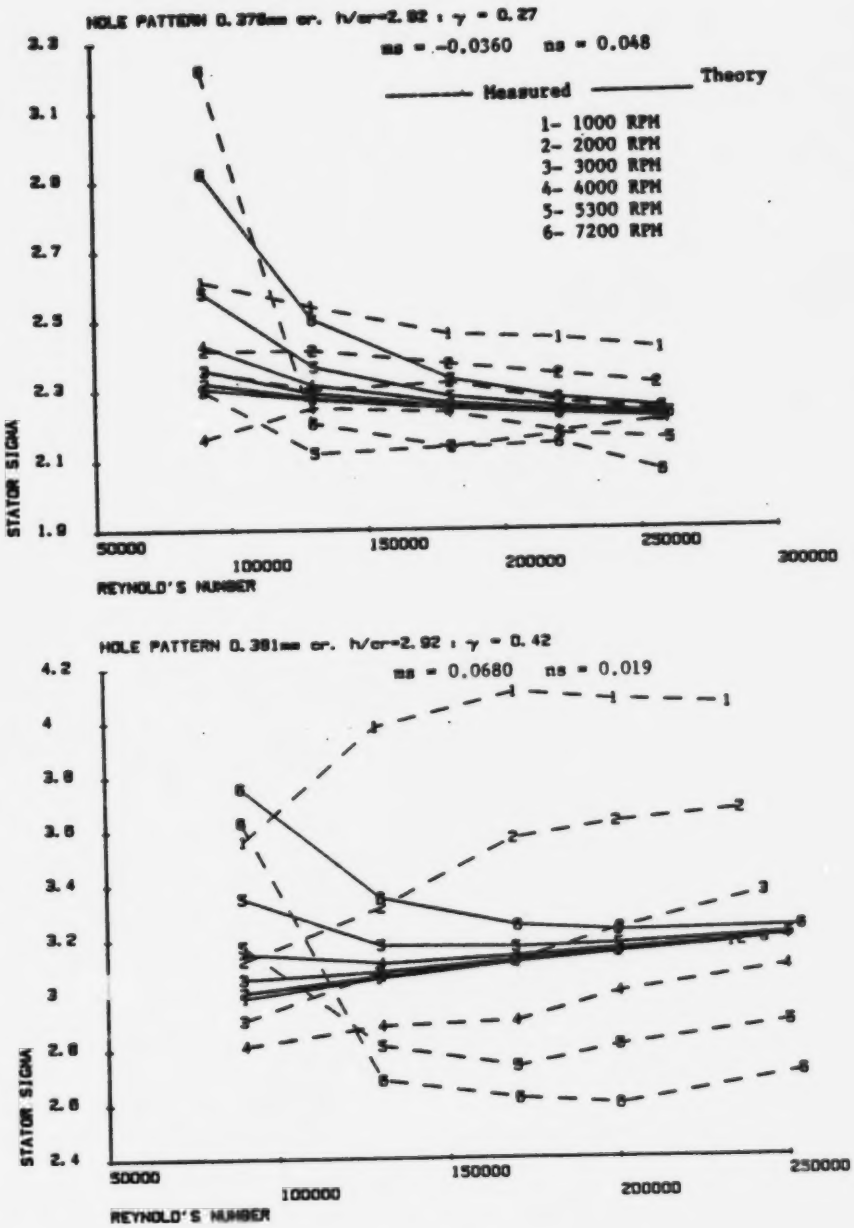

Figure 21. Stator sigma data for hole-pattern-stators 5 and 6

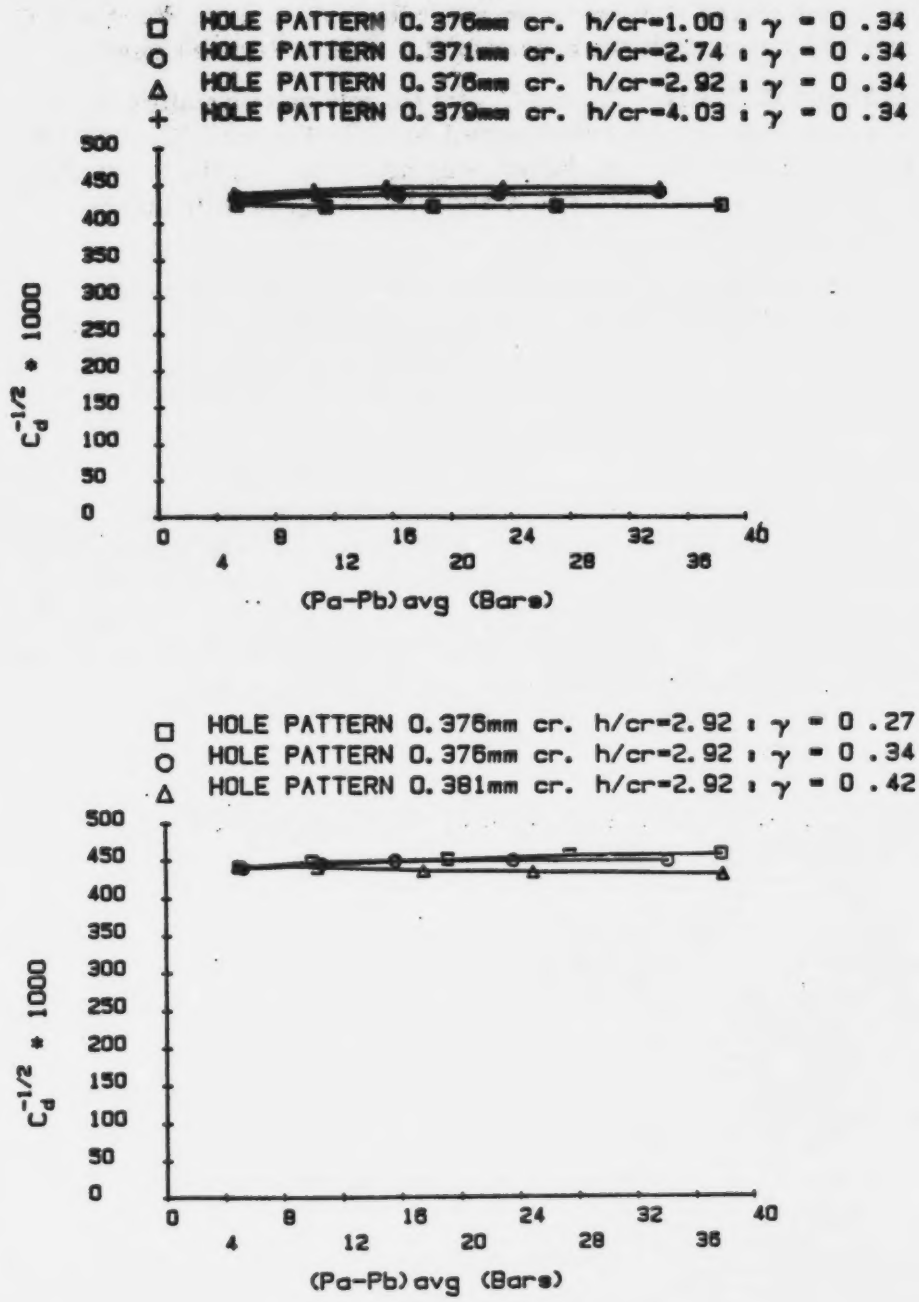

Figure 22. $C_d^{-1/2}$ for hole-pattern-stator seals.

Figures 29 and 30 illustrate K_{ef} and $\overline{K}_{ef}$ for the hole-pattern stators. For the $\gamma = 0.34$ stators, the largest overall stiffness values result for $h/C_r = 2.92$. For the $h/C_r = 2.92$ data, the $\gamma = 0.27$ stator yields the maximum K_{ef} at high Reynolds numbers.

Figures 31 and 32 illustrate C_{ef} and $\overline{C}_{ef}$ for the hole-pattern stators. For the $\gamma = 0.34$ stators, there is no clear optimum with respect to h/C_r. For the $h/C_r = 2.92$ stators, the $\gamma = 0.27$ and $\gamma = 0.34$ stators yield larger damping values than the $\gamma = 0.42$ stator. The absence of clear optima with respect to γ and h/C_r is significantly different from earlier tests at $0.51mm$ clearances.

Table 5 provides measured data for K_{ef}, C_{ef}, and M_{ef} and comparisons to theory for the hole-pattern-stator seals. The comparison betwen theory and experiment is generally good for K_{ef} and C_{ef}. Predictions for M_{ef} continue to be erratic and small, as compared to measured data, but the correlation is better for hole-pattern stators than smooth stators (compare with Table 3).

4.5 Conclusions

The test results presented in this chapter support the following conclusions:

(a) The test results for pressure gradients in damper seals raise serious questions with respect to our understanding of the correct model for friction factors versus running speed and Reynolds numbers. Neither a Hirs model or a Moody model will correctly predict the measured test data, and the correlation capability drops sharply as γ is increased from 0.34 to 0.42.

(b) Despite the poor capability of the Hirs formulation for predicting σ_s, the theory of [2] does a good job of predicting K_{ef} and C_{ef}. The predictions are actually better for the hole-pattern stators than smooth stators.

(c) Test results for hole-pattern stators at reduced clearances (0.38 versus $0.51mm$) show no clear optimum of C_{ef} versus h/C_r. With $h/C_r = 2.92$, a dropoff in C_{ef} is observed when γ is increased from 0.34 to 0.42.

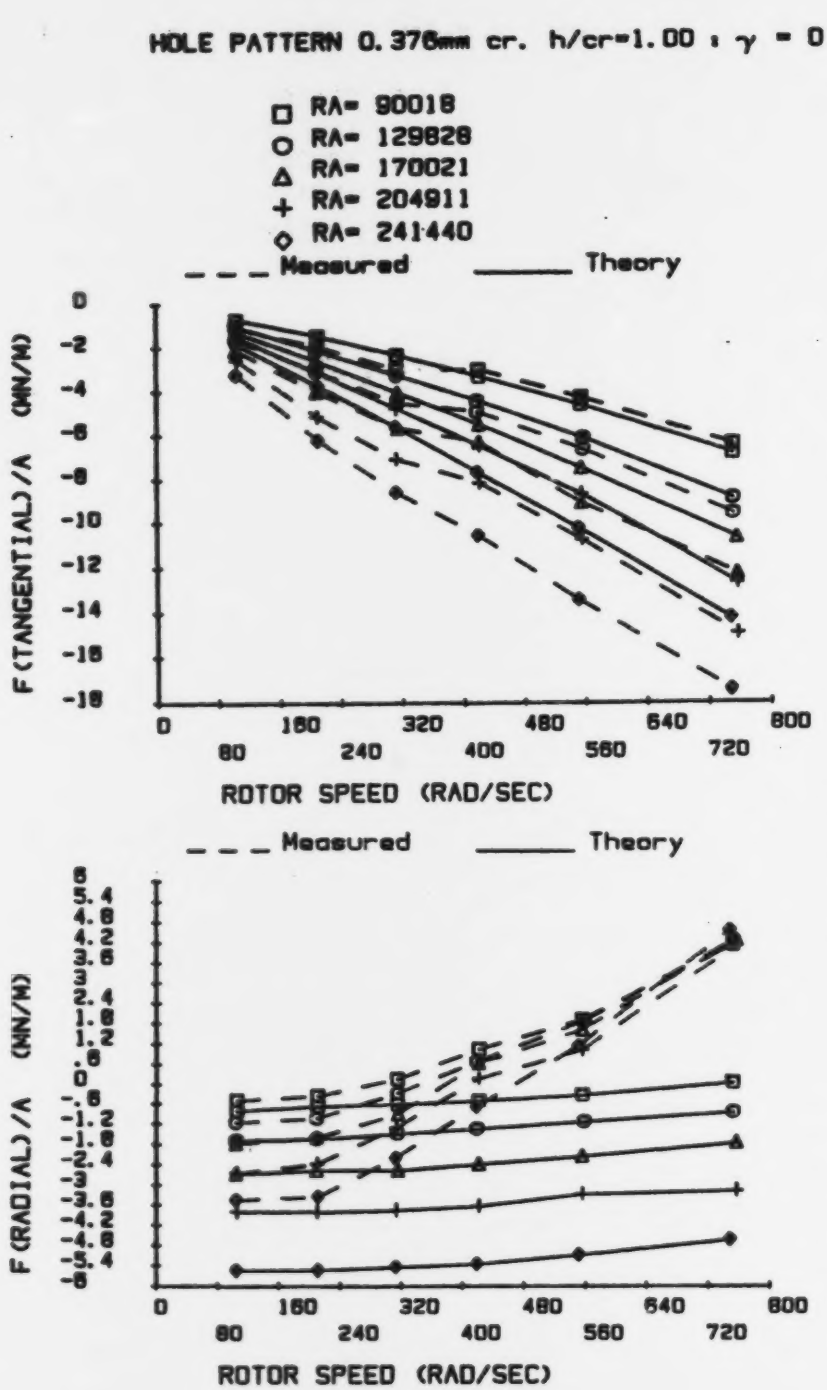

Figure 23. Measured and theoretical [2] results for F_r/A and F_θ/A; hole-pattern stator 1.

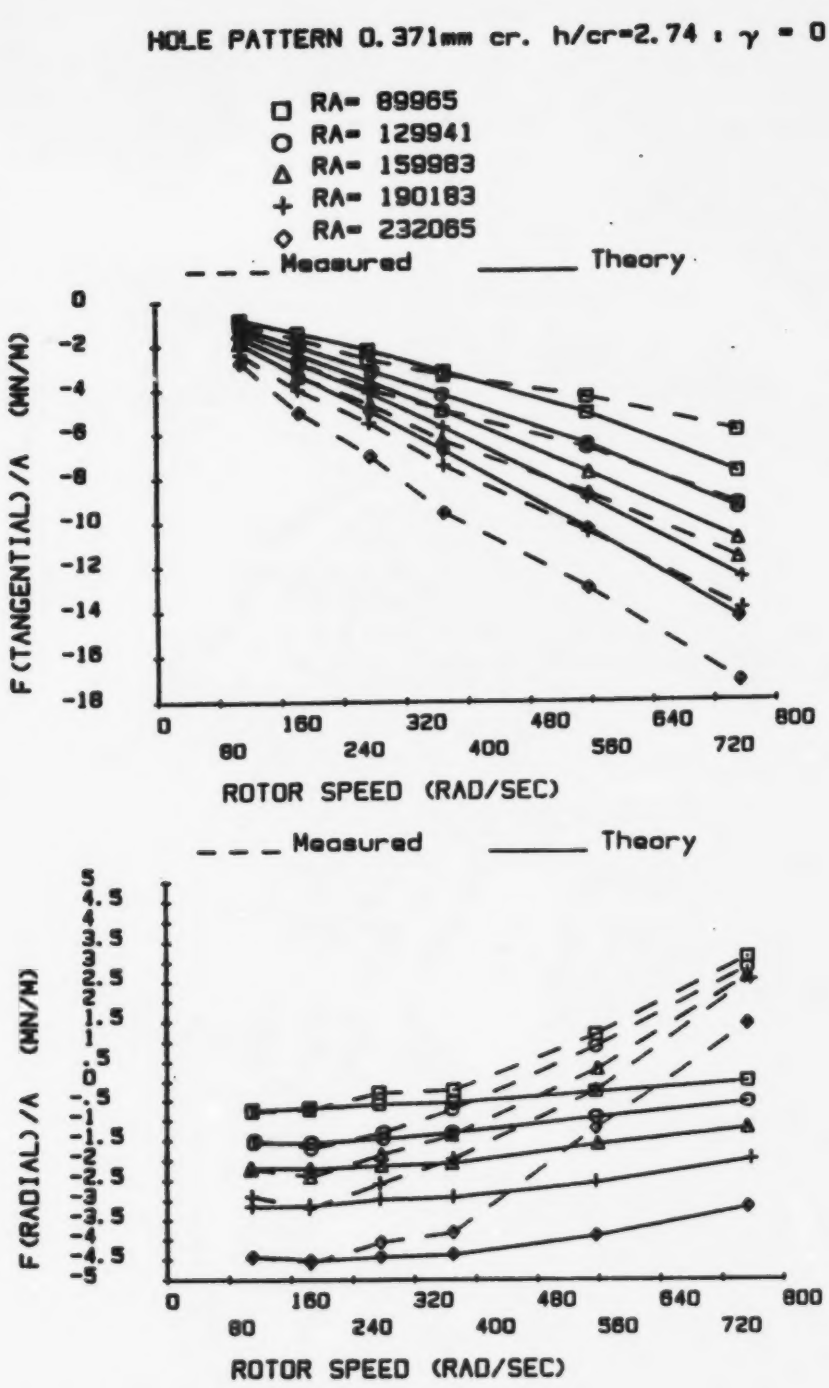

Figure 24. Measured and theoretical [2] results for F_r/A and F_θ/A; hole-pattern stator 2.

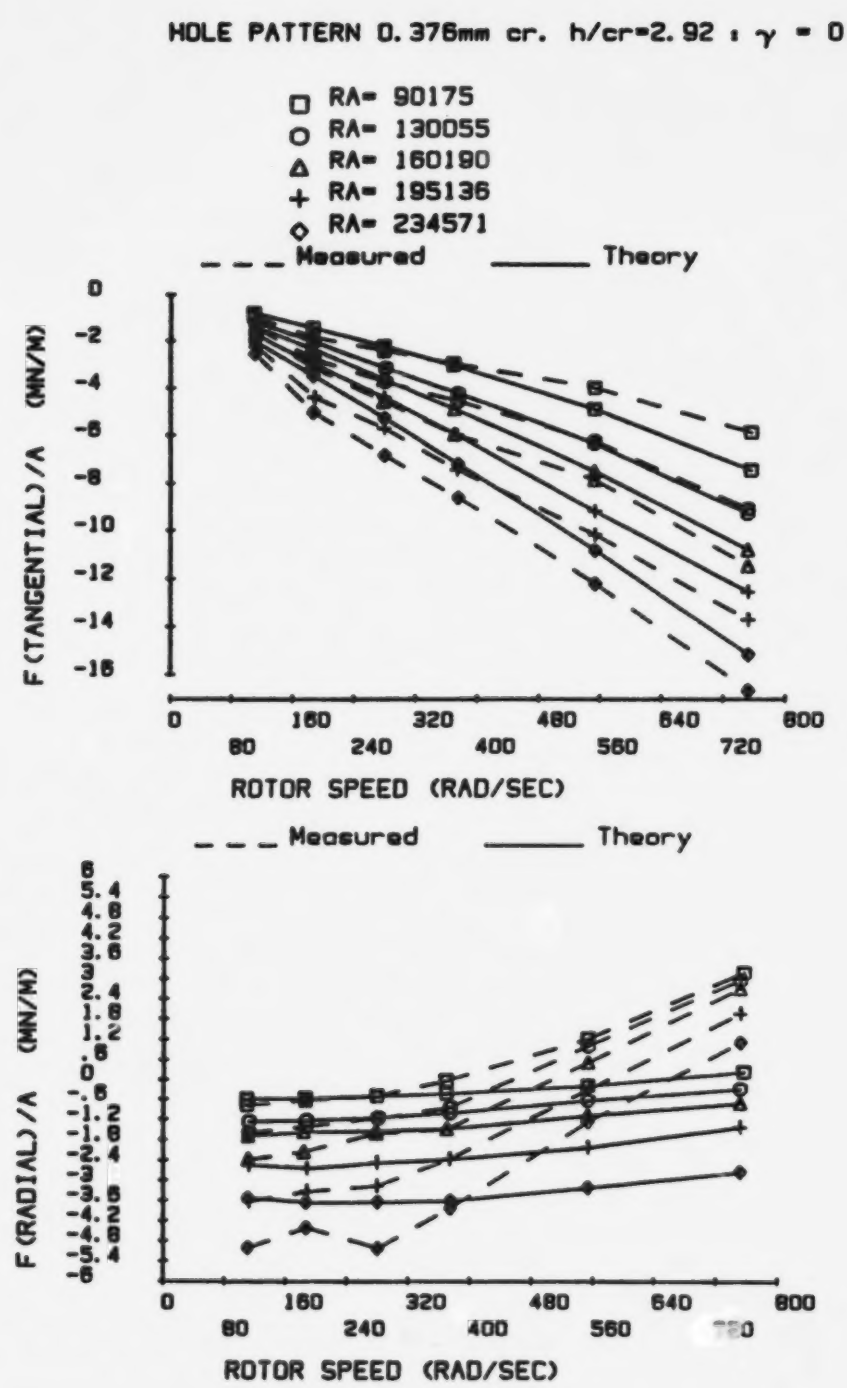

Figure 25. Measured and theoretical [2] results for F_r/A and F_θ/A; hole-pattern stator 3.

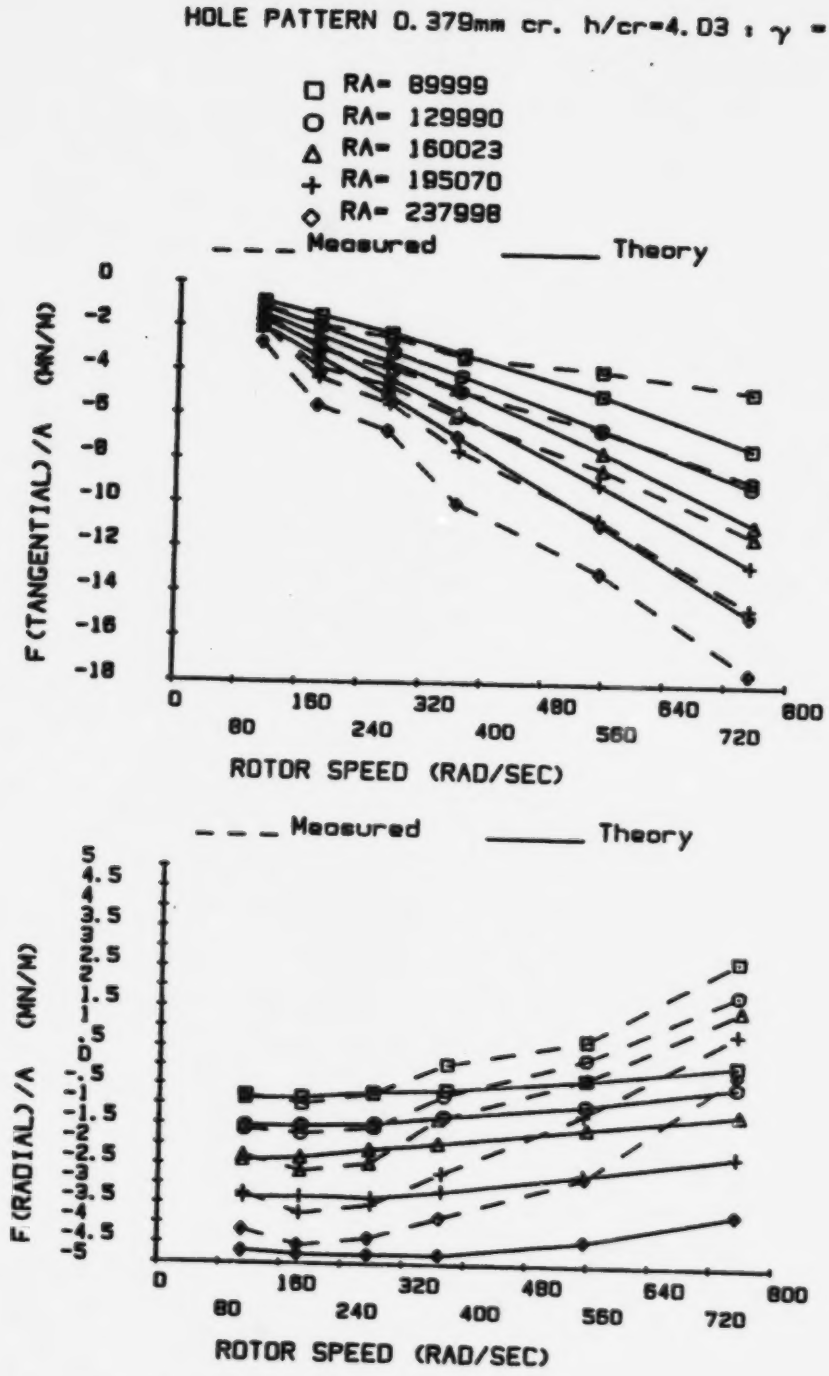

Figure 26. Measured and theoretical [2] results for F_r/A and F_θ/A; hole-pattern stator 4.

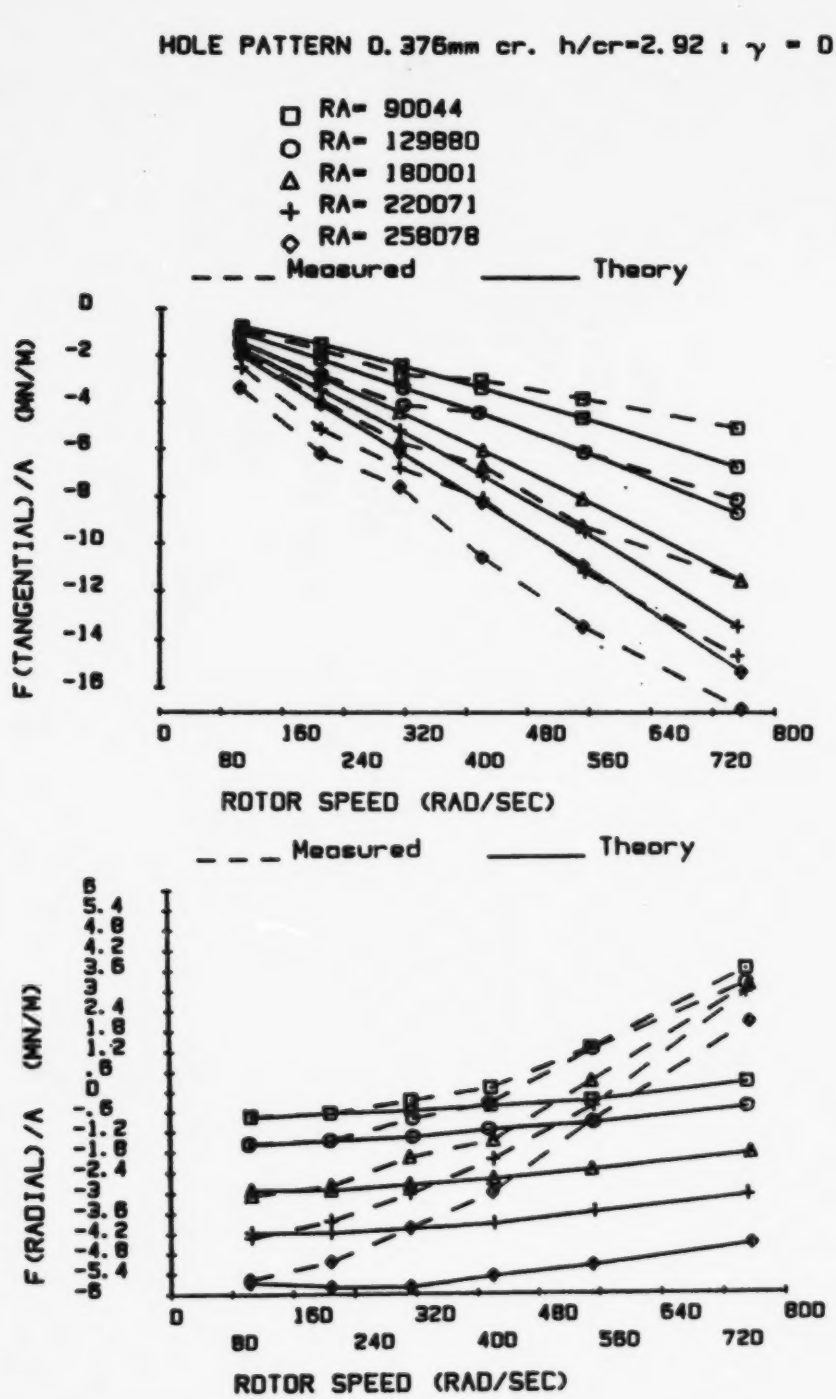

Figure 27. Measured and theoretical [2] results for F_r/A and F_θ/A; hole-pattern stator 5

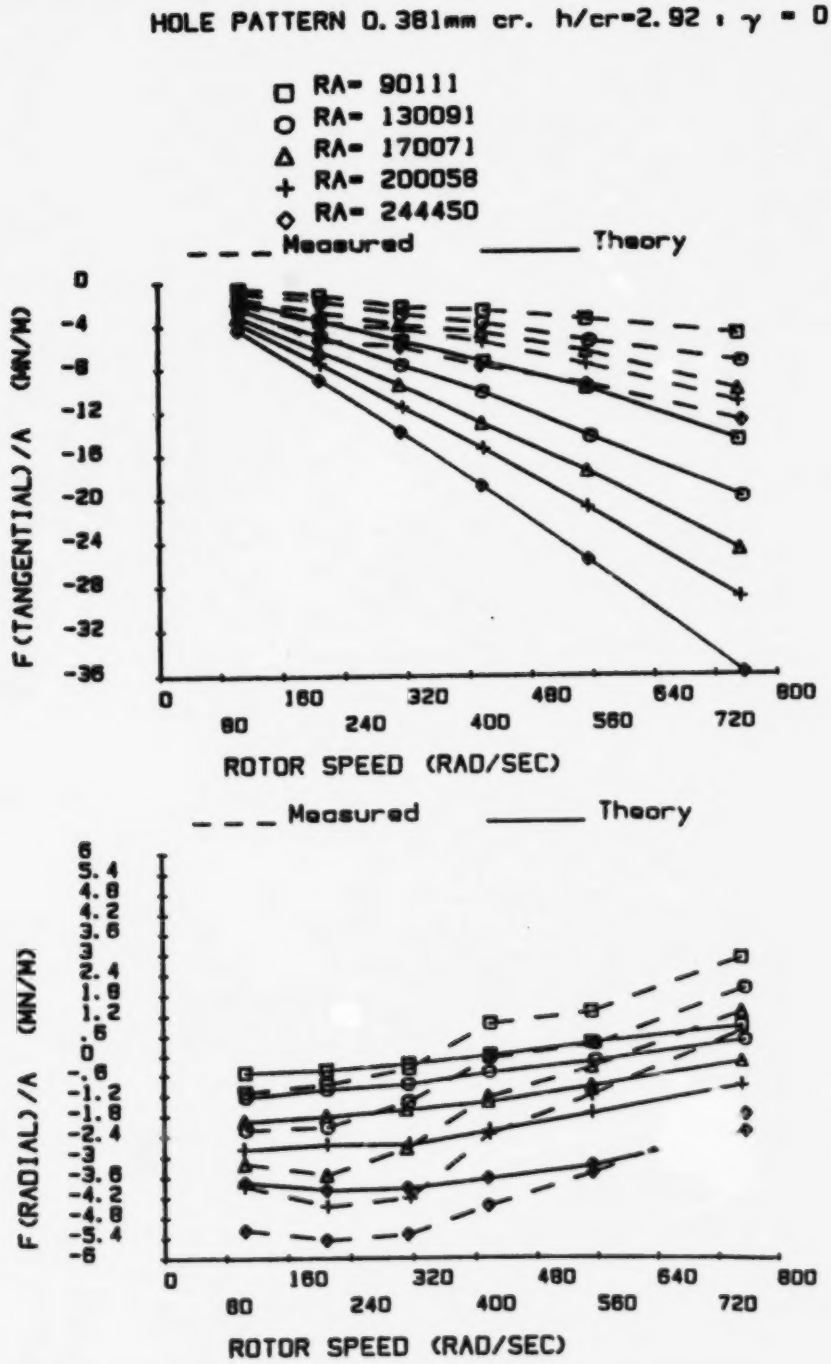

Figure 28. Measured and theoretical [2] results for F_r/A and F_θ/A; hole-pattern stator 6.

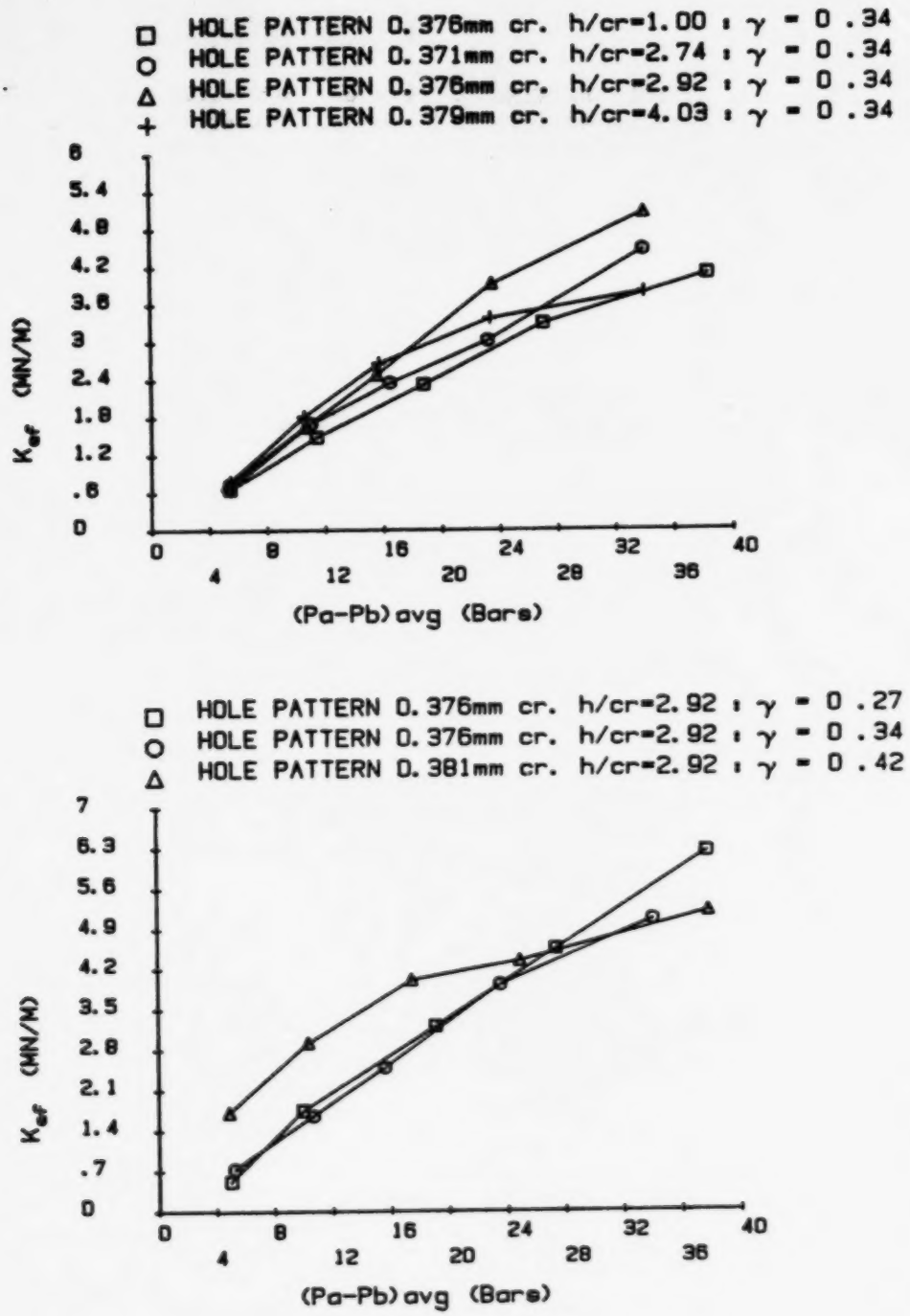

Figure 29. K_{ef} **for hole-pattern stators 1 through 6.**

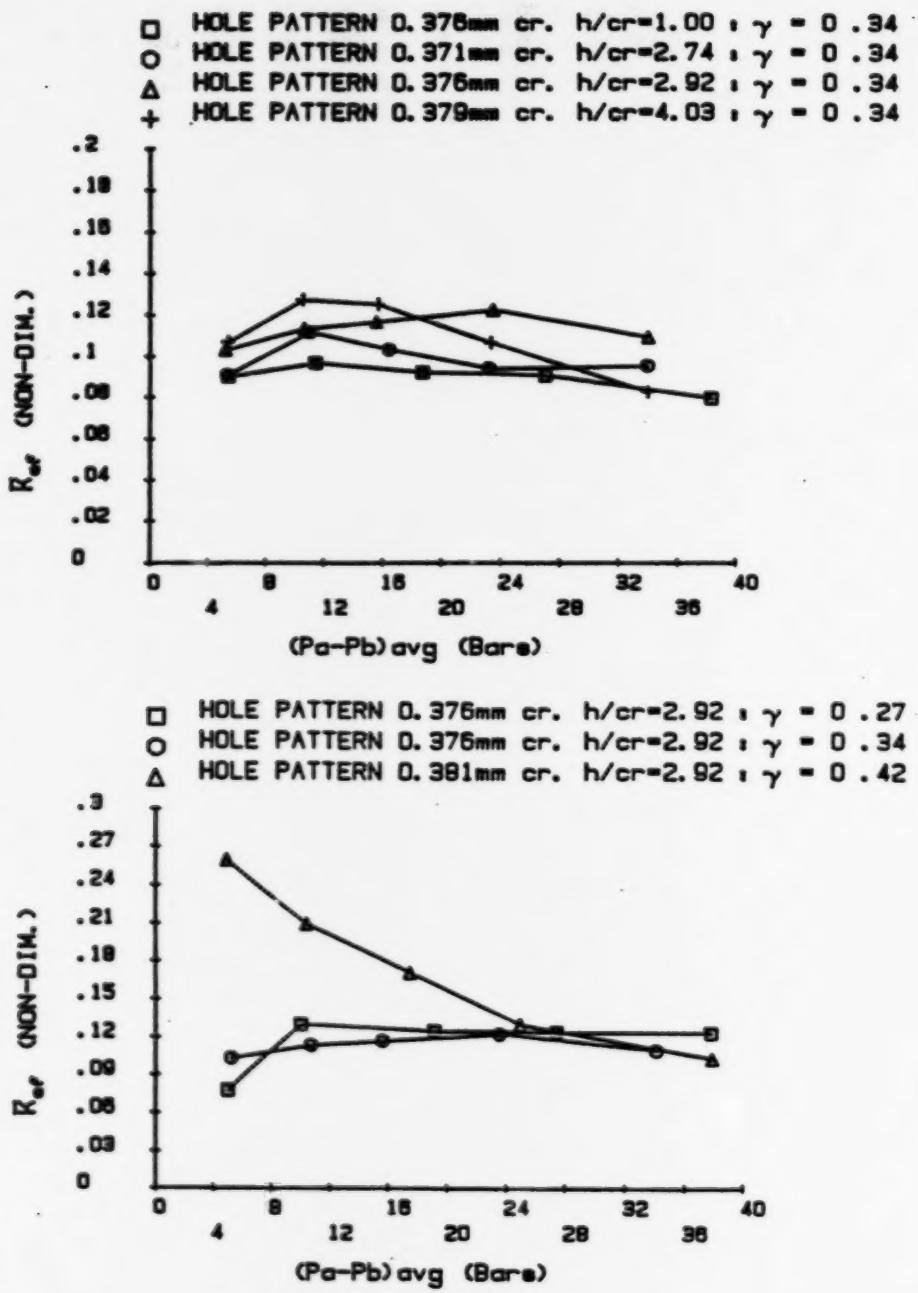

Figure 30. $\overline{K}_{ef}$ for hole-pattern stators 1 through 6.

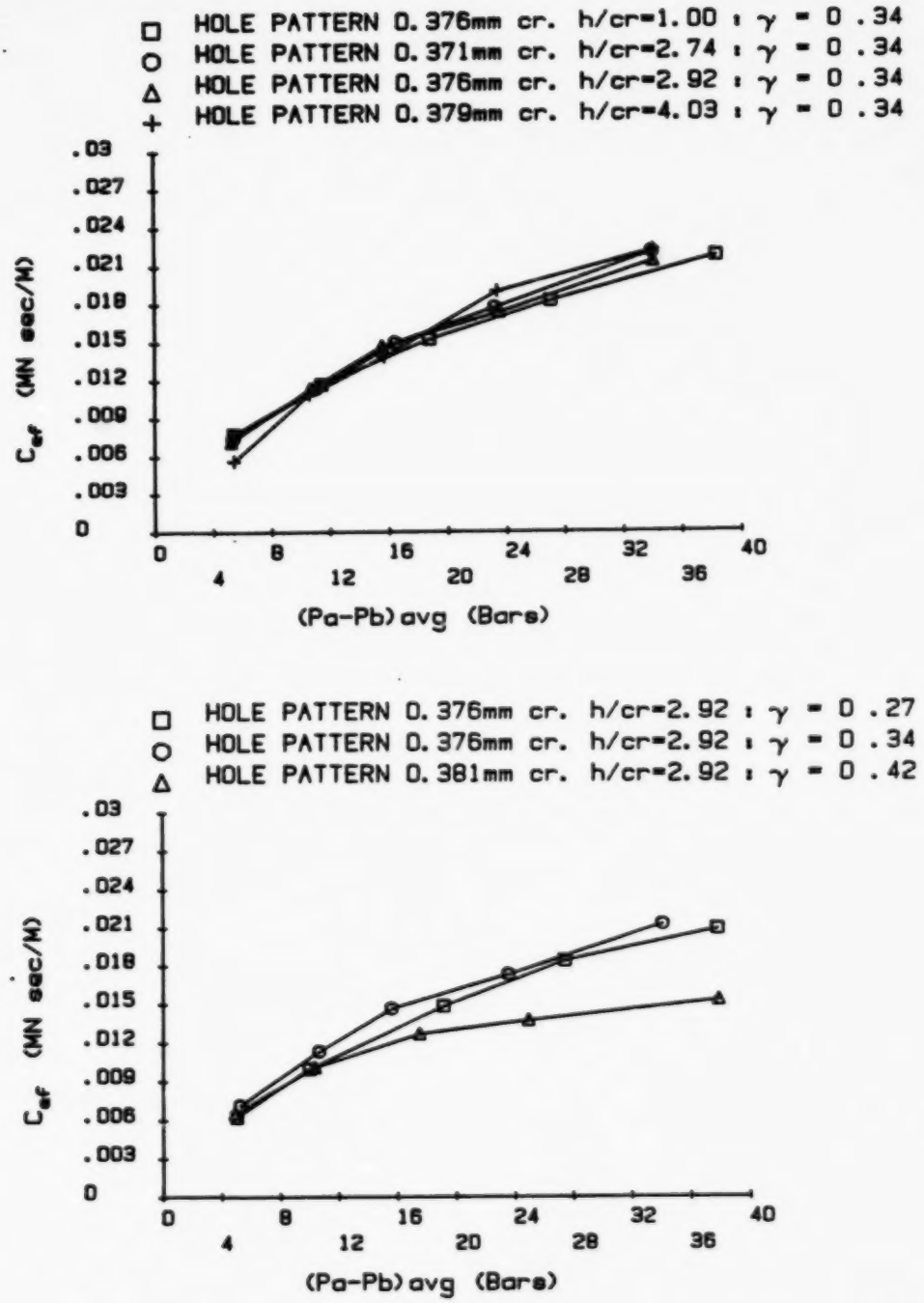

Figure 31. C_{ef} **for hole-pattern stators 1 through 6.**

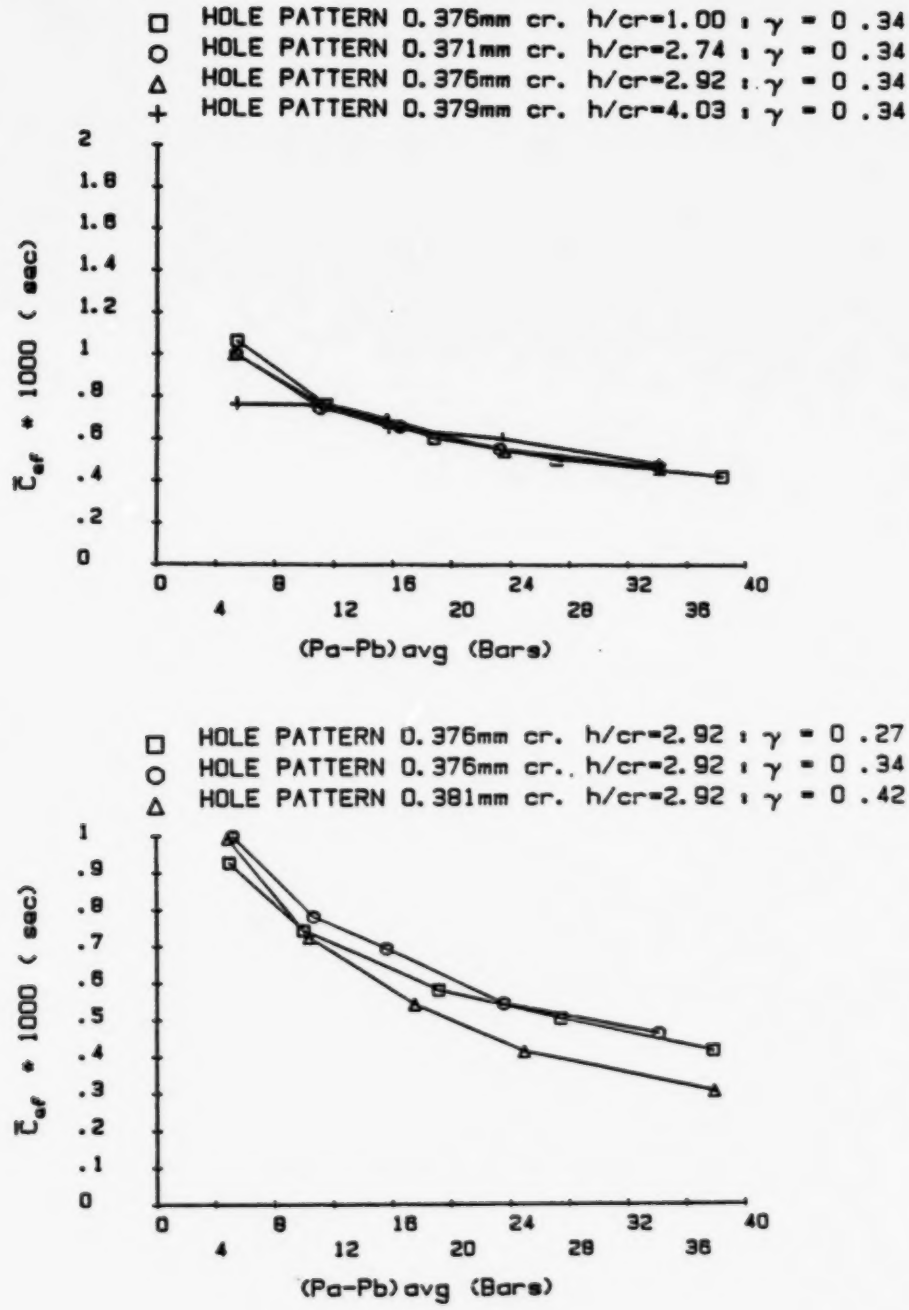

Figure 32. $\overline{C}_{ef}$ for hole-pattern stators 1 through 6.

S.I. Units	K_{ef} (EXP)	C_{ef} (EXP)	M_{ef} (EXP)	K_{ef} (EXP/TH)	C_{ef} (EXP/TH)	M_{ef} (EXP/TH)
HOLE PATTERN 0.376mm cr. h/cr=1.00 : γ =0.34						
R_e=90020	654200	7737	8.303	0.7999	0.8222	7.436
R_e=129800	1482000	11640	8.509	0.8166	0.9726	14.74
R_e=170000	2316000	15200	7.947	0.8636	1.059	5.022
R_e=204900	3282000	18190	7.526	0.8385	1.07	9.615
R_e=241400	4070000	21680	12.24	0.7382	1.125	5.454
HOLE PATTERN 0.371mm cr. h/cr=2.74 : γ =0.34						
R_e=89970	669600	7378	8.943	0.8491	0.6877	12.37
R_e=129900	1699000	11330	9.155	1.019	0.8919	6.529
R_e=160000	2343000	14910	10.40	1.057	1.015	4.804
R_e=190200	3010000	17670	12.17	0.9500	1.044	5.698
R_e=232100	4458000	21990	14.12	1.029	1.143	3.415
HOLE PATTERN 0.376mm cr. h/cr=2.92 : γ =0.34						
R_e=90180	735700	7135	8.505	1.255	0.6997	5.155
R_e=130100	1645000	11290	9.233	1.217	0.9009	7.738
R_e=160200	2475000	14640	9.167	1.441	0.9998	6.459
R_e=195100	3912000	17310	9.331	1.520	1.018	3.466
R_e=234600	5051000	21270	12.77	1.465	1.037	3.708
HOLE PATTERN 0.379mm cr. h/cr=4.03 : γ =0.34						
R_e=90000	783500	5596	8.361	0.8748	0.5509	6.477
R_e=130000	1811000	10840	6.836	1.161	0.8742	3.215
R_e=160000	2648000	13840	7.209	1.019	0.9545	24.45
R_e=195100	3360000	18930	11.26	1.009	1.108	4.140
R_e=238000	3782000	22120	14.10	8453	1.096	3.009
HOLE PATTERN 0.376mm cr. h/cr=2.92 : γ =0.27						
R_e=90040	520100	6217	11.28	0.6777	0.6680	6.635
R_e=129900	1738000	9934	8.718	1.044	0.8455	7.481
R_e=180000	3194000	14830	11.09	1.07	0.9568	6.211
R_e=220100	4539000	18400	11.68	1.081	1.016	5.051
R_e=258100	6214000	20880	8.742	1.105	1.022	2.298
HOLE PATTERN 0.381mm cr. h/cr=2.92 : γ =0.42						
R_e=90110	1712000	6551	2.448	2.606	0.3304	1.570
R_e=130100	2915000	10060	2.365	2.049	0.3750	1.903
R_e=170100	3996000	12670	4.833	1.972	0.3812	1.834
R_e=200100	4330000	13740	10.31	1.564	0.3507	2.660
R_e=244500	5192000	15320	9.461	1.448	0.3166	1.547

Table 5. Measured values for K_{ef}, C_{ef}, and M_{ef}; comparison of theory and experiments for hole-pattern stators.

CHAPTER V
TEST RESULTS FOR HELICALLY-GROOVED STATORS

5.1 Introduction

As noted in Chapter I, Kim and Childs developed a theory for helically grooved seals which predicted reductions in the cross-coupled stiffness coefficient for a properly-designed helically-grooved seal. In fact, his theory predicted a reversal in the sign of k. Test results are presented in this chapter for the helically-grooved stators illustrated in figure 33. The helix angle α is the principal parameter which is studied, ranging from 0 to 70 degrees. The groove depth and width is held constant. A 30° -helix stator was made with end lands. The same type of test results are presented here as in the preceding chapter for smooth and hole-pattern stators. However, no theoretical predictions of forces are presented because the test and theory are completely at odds with respect to C_{ef}.

5.2 Friction-Factor Data

Figures 34 through 37 illustrate σ_c for the helically-grooved-stator seals. For the 0° degree stator, σ_c increases with increasing running speed at lower values of R_a, but decreases with increasing ω at higher values of R_a. Figure 38 illustrates σ_c versus R_a at 7200 rpm for helix angel 0° through 70°. Observe that σ_c is maximum for the 0°-helix-angle stator at R_a greater than approximately 175,000. The 15°-helix-angle stator yields the highest value for σ_c for R_a less than 175,000. Generally speaking, σ_c decreases uniformly as the helix angle increases.

5.3 Leakage Data

Figure 39 illustrates $C_d^{-1/2}$ for the helically-grooved stators. As expected, leakage increases with increasing helix angles. Also, adding the end seals to the 30° helix stator is seen to reduce leakage. By comparison to figure 8 for smooth seals, helically-grooved stators leak more than smooth seals for α greater than 30°.

5.4 Dynamic Test Data

Figures 40 through 47 illustrate F_r/A and F_θ/A versus ω and R_a for the eight helically-grooved stators. The F_θ/A results of these figures is similar to test results in the previous chapter for smooth and hole-pattern-damper stators. However, much of the F_r data differ as follows. For the smooth and hole-pattern-damper stators, F_r/A decreases with increasing R_a at all speeds. For most of the grooved seals, F_r/A decreases with increasing R_a at lower speeds, but increases at high speeds.

Figure 48 illustrates $\overline{K}_{ef}$ versus ΔP for the helically-grooved seals. Generally speaking, $\overline{K}_{ef}$ first decreases and then increases as the helix angle increases. This result is predicted by the theory of [8]. Adding end lands to the 30° helix-angle stator is seen to increase $\overline{K}_{ef}$. A comparison of the helically-grooved-seal test results with the smooth-seal results of figure 12 and the hole-pattern-seal results of figure 30 shows helically-grooved seals to have substantially lower stiffness values for helix angles less than 40°.

STATOR 1
HELIX ANGLE - 0°
GROOVE DEPTH - 0.38mm
OF GROOVES - 9
GROOVE WIDTH - 2.38mm
LAND WIDTH - 2.38mm

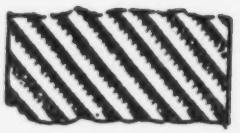

STATOR 5
HELIX ANGLE - 40°
GROOVE DEPTH - 0.38mm
OF GROOVES - 43
GROOVE WIDTH - 2.38mm
LAND WIDTH - 2.40mm

STATOR 2
HELIX ANGLE - 15°
GROOVE DEPTH - 0.38mm
OF GROOVES - 17
GROOVE WIDTH - 2.38mm
LAND WIDTH - 2.48mm

STATOR 6
HELIX ANGLE - 50°
GROOVE DEPTH - 0.38mm
OF GROOVES - 51
GROOVE WIDTH - 2.38mm
LAND WIDTH - 2.41mm

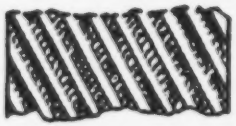

STATOR 3
HELIX ANGLE - 30°
GROOVE DEPTH - 0.38mm
OF GROOVES - 32
GROOVE WIDTH - 2.38mm
LAND WIDTH - 2.60mm

STATOR 7
HELIX ANGLE - 60°
GROOVE DEPTH - 0.38mm
OF GROOVES - 57
GROOVE WIDTH - 2.38mm
LAND WIDTH - 2.47mm

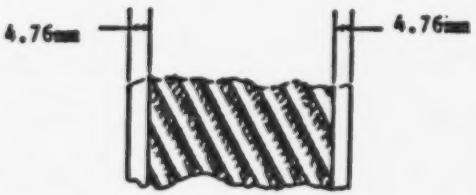

STATOR 4
HELIX ANGLE - 30°
GROOVE DEPTH - 0.38mm
OF GROOVES - 32
GROOVE WIDTH - 2.38mm
LAND WIDTH - 2.60mm

STATOR 8
HELIX ANGLE - 70°
GROOVE DEPTH - 0.38mm
OF GROOVES - 62
GROOVE WIDTH - 2.38mm
LAND WIDTH - 2.46mm

Figure 33. Helically-grooved stator, detail A.

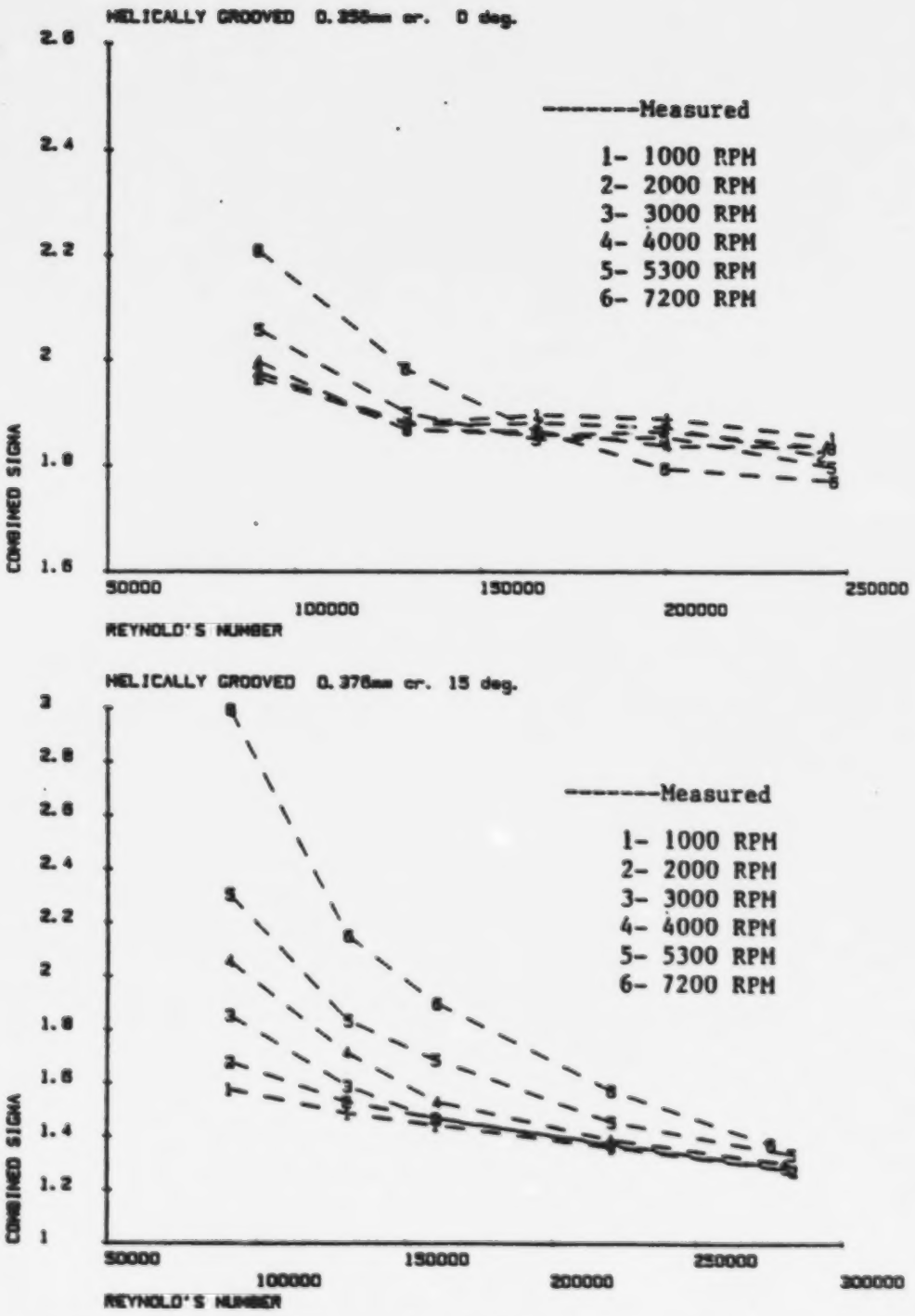

Figure 34. Combined-sigma, σ_c, data for helically-grooved-stators 1 and 2 versus R_a and ω.

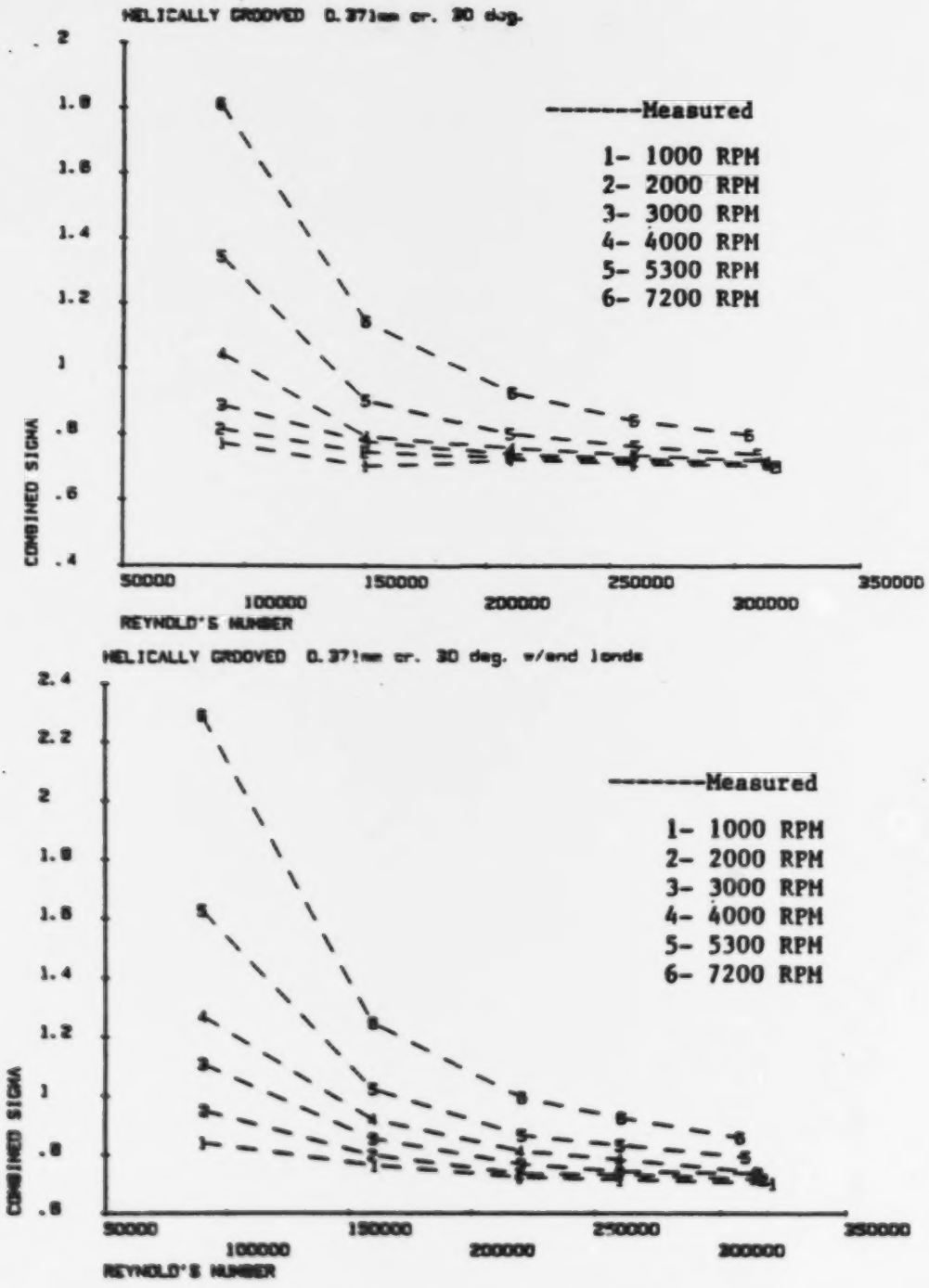

Figure 35. Combined-sigma, σ_c, data for helically-grooved-stators 3 and 4 versus R_a and ω.

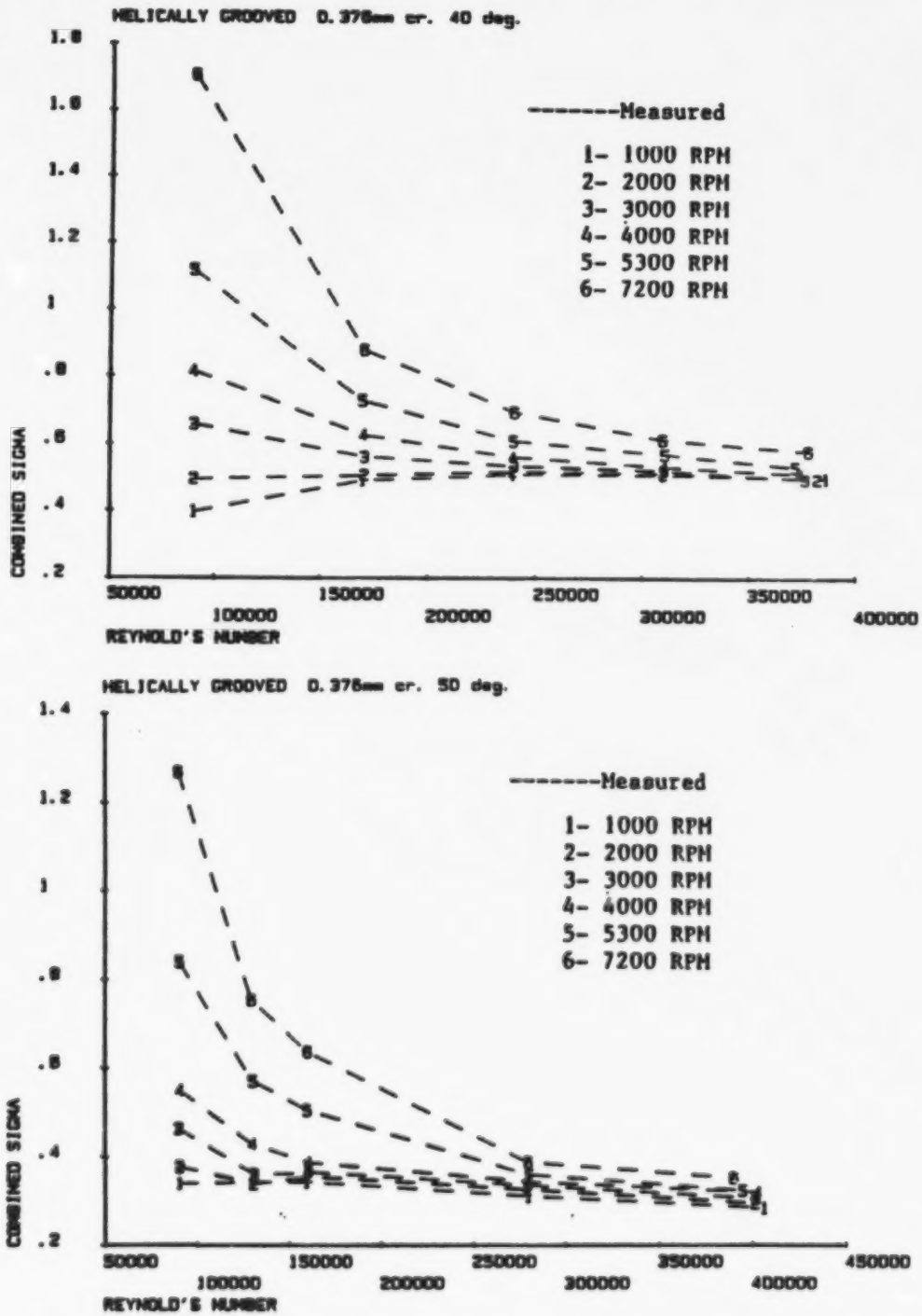

Figure 36. Combined-sigma, σ_c, data for helically-grooved-stators 5 and 6 versus R_a and ω.

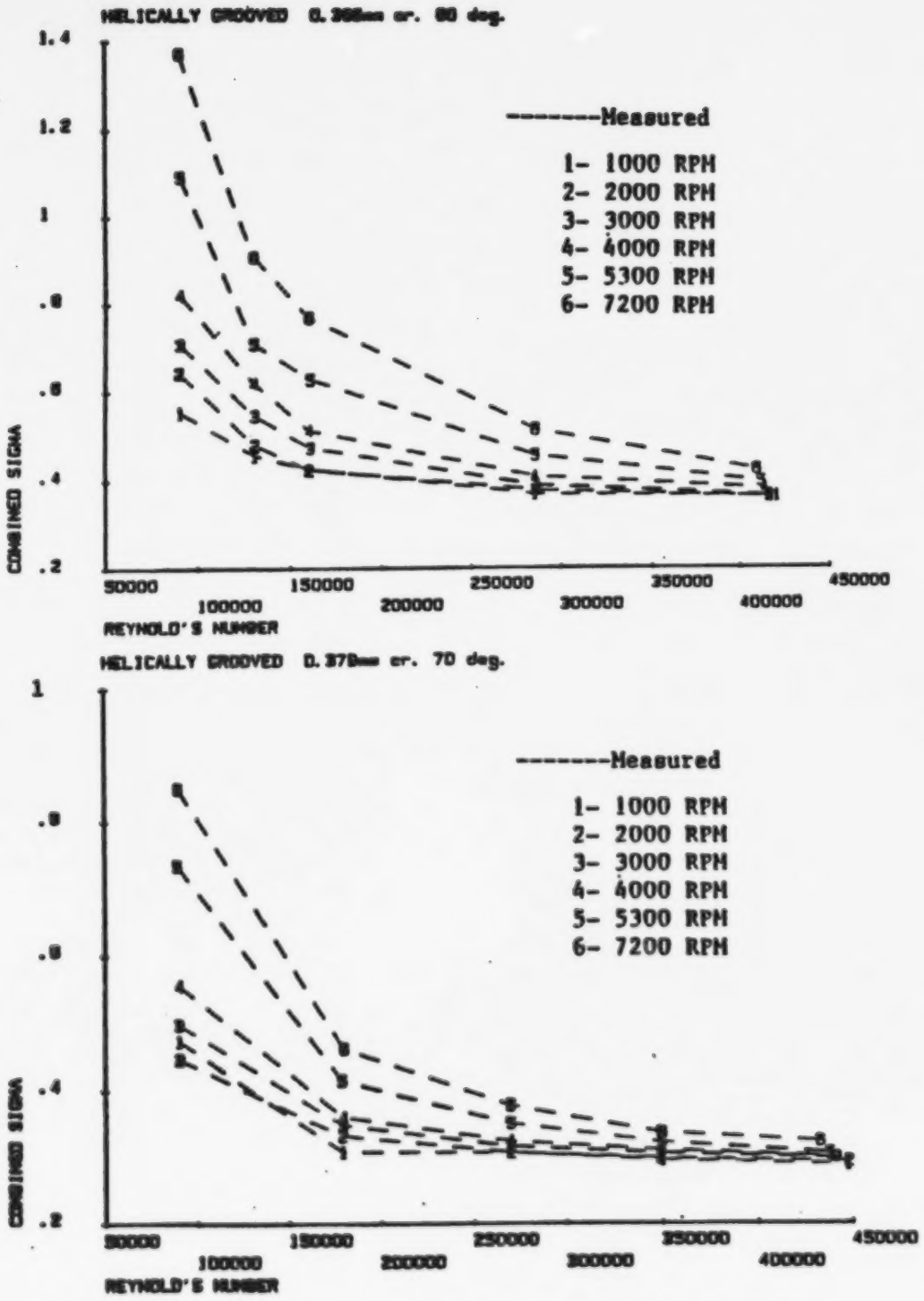

Figure 37. Combined-sigma, σ_c, data for helically-grooved-stators 7 and 8 versus R_a and ω.

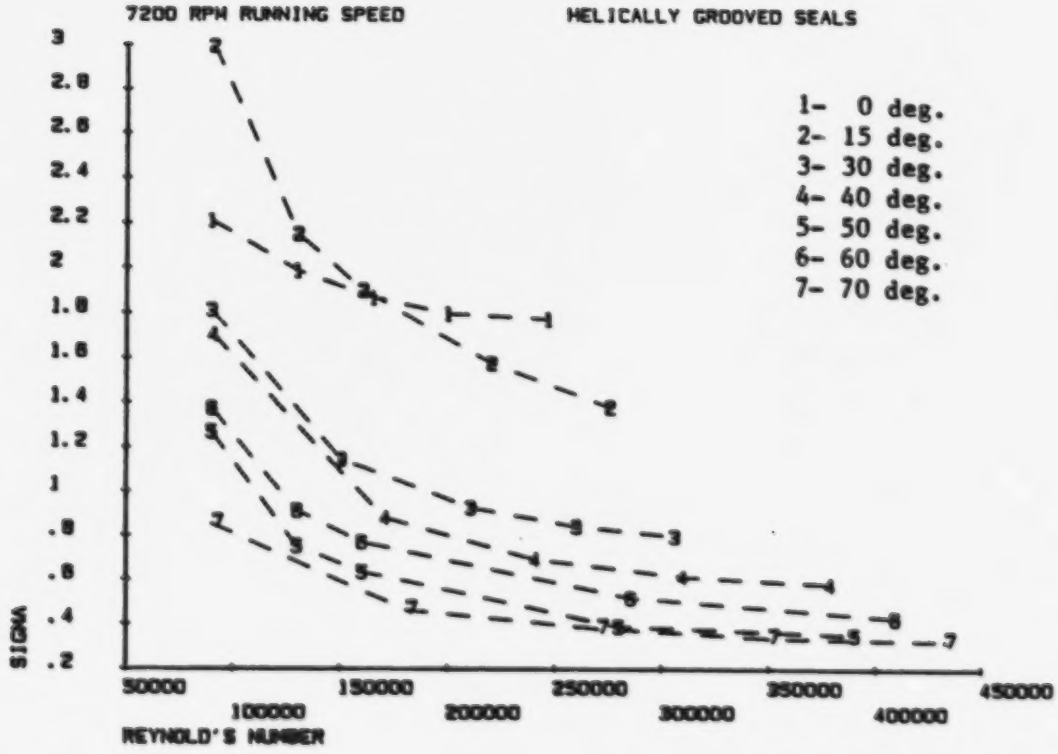

Figure 38. Combined-sigma data, σ_e, for helix-angles 0° through 70° at 7200 rpm, versus R_a.

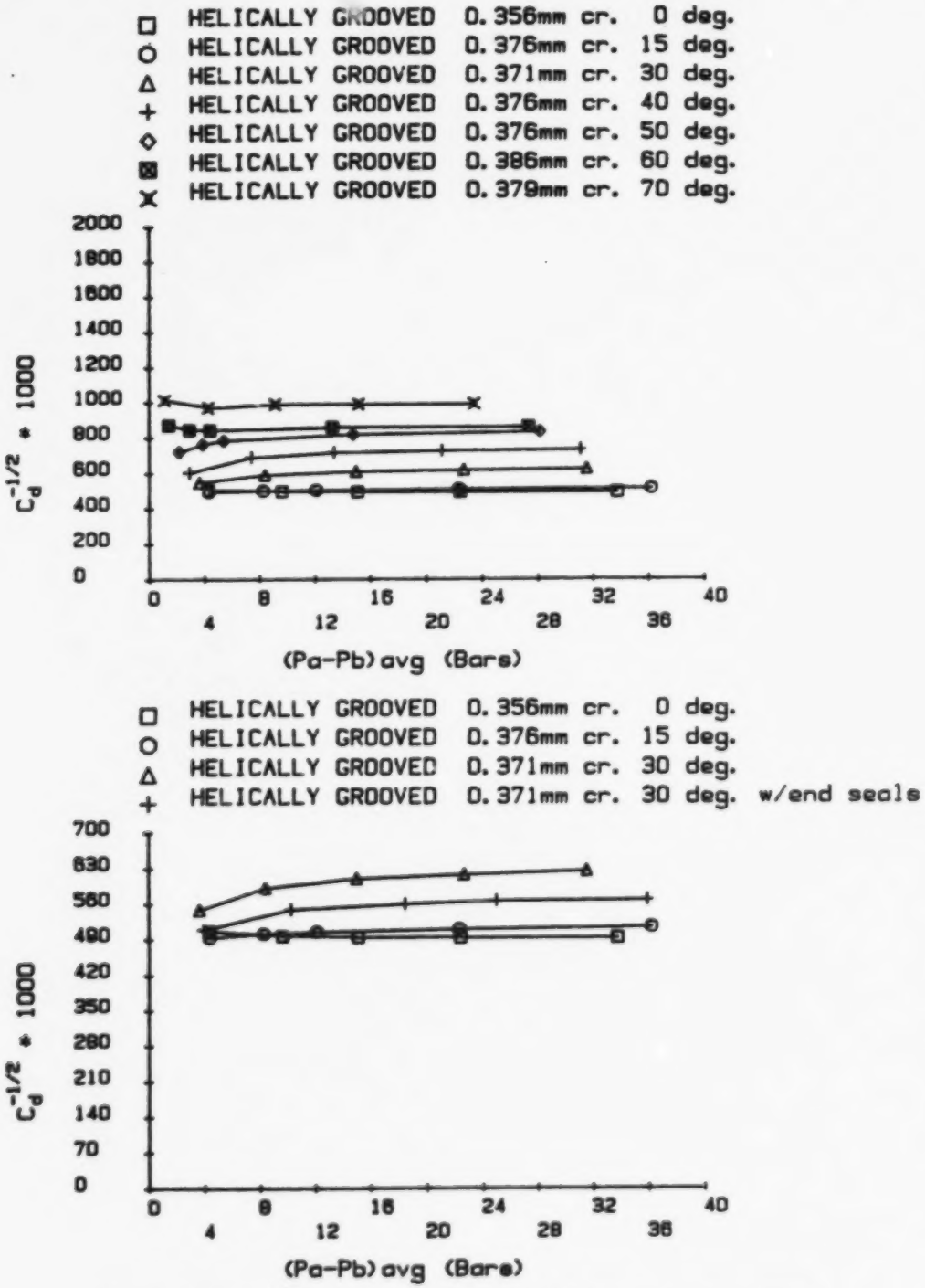

Figure 39. $C_d^{-1/2}$ versus ΔP for helically-grooved-stator seals.

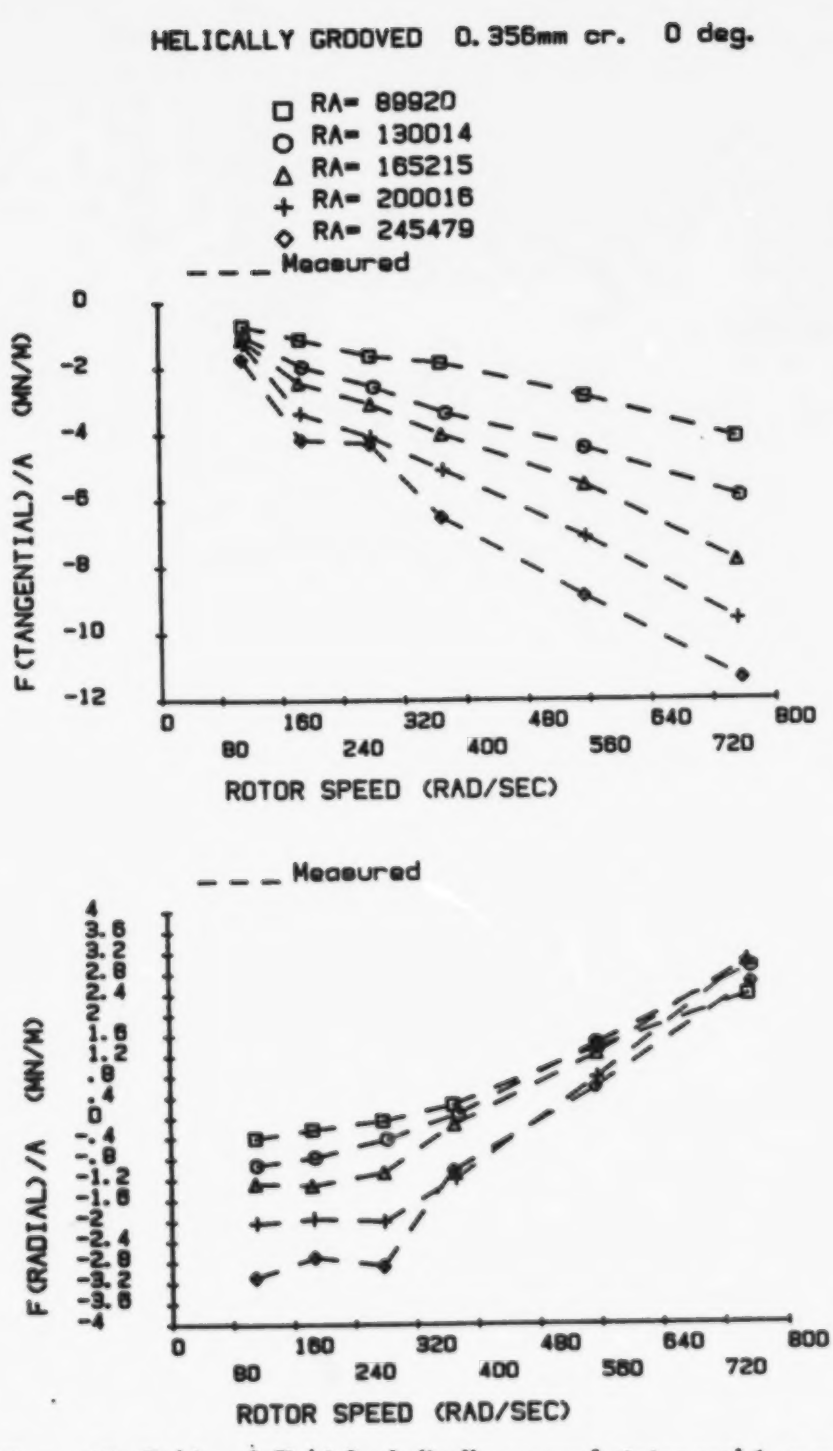

Figure 40. F_r/A and F_θ/A for helically-grooved-stator seal 1, $\alpha = 0°$.

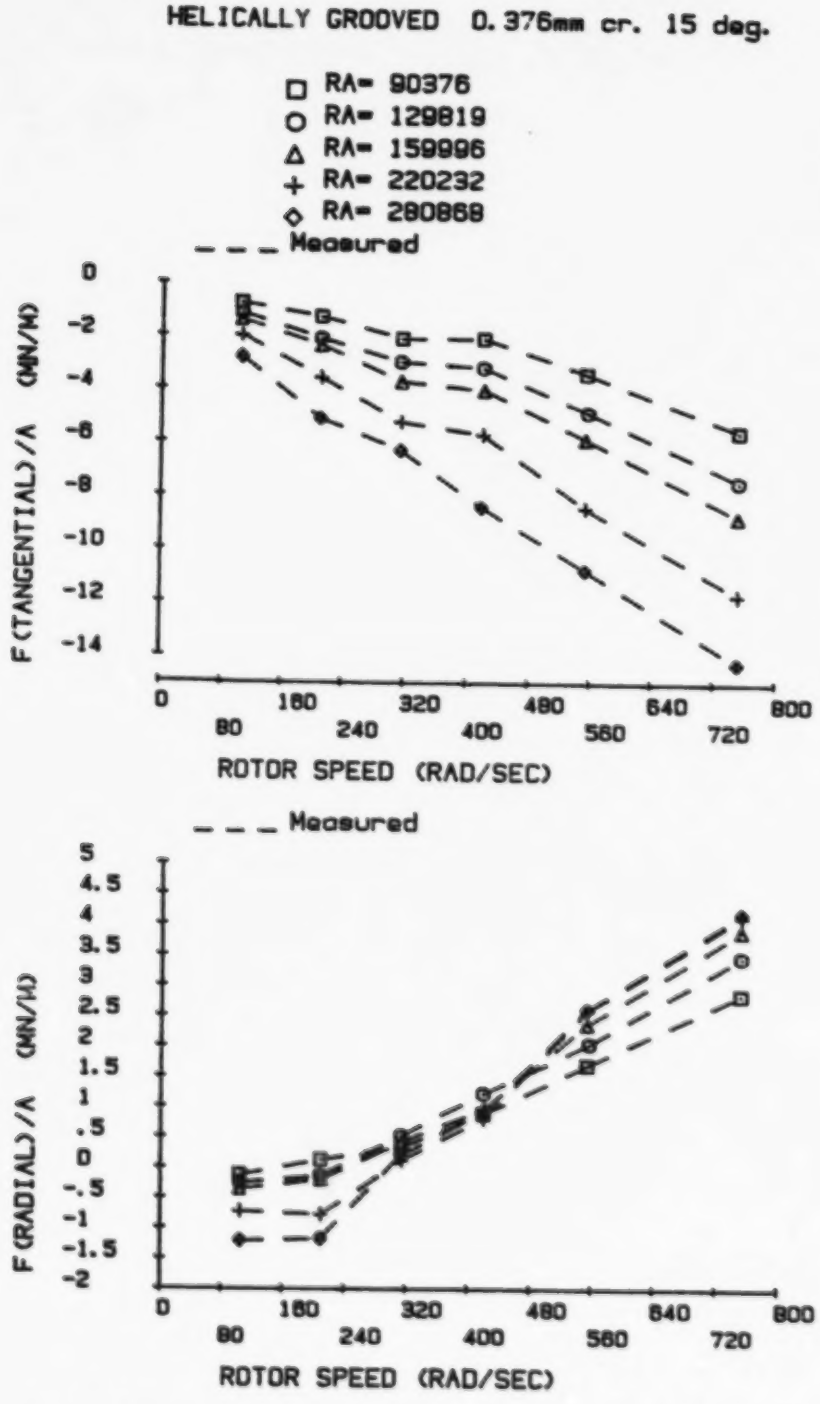

Figure 41. F_r/A and F_θ/A for helically-grooved-stator seal 2, $\alpha = 15°$.

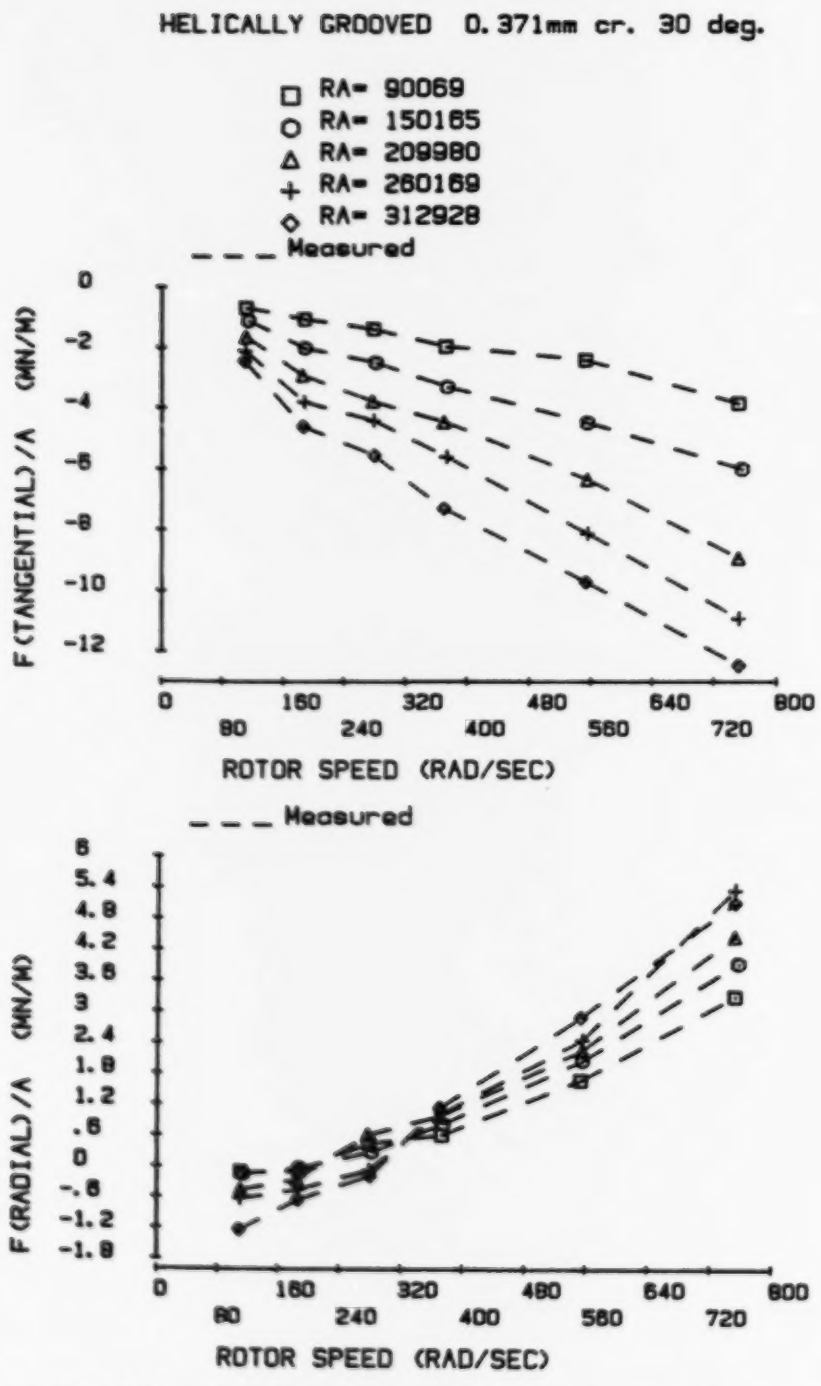

Figure 42. F_r/A and F_θ/A for helically-grooved-stator seal 3, $\alpha = 30°$.

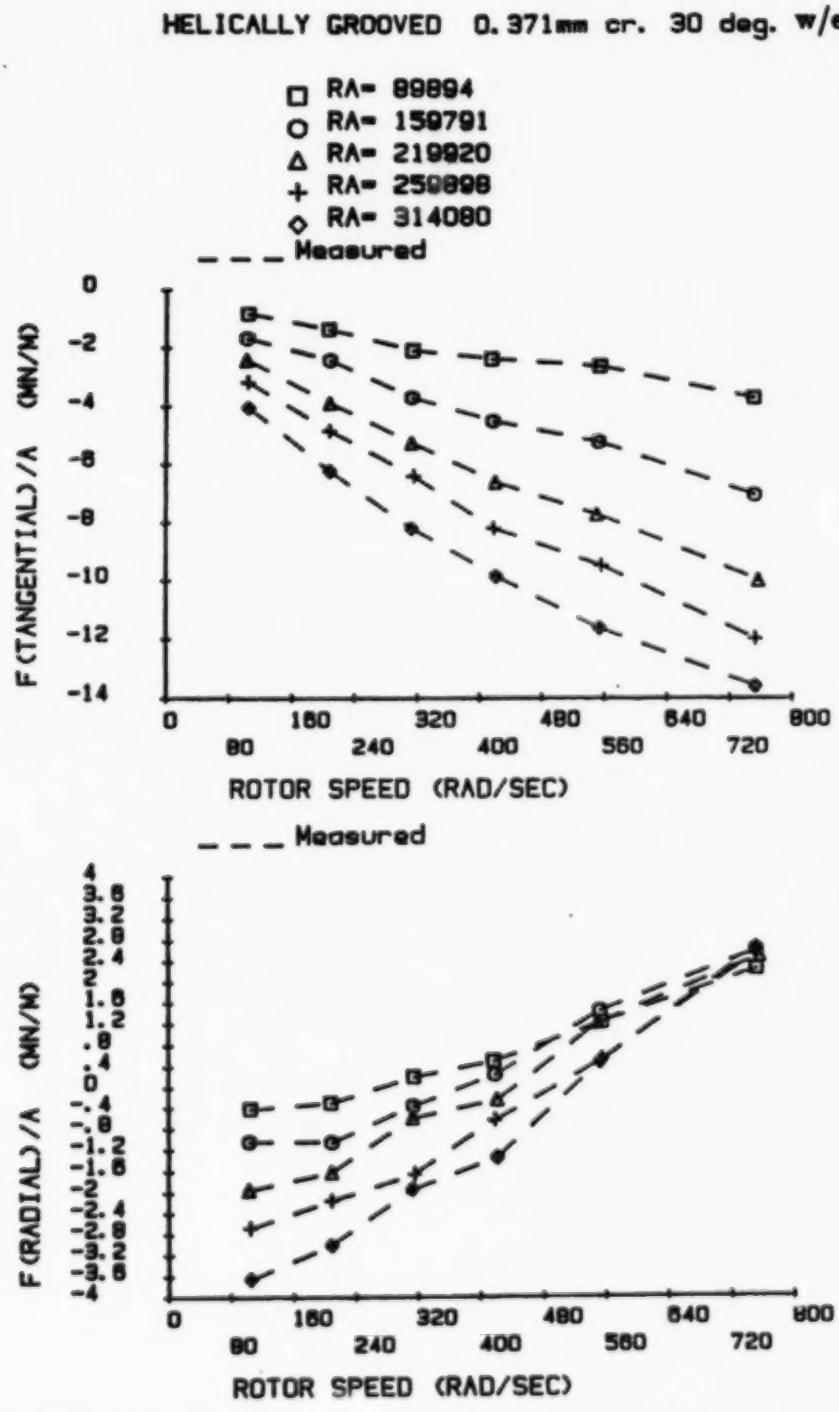

Figure 43. F_r/A and F_θ/A for helically-grooved-stator seal 4, $\alpha = 30°$ with end lands.

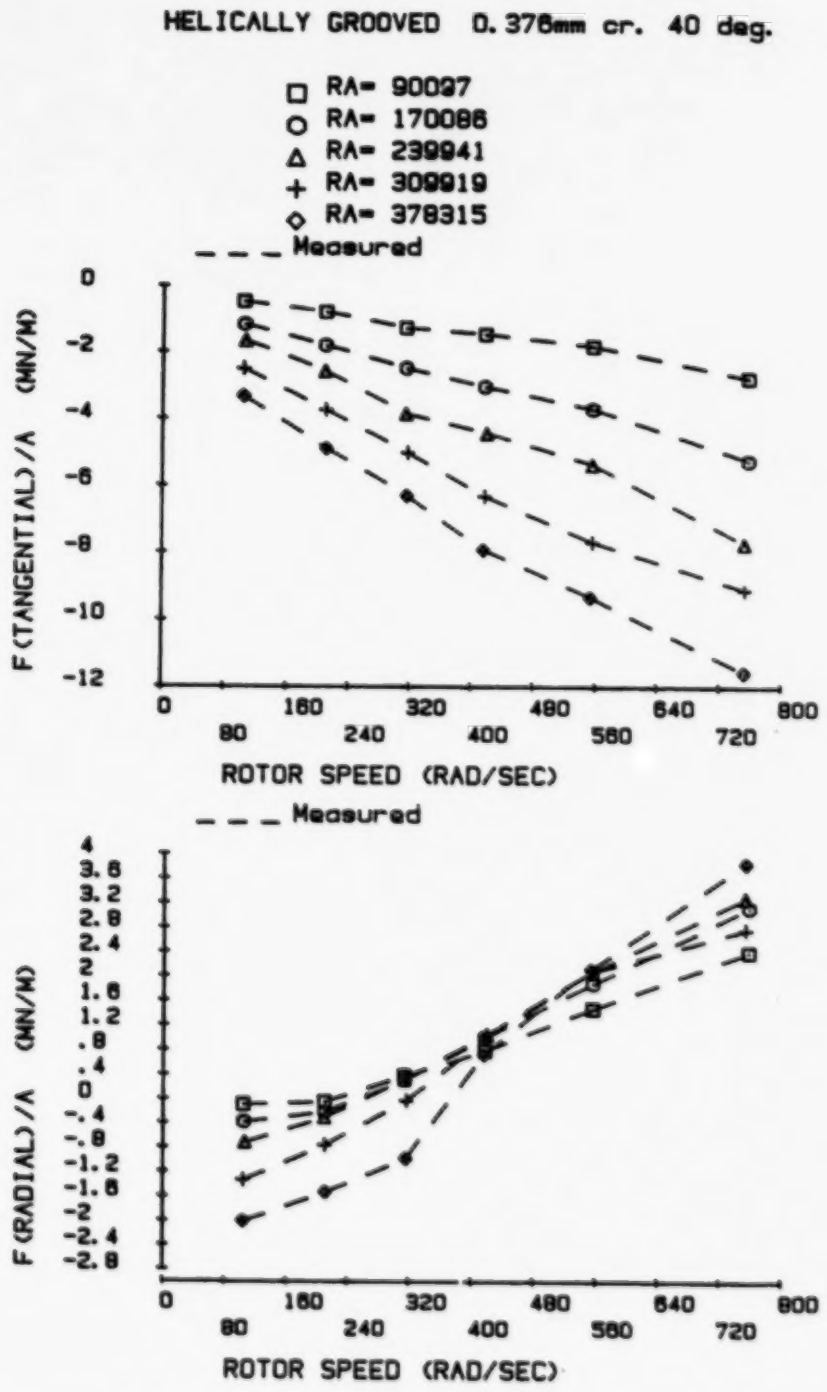

Figure 44. F_r/A and F_θ/A for helically-grooved-stator seal 5, $\alpha = 40°$.

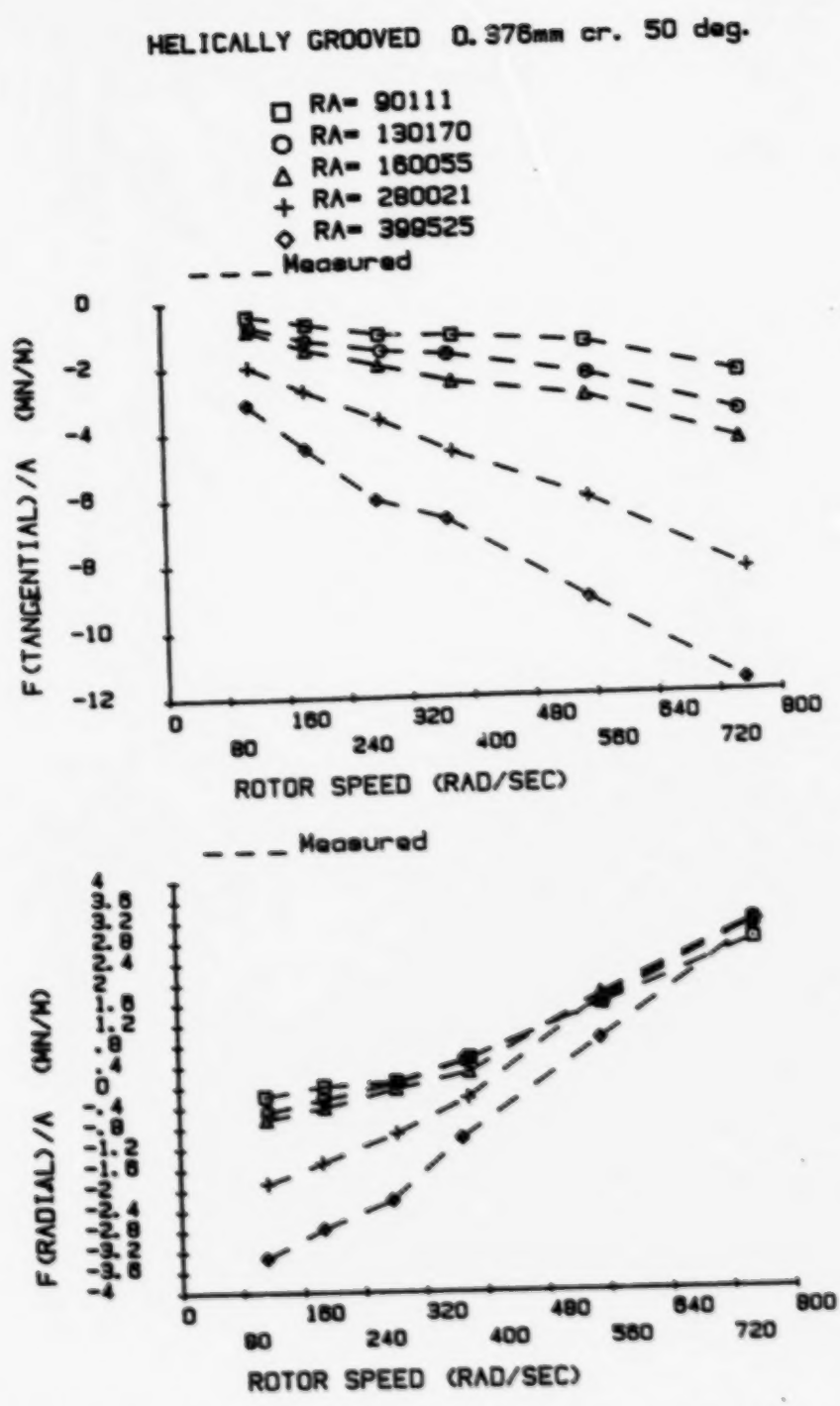

Figure 45. F_r/A and F_θ/A for helically-grooved-stator seal 6, $\alpha = 50°$.

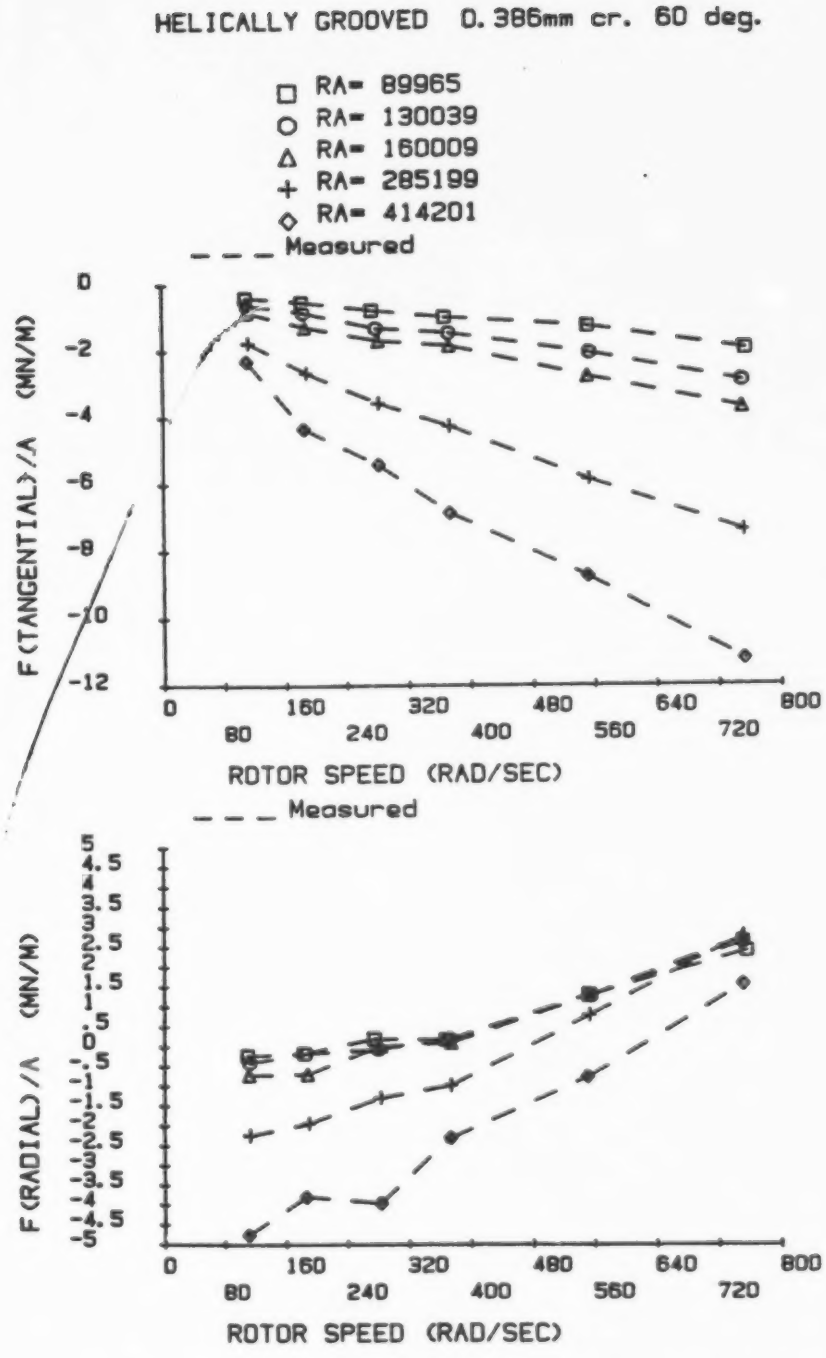

Figure 46. F_r/A and F_θ/A for helically-grooved-stator seal 7, $\alpha = 60°$.

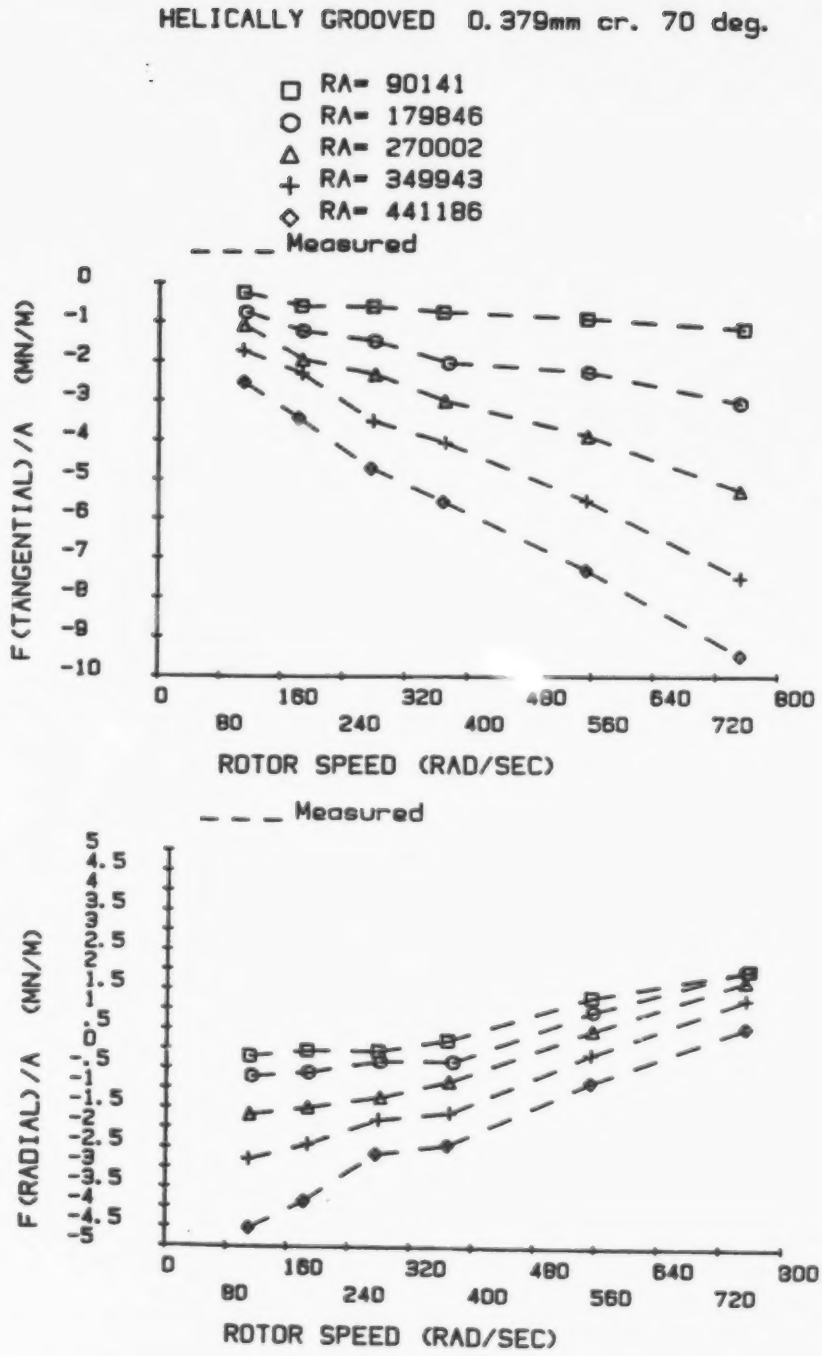

Figure 47. F_r/A and F_θ/A for helically-grooved-stator seal 8, $\alpha = 70°$.

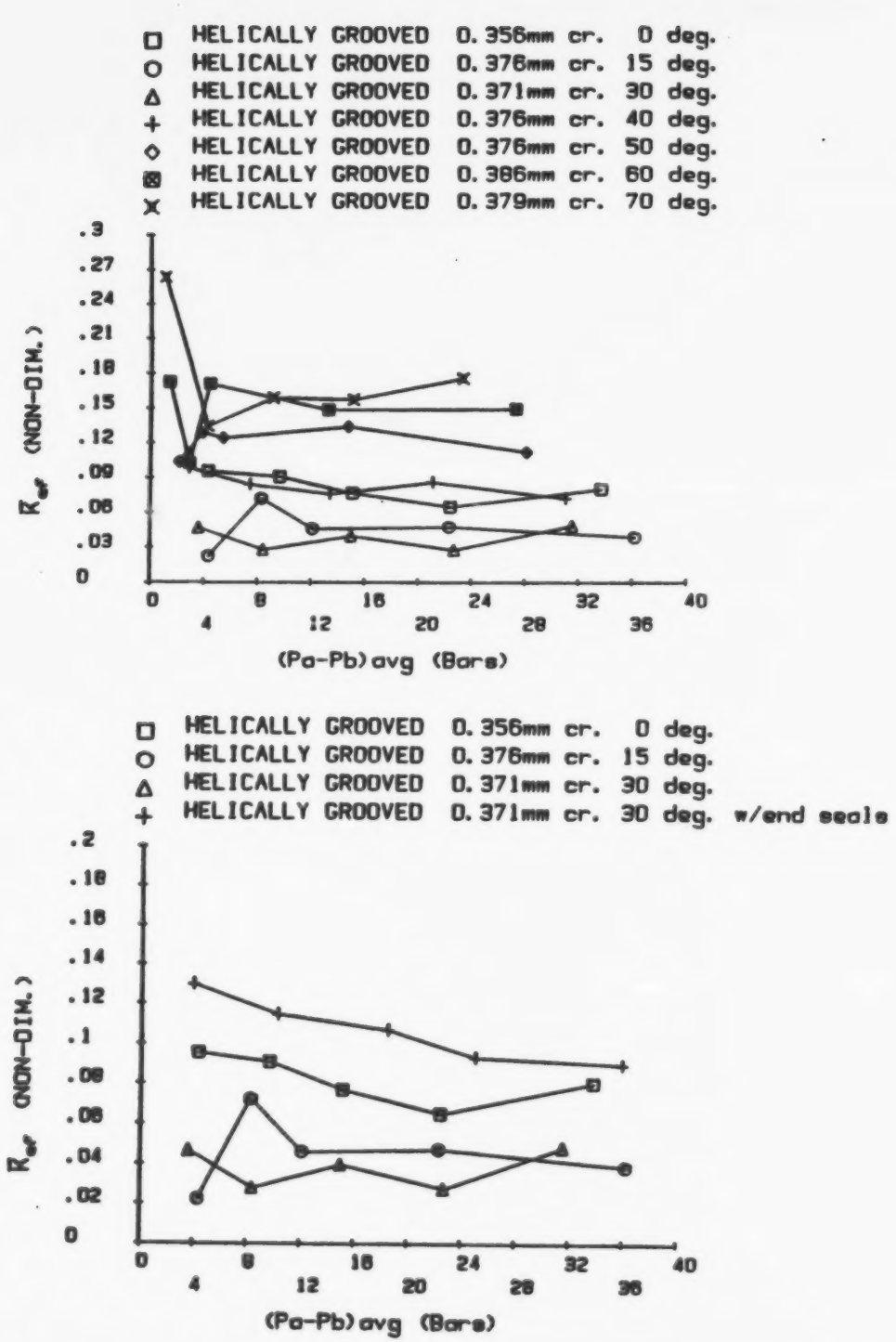

Figure 48. $\overline{K}_{ef}$ **versus** ΔP **for the helically-grooved stator seals.**

Figure 49 illustrates $\overline{C}_{ef}$ versus ΔP for the helically-grooved-stator seals. Those results indicate the $\overline{C}_{ef}$ is generally insensitive to changes in the helix angle. The 30° helix-angle stator yields slightly higher damping values than the remaining stators. Adding end lands to the 30° helix-angle stator does not change $\overline{C}_{ef}$. A comparison of the results for figures 14, 32,and 50 indicates that the net damping for helically-grooved stators is less than that for either smooth or hole-pattern-damper stators. This result conflicts with the theoretical predictions of reference [8], which predicted a change in sign for k as the helix angle α is increased, with a small change in C. From Eqs. (3) and (25)

$$F_\theta/A = k - C\omega$$

$$F_\theta/A = -C_{ef}\omega = -C(1 - b_1/2)\omega\,.$$

The theory of [8] predicts a reversal in sign for b_1, and a corresponding increase in C_{ef} for increasing helix angles. The test results generally refute this prediction.

Table 6 contains calculated values for K_{ef}, C_{ef}, and M_{ef} for the helically-grooved-stator seals which were tested in this study.

5.5 Conclusions

The test results of this chapter support the following conclusions with respect to helically-grooved stators:

(a) Helically-grooved seals leak more as the helix angle increases. Of the seals tested, those with helix angles greater than 30° leaked more than smooth seals.

(b) The stiffness of helically-grooved seals first decreases and then increases as the helix angle increases. For helix angles less than 40°, helically-grooved seals have substantially lower direct stiffnesses than either smooth or hole-pattern-stator seals.

(c) $\overline{C}_{ef}$ for the seals tested is insensitive to helix angle. The 30° -helix stator had slightly better damping characteristics than the other seals.

(d) Adding end lands to the 30° -helix stator decreased leakage, increased $\overline{K}_{ef}$, and had little or no effect on $\overline{C}_{ef}$.

(e) The theory of [8] correctly predicted trends in leakage and $\overline{K}_{ef}$; however, its predictions are wrong for $\overline{C}_{ef}$

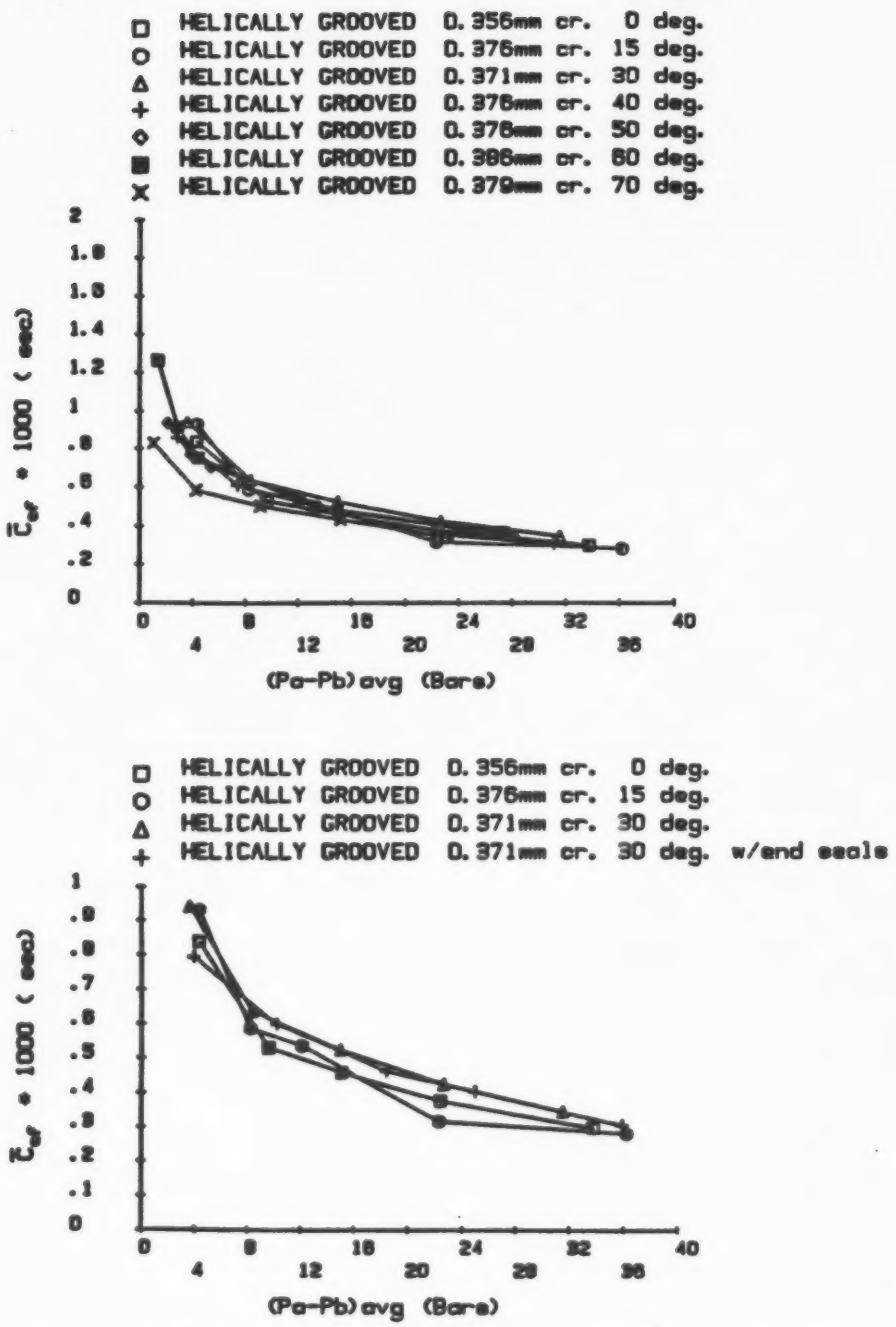
HELICALLY GROOVED D. 356mm cr. 0 deg.
HELICALLY GROOVED D. 376mm cr. 15 deg.
HELICALLY GROOVED D. 371mm cr. 30 deg.
HELICALLY GROOVED D. 376mm cr. 40 deg.
HELICALLY GROOVED D. 376mm cr. 50 deg.
HELICALLY GROOVED D. 386mm cr. 60 deg.
HELICALLY GROOVED D. 379mm cr. 70 deg.
$\bar{C}_{ef}$ * 1000 (sec)
(Pa-Pb) avg (Bars)
HELICALLY GROOVED D. 356mm cr. 0 deg.
HELICALLY GROOVED D. 376mm cr. 15 deg.
HELICALLY GROOVED D. 371mm cr. 30 deg.
HELICALLY GROOVED D. 371mm cr. 30 deg. w/end seals
$\bar{C}_{ef}$ * 1000 (sec)
(Pa-Pb) avg (Bars)

Figure 49. $\bar{C}_{ef}$ versus ΔP for the helically-grooved stator seals.

S.I. UNITS	$K_{ef}(EXP)$	$C_{ef}(EXP)$	$M_{ef}(EXP)$
HELICALLY GROOVED 0.356mm cr. 0 deg.			
R_e=89920	591100	5184	3.862
R_e=130000	1255000	7294	4.914
R_e=165200	1659000	9895	6.723
R_e=200000	2081000	12090	11.64
R_e=245500	3877000	14370	5.016
HELICALLY GROOVED 0.376mm cr. 15 deg.			
R_e=90380	130300	5493	6.835
R_e=129800	807800	6560	1.244
R_e=160000	755500	8775	4.271
R_e=220200	1432000	9580	4.350
R_e=280900	1891000	13740	3.407
HELICALLY GROOVED 0.371mm cr. 30 deg.			
R_e=90070	232400	4698	5.948
R_e=150100	321400	7350	6.993
R_e=201000	814800	10770	5.583
R_e=260200	857400	13240	10.21
R_e=312900	2099000	14990	3.580
HELICALLY GROOVED 0.376mm cr. 30 deg. w/end lands			
R_e=89890	686500	4200	2.908
R_e=159800	1580000	8237	3.702
R_e=219900	2657000	11460	1.768
R_e=314100	3133000	13550	5.395
R_e=367200	4320000	14730	4.933
HELICALLY GROOVED 0.376mm cr. 40 deg.			
R_e=90100	382800	3341	2.787
R_e=170100	840800	6078	3.080
R_e=239900	1372000	9045	1.443
R_e=276200	2437000	10380	-2.928
R_e=378300	3012000	12710	2.917
HELICALLY GROOVED 0.371mm cr. 50 deg.			
R_e=90110	302300	2731	5.082
R_e=130200	678000	4055	5.302
R_e=160100	912200	5156	5.234
R_e=280000	2689000	9695	2.385
R_e=399500	4272000	12930	3.045
HELICALLY GROOVED 0.386mm cr. 60 deg.			
R_e=89970	320200	2343	4.672
R_e=130000	394500	3518	5.997
R_e=160000	998900	4386	4.587
R_e=285200	2608000	8703	6.352
R_e=414200	5396000	13210	4.660
HELICALLY GROOVED 0.379mm cr. 70 deg.			
R_e=90140	389500	1222	2.983
R_e=179800	772900	3345	5.107
R_e=270000	1958000	6166	4.454
R_e=349900	3221000	8819	2.921
R_e=441200	5551000	10560	-2.600

Table 6. Measured values for K_{ef}, C_{ef}, and M_{ef} for helically-grooved-stator seals.

CHAPTER VI
TEST RESULTS FOR A 30°-HELICALLY-GROOVED STATOR IN AN AIR-SEAL TEST FACILITY

6.1 Introduction

As noted earlier, the liquid-seal test apparatus used in this study is limited in the following respects:

(a) There is no capability for prerotating the flow entering the seal.
(b) While a net damping coefficient can be measured, the direct-damping and cross-coupled-stiffness coefficients k and C can not be separately identified.

Fortunately, a dynamic, seal-test apparatus and facility have been developed and is available at TAMU which eliminates those shortcomings [12]. Unfortunately, this facility only uses air as a test media. The contents of this chapter concern test results for a 30°-helix, 151.9*mm* diameter seal tested in air. Dimension's for the stator of this seal are provided in figure 50. A nominally smooth rotor was used with this stator.

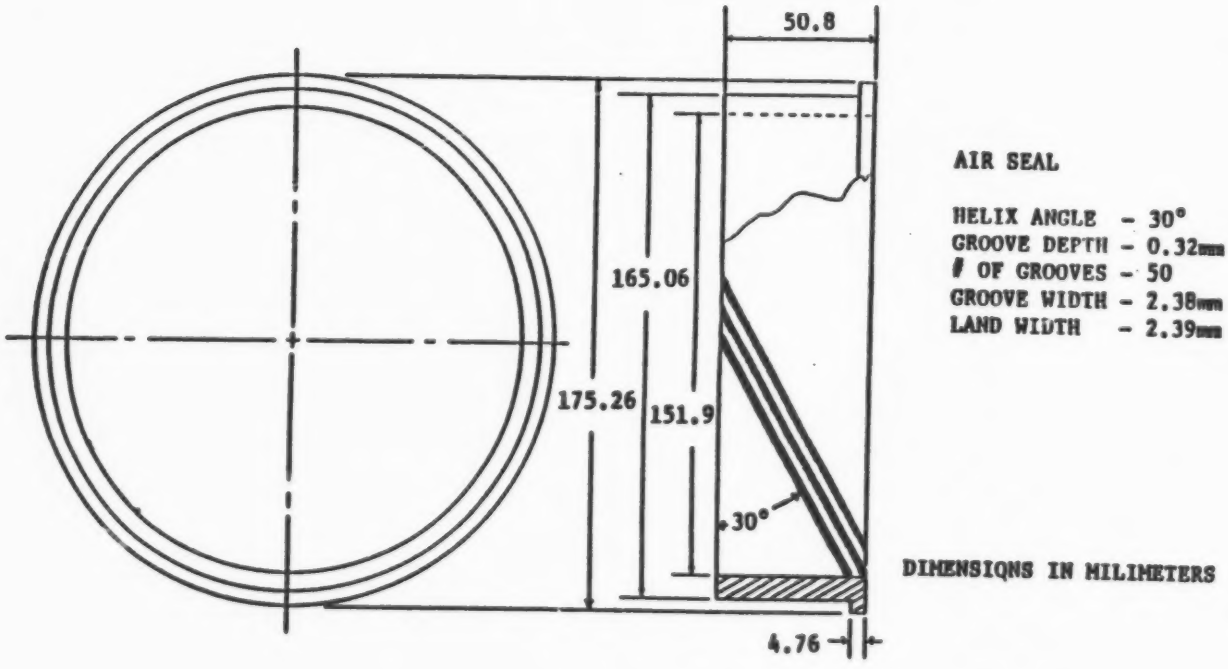

Figure 50. Helically Grooved Air Seal

6.2 Test Facility

Figures 51 through 53 illustrate the air-seal test apparatus and facility. Observe that the flow can be preswirled immediately before entering the seal. Two preswirl vanes are used to rotate the fluid in the direction of shaft rotation, two are used for prerotation against shaft rotation, and one inlet provides no intentional prerotation.

The housing supporting the shaft is vibrated horizontally while the shaft is rotating. Simultaneous measurements of the seal's rotor motion relative to the stator and seal reaction forces yield data from which the direct and cross-coupled stiffness and damping coefficients can be determined.

The test facility is supplied by a screw compressor which can provide air at pressures up to approximately 7 bars. Since the seal configuration of figure 54 is intended only for liquid applications, only test data at comparatively low pressures and unchoked conditions are examined.

Test results for the helically-grooved stator will be compared to results for a smooth stator and a honeycomb stator. The honeycomb stator has a cell width of $0.79mm$ (.031 in) and a cell depth of $1.47mm$ (.058 in).

6.3 Test Results

Figure 54(a) illustrates the direct and cross-coupled stiffness coefficients K_{zz}, K_{zy} versus $u_{\theta o} = U_{\theta o}/R\omega$, the normalized inlet tangential velocity. The results are presented at 3000 CPM and 3.08 bars supply pressure for smooth, honeycomb, and helically-grooved stators. Figure 54 (b) illustrates C_{zz} and $K_{zy}/\omega C_{zz}$ versus $u_{\theta o}$ for the same operating conditions. The data in those figures which is of practical interest concerns positive $u_{\theta o}$. A review of these figures supports the following conclusions:

(a) K_{zz} is positive for the helically-grooved stator but is much smaller than comparable values for a smooth stator.

(b) K_{zy} is smaller for the helically-grooved stator than either the smooth or honeycomb stator.

(c) C_{zz} is smaller for the helically-grooved stator than for either the smooth stator or honeycomb stator.

(d) The whirl-frequency ratio $K_{zy}/\omega C_{zz}$ is comparable for honeycomb and helically-grooved stators.

Note in comparing these figures that the tangential velocity is highest for the smooth seal, intermediate for the helically-grooved stator, and a minimum for the honeycomb stator. This results is a consequence of the leakage performance of the seals with leakage-rate increasing as one moves from the honeycomb, to helix, to smooth stators. For a given preswirl vane, the inlet tangential velocity goes up with the leakage rate.

Figures 55(a) and (b) provide parallel results for the three stators with running speed increased to 16,000 CPM. Observe that K_{zy} for the helically-grooved stator is now less than the comparable results for the honeycomb stator. Also, while C_{zz} continues to be less for the helix stator than the honeycomb stator, the margin has been reduced. The whirl frequency ratio's for the honeycomb and helix stators are about equal for positive $u_{\theta o}$.

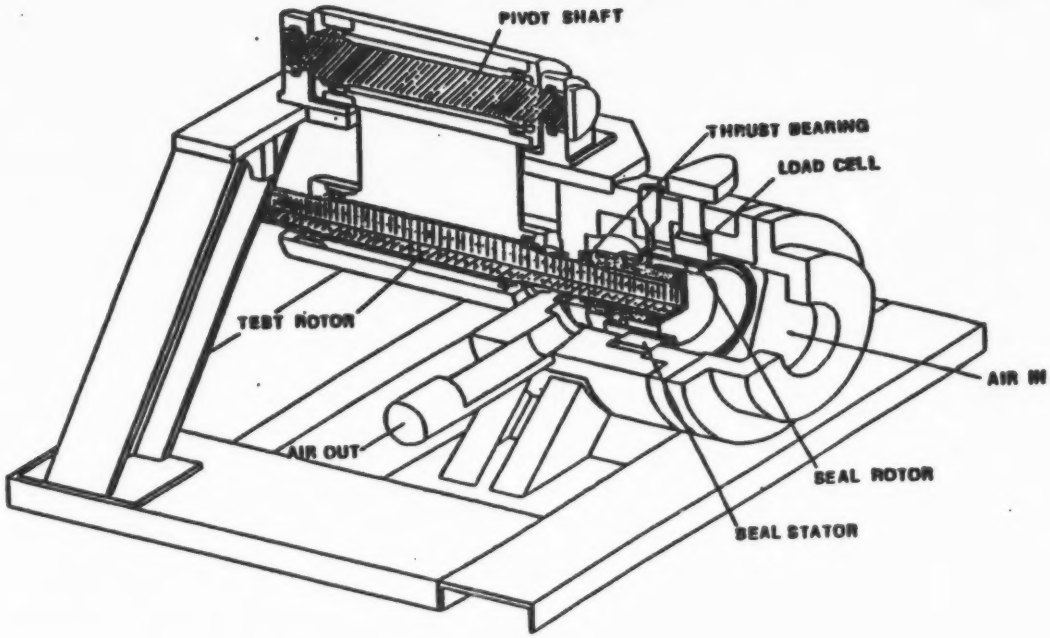

Figure 51. Test-apparatus, isometric view.

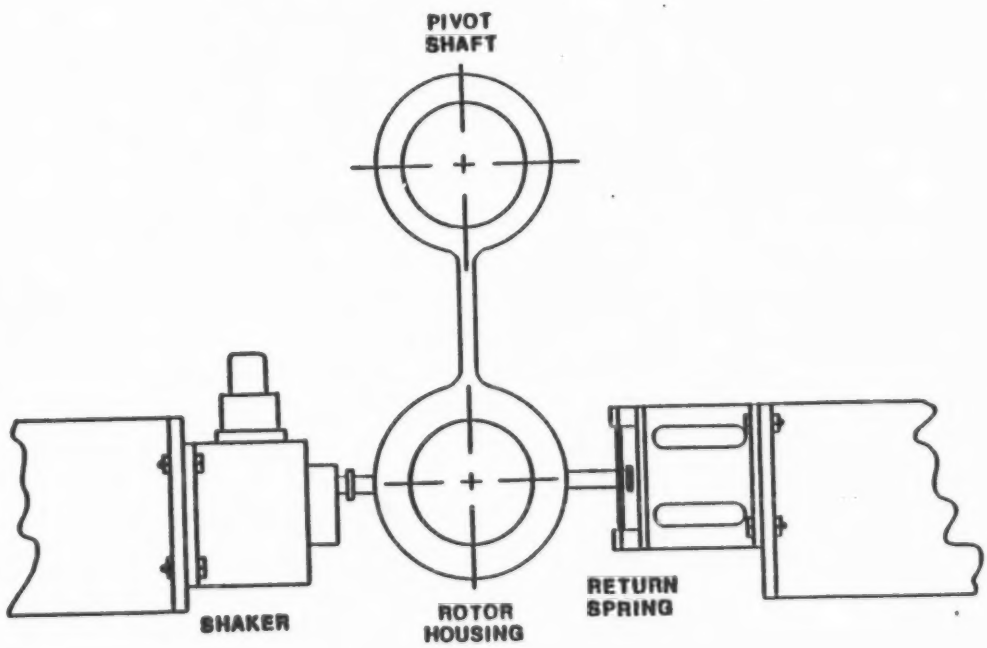

Figure 52. Components used for static and dynamic displacement of seal rotor.

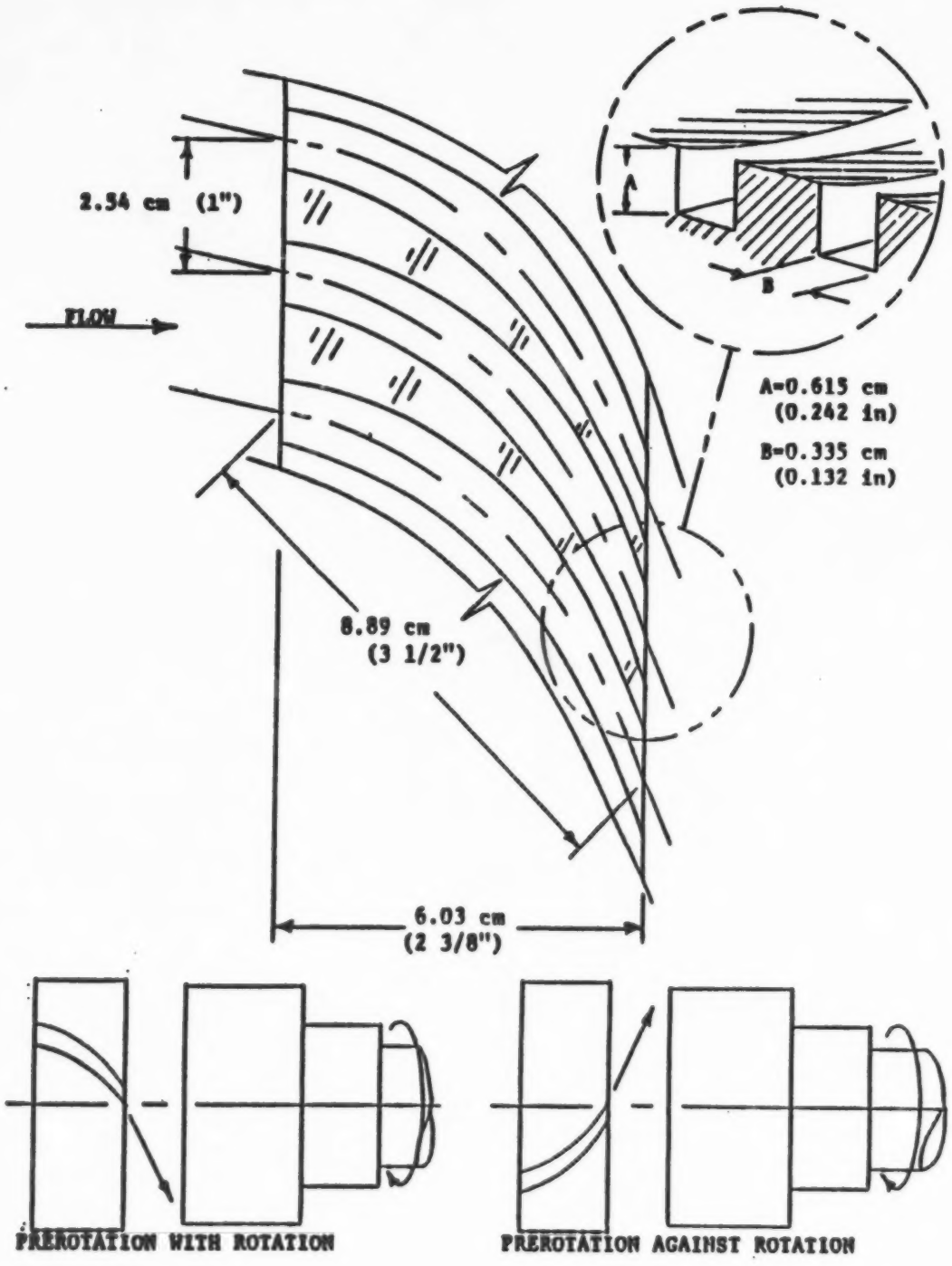

Figure 53.Inlet guide vane detail.

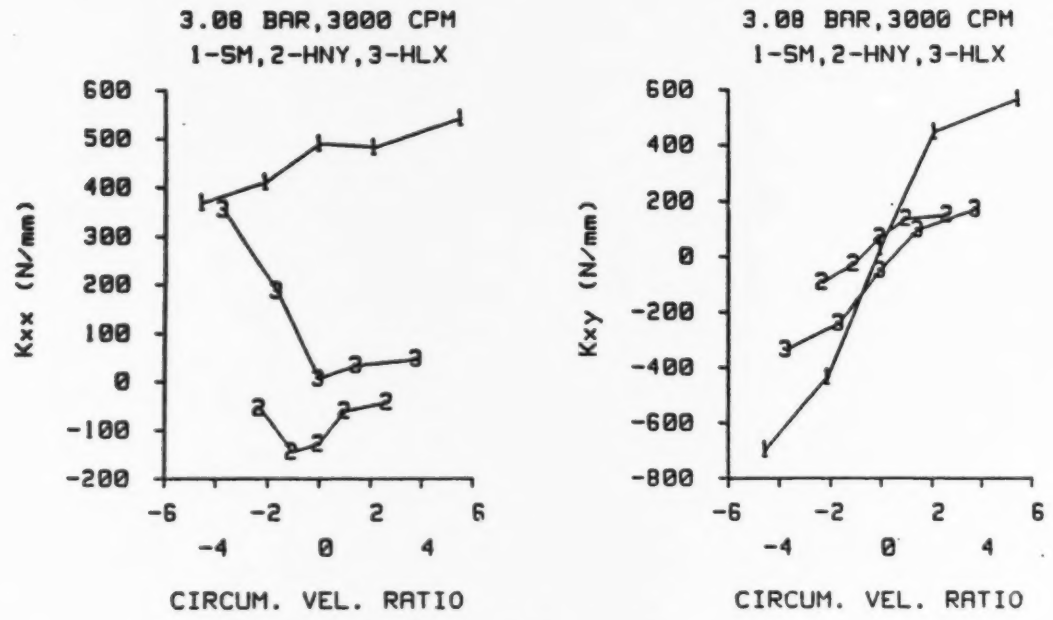

Figure 54(a). K_{xx} and K_{xy} versus $u_{\theta o}$ for smooth (1), honeycomb (2), and helix (3) stators at 3,000 CPM.

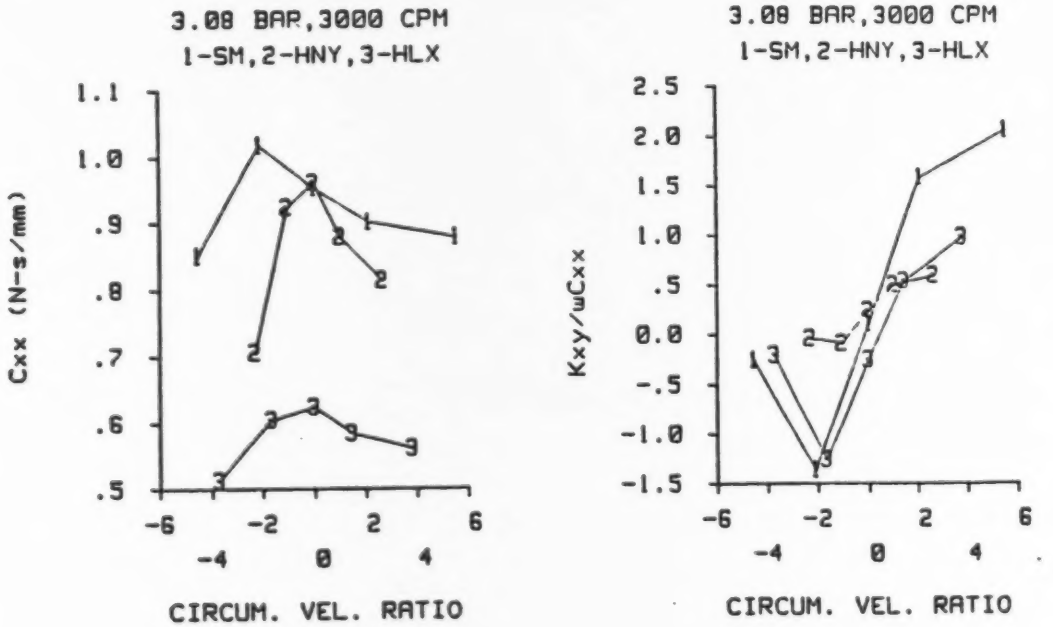

Figure 54(b). C_{xx} and $K_{xy}/\omega C_{xx}$ versus $u_{\theta o}$ for smooth (1), honeycomb (2), and helix (3) stators at 3,000 CPM.

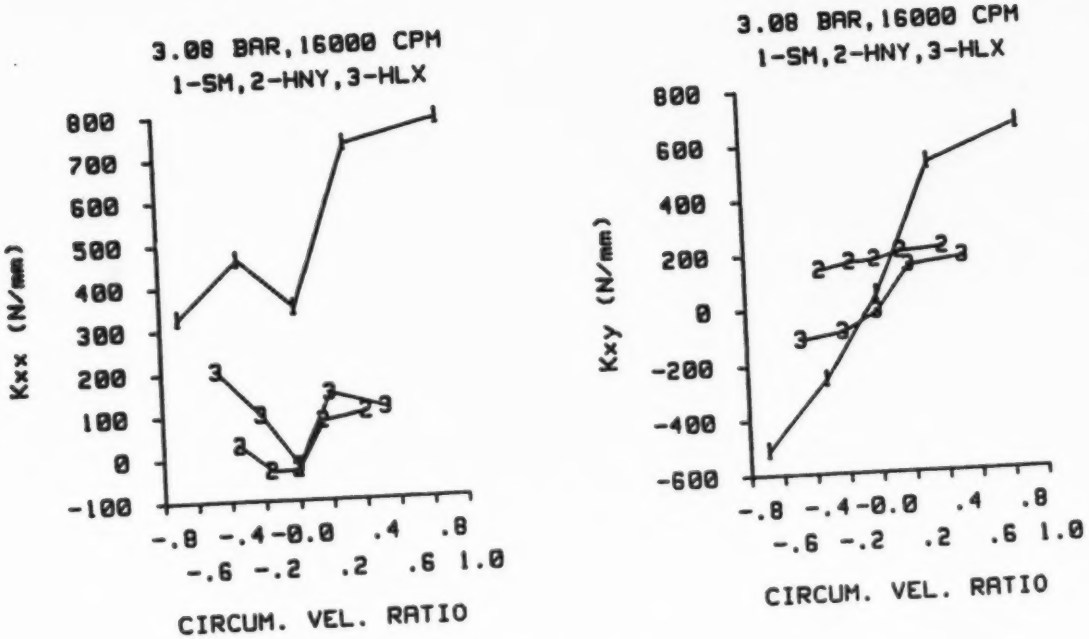

Figure 55(a). K_{xx} and K_{xy} versus $u_{\theta o}$
for smooth (1), honeycomb (2), and helix (3) stators at
16,000 CPM.

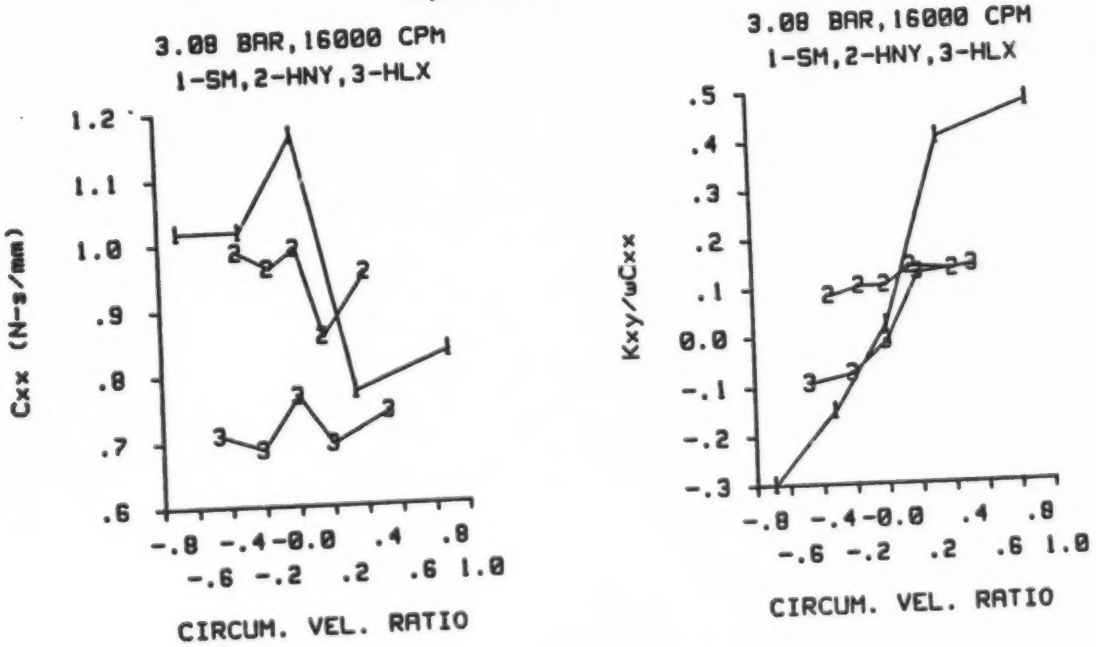

Figure 55(b). C_{xx} and $K_{xy}/\omega C_{xx}$ versus $u_{\theta o}$
for smooth (1), honeycomb (2), and helix (3) stators at
16,000 CPM.

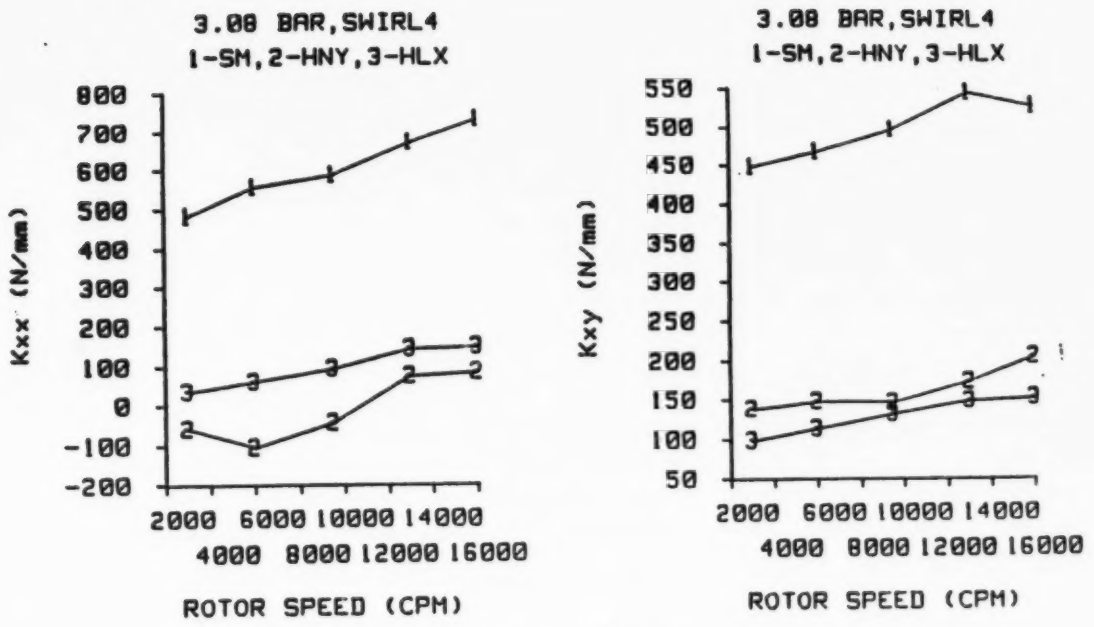

Figure 56(a). Test results for K_{xx} and K_{xy} versus running speed for smooth (1), honeycomb (2), and helix (3) stators versus running speed for maximum inlet-flow prerotation in the direction of shaft rotation.

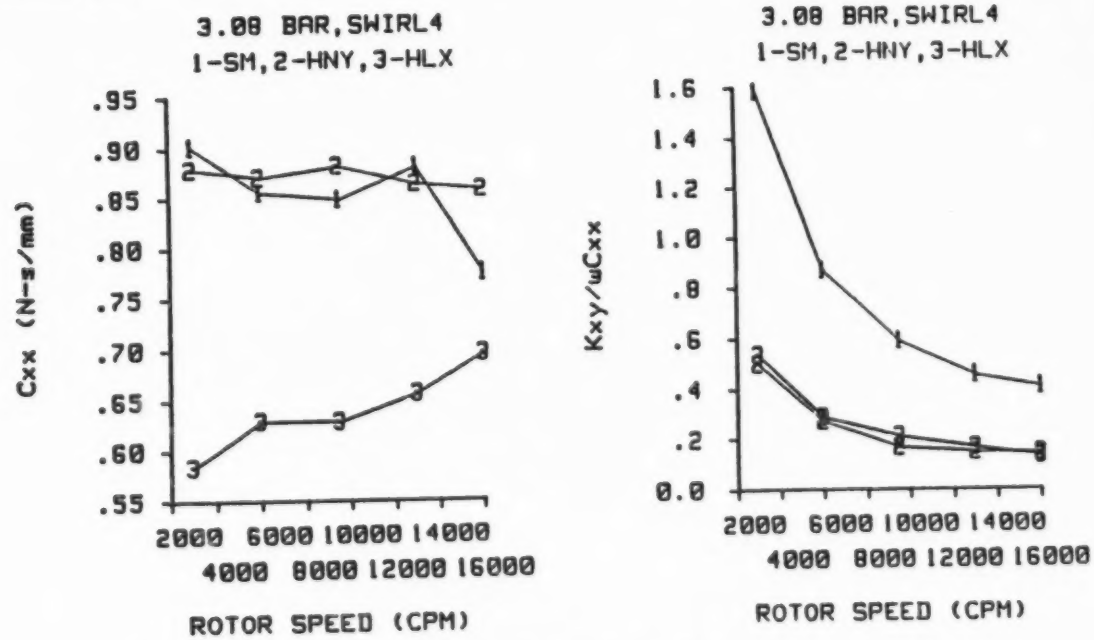

Figure 56(b). Test results for C_{xx} and $K_{xy}/\omega C_{xx}$ versus running speed for smooth (1), honeycomb (2), and helix (3) stators versus running speed for maximum inlet-flow prerotation in the direction of shaft rotation.

Figures 56(a) and (b) illustrate the rotordynamic coefficients of figure 54 and 55 versus running speed for maximum preswirl in the direction of shaft rotation. Observe that K_{xy} is smaller for the helix stator than the honeycomb stator and does not increase as rapidly with increasing running speed. Observe in figure 56(b) that C_{xx} is smaller for the helix stator then the honeycomb stator but increases more rapidly with running speed. Finally, note that the whirl-frequency ratio is generally slightly smaller for the honeycomb stator than the helix stator, except at the highest speed.

Recall in reviewing the results of figure 56 that the helically-grooved stator has a higher leakage rate and accordingly higher inlet tangential velocity. Given that a higher $u_{\theta o}$ yields higher K_{xy}, the helix stator suffer an unfair direct comparison in these figures. Even so, the helix stator has comparable rotordynamic-stability performance to the honeycomb stator and its performance is increasing rapidly with speed.

6.4 Conclusions

The test results reported here for smooth, honeycomb, and helically-grooved stators shows comparable performance between honeycomb and helically-grooved stators. From a stability viewpoint, the helically-grooved stator's performance is increasing rapidly with speed. An extrapolation of the data presented here predicts substantially better rotordynamic-stability performance for the helically-grooved stator than a comparable honeycomb stator at higher speeds.

Chapter VII
SUMMARY AND CONCLUSIONS

7.1 Summary and Conclusions

Test results are presented for the following seals:

(a) smooth, concentric seals at four clearances (static-test-data only),
(b) smooth seals at three clearances,
(c) hole-pattern-damper seals, six configurations, and
(d) helically-grooved-stator seals, seven helix angles

All of the above seals are tested in a liquid Halon test facility at high Reynolds numbers. In addition, a helically-grooved-stator seal was tested in an air-seal test facility.

An analysis of the test results with comparisons to theoretical predictions supports the following conclusions:

(a) For small seals, the Hirs' friction-factor model is more restricted than had been through previously. Experimentally-derived-Hirs empirical coefficients apply for a reasonable Reynolds number range but are clearly a function of clearance. Further, there are significant differences between measured σ values with centered concentric seals and a seal with the rotor orbiting. Fortunately, the difference between concentric and orbiting-rotor friction factor data is reduced as the radial clearance is reduced.
(b) For smooth seals, predictions of stiffness and damping improve markedly as the radial clearance is reduced.
(c) Friction factor data for hole-pattern-seal stators frequently deviates from the Hirs model.
(d) Predictions of stiffness and damping coefficients for hole-pattern-stator seals is generally reasonable.
(e) Test for the hole-pattern stators at reduced clearances (0.30 mm versus 0.51 mm) show no clear optimum for hole-pattern seals with respect to either hole-area ratio or hole depth to minimum-clearance ratios.
(f) Tests of these hole-pattern stators show no significant advantage in net damping over smooth seals; however, the seals leak about 30% less than smooth seals.
(g) Tests of helically-grooved seal stators in Halon show reasonable agreement between theory and prediction for leakage and direct stiffness but poor agreement for the net damping coefficient.
(h) Tests of a helically-grooved stator in the air seal facility shows superior stability characteristics at high speeds (16,000 rpm) as compared to a honeycomb seal.

7.2 Comments on Friction Factors

The values of Hirs coefficients which are provided in tables 1, 2, and 4 for the smooth and hole-pattern stators, are not of themselves particularly informative. To provide some perspective, the m and n values have been used to calculate friction factors which are illustrated in figure 57. The λ friction factors of this report have been multiplied by a

ORIGINAL PAGE IS
OF POOR QUALITY

factor of 4 to yield the friction factor values for this figure. The identification on the figure for the smooth stators can best be explained by example. Specifically, .508(S) identifies the curve belonging to the .508mm radial clearance stator with concentric (static) operating conditions, while .508 (D) identifies the curve belonging to the .508 mm radial clearance stator when tested dynamically, i.e., with an orbiting rotor.

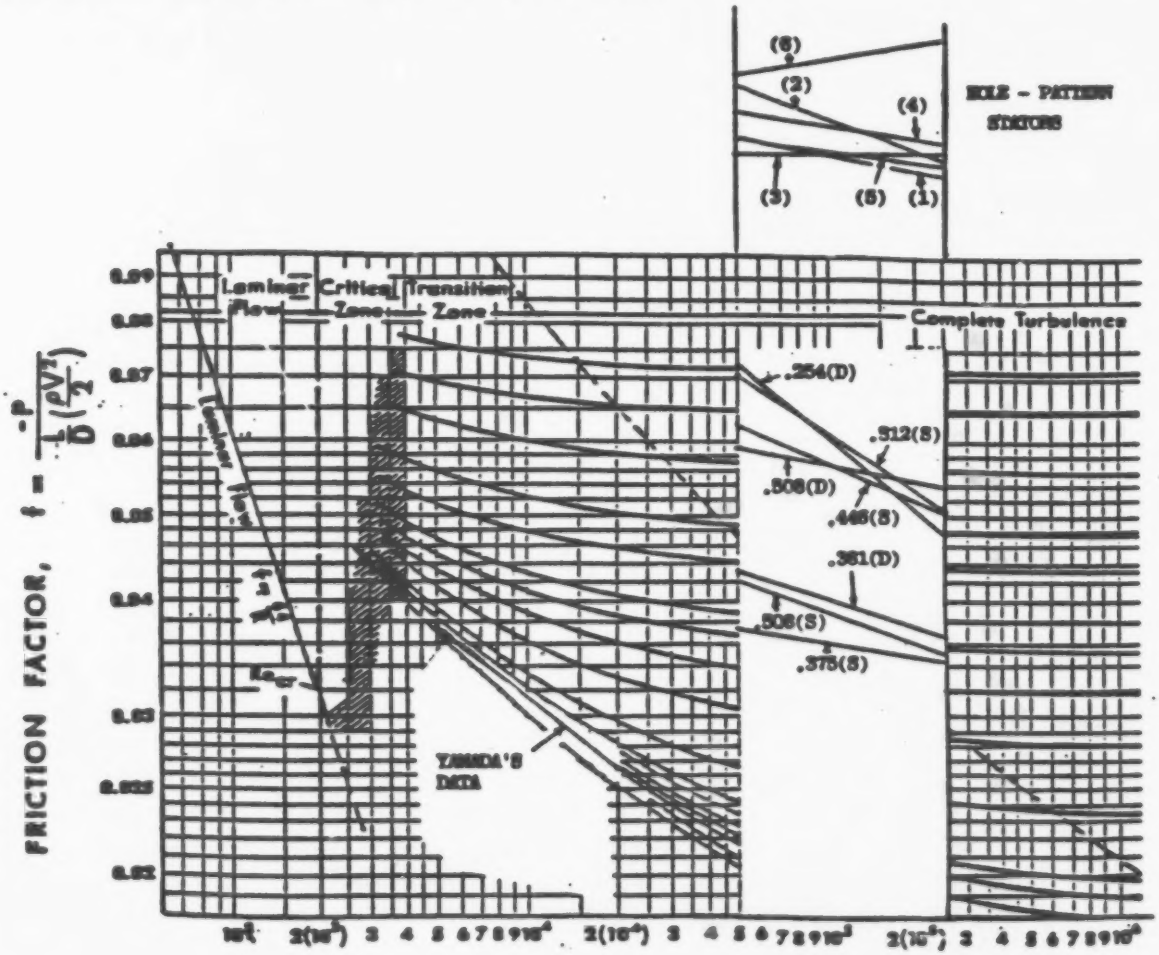

Figure 57. Measured friction-factor data plotted on a Moody diagram.

Observe that the friction-factor data for concentric seals generally proceeds reasonably (f increases as C_r decreases) except for the 0.375 (S) curve. The friction factors corresponding to orbiting rotor cases do not proceed as expected since the friction factors are higher for the .508 (D) than the 0.381 (D) curve. Note where the clearances are approximately the same in concentric and orbiting-rotor cases that the dynamic friction factor is always higher, but the the difference decreases as the clearance decreases.

The line of the lower left hand side of the turbulent friction factors illustrates Yamada's test-data correlation. Obviously, the "smooth" seals tested in this program have markedly higher friction factors than those measured by Yamada. Differences in surface finishes

between the current seals and Yamada's could possible account for those differences.

Friction-factor curves corresponding to the hole-pattern stators are illustrated above the normal expent of the Moody diagram. The circled numbers identify the stators. Note that curves 3 and 6 have positive slopes corresponding to positive ms values in Table 4. Obviously, the hole-pattern stators have markedly higher λ values than the smooth stators.

Despite the fact that the analysis for smooth and hole-pattern stators does a reasonably good job of calculating force coefficients, an inspection of figure 57 suggests a discouraging and generally comprehensive failure to model and understand friction factors in seals. Given that the speed and Reynolds-number dependency of λ provides the basic foundation for rotordynamic-coefficient calculation, these are particularly discouraging results. They provide a strong argument for additional and more fundamental measurements of friction-factor data, possibly in a flat-plate tester.

REFERENCES

1. von Pragenau, G. L., "Damping Seals for Turbomachinery," NASA Technical Paper 1987, 1982.
2. Childs, D. W. and Kim, C-H, "Analysis and Testing of Turbulent Annular Seals with Different, Directionally Homogeneous Surface Roughness Treatments for Rotor and Stator Elements," *ASME Transaction, Journal of Tribology Technology,* Vol. 107, July 1985, pp. 296-306.
3. Childs, D. W., "SSME HPFTP Interstage Seals: Analysis and Experiments for Leakage and Reaction-Force Coefficients," Progress Report, NAS8-33716, Texas A&M University-Turbomachinery Laboratories Report, Seal-1-83, 15 February 1983.
4. Childs, D. W., "SSME HPFTP Interstage Seals: Analysis and Experiments for Leakage and Reaction-Force Coefficients," Supplementary Progress Report, NASA Contract NAS8-33716, Texas A&M University-Turbomachinery Laboratories Report Seal-2-83, 15 July 1983.
5. Childs, D. W., "SSME Seal Program: Leakage Tests for Helically-Grooved Seals," Progress Report NASA Contract NAS8-33716, Texas A&M University, Turbomachinery Laboratories Report, Seal-3-83, November 1983.
6. Childs, D. W., "SSME Interstage Seal Research," Progress Report NASA Contract NAS8-33716, Texas A&M University, Turbomachinery Laboratories Report, RD-1-84, January 1984.
7. Childs, D. W., "SSME Seal Test Program: Test Results for Hole Pattern Damper Seals," Interim Progress Report, NASA Contract NAS8-35824, Turbomachinery Laboratories Report TRC-Seal-4-85, July 1985.
8. Kim, C-H and Childs, D. W., "Analysis for Rotordynamic Coefficients of Helically-Grooved Turbulent Annular Seals," ASME Paper 86-Trib-18, presented at ASME-ASLE Joint Lubrication Conference, Pittsburgh, PA, 20-22 October 1986.
9. Yamada, Y., "Resistance of Flow through Annulus with an Inner Rotating Cylinder," *Bulletin of Japanese Society of Mechanical Engineers,* 1962, Vol.5, No. 18, pp. 302-310.
10. Hirs, G. G., "A Bulk-Flow Theory for Turbulence in Lubricant Films," *ASME Journal of Lubrication Technology,* April 1973, pp. 137-146.
11. Nelson, C. and Nguyen, D., "Comparisons of Hirs' Equation with Moody's Equation for Determining Rotordynamic Coefficients of Annular Pressure Seals," *ASME Journal of Tribology,* January 1987, Vol. 109, No. 1, pp. 144-148.
12. Childs, D. W., Nelson, C. E., Nicks, C., Scharrer, J., Elrod, D., and Hale, K., "Theory Versus Experiment for the Rotordynamic Coefficients of Annular Gas Seals: Part 1-Test Facility and Apparatus," *ASME Transaction, Journal of Tribology Technology,* Vol. 108, July 1986, pp. 426-432.

APPENDIX A.
STATIC TEST CONDITIONS FOR TESTED SEALS

SMOOTH SEAL 0.254mm cr.

$Pa - Pb$ $(Bars)$	ρ (Kg/M^3)	μ $(Nsec/M^2)$	$\dot{m}$ (Kg/sec)	CPM (C_{yc}/min)	$1+\zeta$	λ
3.847	1569.970	.151E-03	1.423	1007.	1.0828	.0199
3.896	1570.592	.151E-03	1.432	2007.	1.0144	.0197
3.991	1566.448	.150E-03	1.431	3000.	1.0750	.0198
4.154	1566.659	.150E-03	1.421	4000.	1.0691	.0214
4.410	1571.417	.151E-03	1.435	5310.	1.1794	.0219
4.723	1562.182	.149E-03	1.409	7186.	1.1958	.0248
8.755	1559.288	.148E-03	2.102	987.	1.1750	.0166
8.553	1556.093	.147E-03	2.097	2000.	1.1184	.0169
9.001	1564.979	.149E-03	2.117	3008.	1.1665	.0169
8.945	1551.496	.146E-03	2.077	4013.	1.1405	.0177
9.171	1556.367	.147E-03	2.101	5263.	1.1452	.0181
10.380	1569.112	.150E-03	2.146	7186.	1.2375	.0193
18.557	1555.611	.147E-03	3.010	1007.	1.2122	.0156
18.388	1549.342	.145E-03	2.989	2000.	1.2228	.0155
18.476	1553.456	.146E-03	3.015	3000.	1.2360	.0151
18.562	1552.989	.146E-03	3.003	4013.	1.1996	.0154
18.695	1551.470	.145E-03	2.994	5286.	1.2036	.0154
20.389	1560.274	.148E-03	3.033	7229.	1.2413	.0164
28.529	1562.954	.148E-03	3.757	1017.	1.1940	.0149
28.565	1565.465	.149E-03	3.771	2000.	1.2341	.0144
28.673	1564.047	.149E-03	3.772	3000.	1.2169	.0146
28.707	1564.110	.149E-03	3.765	4000.	1.2547	.0143
28.991	1558.308	.147E-03	3.742	5286.	1.2582	.0145
29.828	1563.025	.149E-03	3.770	7186.	1.1886	.0152
38.922	1559.955	.147E-03	4.442	1003.	1.2402	.0138
39.095	1565.338	.149E-03	4.455	1993.	1.2346	.0137
39.251	1565.809	.149E-03	4.478	2978.	1.2442	.0135
39.279	1566.370	.149E-03	4.458	4027.	1.2370	.0137
39.324	1564.795	.149E-03	4.413	5263.	1.2342	.0139
39.749	1571.649	.150E-03	4.429	7143.	1.1723	.0142

Table A.1. Operating conditions and parameters, smooth stator; $C_r = 0.254mm$.

SMOOTH SEAL 0.381mm cr.

$Pa-Pb$ ($Bars$)	ρ (Kg/M^3)	μ ($Nsec/M^2$)	$\dot{m}$ (Kg/sec)	CPM (C_{yc}/min)	$1+\zeta$	λ
2.279	1565.559	.150E-03	2.130	1071.	1.3348	.0114
2.444	1572.731	.151E-03	2.167	1802.	1.3678	.0116
2.526	1571.843	.151E-03	2.155	2703.	1.4053	.0122
2.748	1575.777	.152E-03	2.179	3614.	1.4618	.0123
2.947	1576.919	.153E-03	2.180	5333.	1.4818	.0152
3.233	1563.204	.149E-03	2.123	7186.	1.7082	.0185
6.775	1560.095	.148E-03	3.505	1068.	1.2667	.0102
6.643	1556.840	.147E-03	3.490	1770.	1.2355	.0104
7.016	1565.407	.149E-03	3.551	2673.	1.2377	.0108
7.123	1569.557	.150E-03	3.572	3582.	1.2493	.0105
7.177	1557.353	.147E-03	3.501	5333.	1.3113	.0110
7.918	1569.529	.150E-03	3.569	7186.	1.3372	.0126
13.524	1565.909	.149E-03	4.974	1060.	1.2351	.0097
13.678	1567.498	.150E-03	4.982	1780.	1.2473	.0098
13.760	1564.680	.149E-03	4.961	2667.	1.2586	.0100
13.012	1549.254	.145E-03	4.817	3509.	1.2458	.0101
13.349	1551.633	.146E-03	4.839	5333.	1.2167	.0107
14.239	1557.650	.147E-03	4.902	7186.	1.2426	.0110
22.244	1566.632	.149E-03	6.379	1038.	1.1887	.0097
21.406	1553.214	.146E-03	6.240	1754.	1.2048	.0097
21.886	1560.953	.148E-03	6.335	2643.	1.2097	.0096
21.613	1554.379	.146E-03	6.243	3529.	1.1998	.0099
22.180	1557.007	.147E-03	6.292	5310.	1.1825	.0103
22.833	1558.117	.147E-03	6.303	7186.	1.2023	.0104
35.152	1566.172	.149E-03	8.053	1071.	1.2128	.0092
35.106	1566.122	.149E-03	8.041	1775.	1.2106	.0092
35.171	1564.961	.149E-03	8.034	2667.	1.2191	.0092
35.236	1565.890	.149E-03	8.050	3561.	1.2018	.0093
35.311	1565.489	.149E-03	7.992	5310.	1.2115	.0096
35.675	1556.295	.146E-03	7.981	7186.	1.1960	.0097

Table A.2. Operating conditions and parameters, smooth stator; $C_r = 0.381mm$.

SMOOTH SEAL 0.508mm cr.

$Pa - Pb$ (*Bars*)	ρ (Kg/M^3)	μ ($Nsec/M^2$)	$\dot{m}$ (Kg/sec)	CPM (C_{ye}/min)	$1+\zeta$	λ
2.719	1552.499	.146E-03	2.772	1000.	1.3689	.0167
2.819	1557.358	.147E-03	2.813	2000.	1.3411	.0174
2.783	1563.211	.149E-03	2.840	3008.	1.2670	.0170
2.896	1570.467	.151E-03	2.863	4000.	1.2969	.0182
3.037	1552.601	.146E-03	2.770	5381.	1.3700	.0195
3.314	1567.797	.150E-03	2.859	7186.	1.4115	.0233
7.676	1562.455	.149E-03	4.716	1000.	1.2264	.0151
7.631	1561.310	.148E-03	4.696	2007.	1.2118	.0153
7.606	1553.678	.146E-03	4.633	3023.	1.2150	.0160
7.720	1553.609	.146E-03	4.633	4040.	1.2161	.0163
7.716	1550.629	.146E-03	4.612	5333.	1.2098	.0168
8.121	1556.693	.147E-03	4.671	7186.	1.2420	.0165
13.471	1553.242	.146E-03	6.239	1007.	1.1828	.0149
13.909	1563.392	.149E-03	6.362	2007.	1.1866	.0150
13.513	1551.480	.146E-03	6.221	3038.	1.1866	.0151
13.805	1555.452	.147E-03	6.278	4027.	1.1979	.0153
13.605	1548.451	.145E-03	6.194	5357.	1.1793	.0155
13.741	1546.812	.144E-03	6.176	7186.	1.1841	.0163
21.466	1554.324	.146E-03	7.871	1003.	1.1762	.0143
21.429	1552.662	.146E-03	7.862	2000.	1.1858	.0143
21.488	1553.358	.146E-03	7.860	3000.	1.1880	.0144
21.593	1553.172	.146E-03	7.873	3987.	1.1634	.0147
22.242	1563.361	.149E-03	8.007	5310.	1.1560	.0149
22.455	1561.094	.148E-03	7.980	7186.	1.1735	.0148
32.122	1561.016	.148E-03	9.735	1014.	1.1415	.0139
32.143	1561.021	.148E-03	9.751	2007.	1.1434	.0139
32.107	1553.930	.146E-03	9.699	3030.	1.1492	.0138
32.247	1560.833	.147E-03	9.756	3987.	1.1540	.0138
32.290	1559.380	.147E-03	9.736	5333.	1.1461	.0141
32.443	1551.717	.145E-03	9.656	7186.	1.1176	.0149

Table A.3. Operating conditions and parameters, smooth stator; $C_r = 0.508mm$.

HOLE PATTERN 0.376mm cr. h/cr=1.00 : $\gamma = 0.34$

$Pa - Pb$ $(Bars)$	ρ (Kg/M^3)	μ $(Nsec/M^2)$	$\dot{m}$ (Kg/sec)	CPM (C_{yc}/min)	$1+\zeta$	λ
4.902	1554.290	.147E-03	2.091	1007.	1.2614	0223
5.032	1560.106	.148E-03	2.113	2013.	1.1223	.0237
5.318	1566.244	.150E-03	2.146	3008.	1.1402	.0243
5.462	1571.857	.151E-03	2.157	4027.	1.1588	.0238
5.634	1565.951	.150E-03	2.124	5310.	1.2386	.0258
6.237	1561.896	.149E-03	2.113	7186.	1.3562	.0308
11.341	1569.992	.151E-03	3.090	997.	1.2167	.0224
11.356	1572.294	.151E-03	3.106	2000.	1.2172	.0220
11.362	1569.160	.150E-03	3.089	3008.	1.1813	.0227
11.120	1559.856	.148E-03	3.039	4000.	1.1976	.0225
11.184	1556.427	.147E-03	3.028	5333.	1.2086	.0227
12.248	1564.611	.149E-03	3.067	7186.	1.2679	.0240
18.819	1558.795	.148E-03	3.970	997.	1.1452	.0218
18.058	1545.118	.144E-03	3.880	2000.	1.1700	.0213
18.685	1551.862	.146E-03	3.928	3015.	1.1907	.0214
18.687	1551.521	.146E-03	3.921	4027.	1.1758	.0214
18.798	1550.450	.145E-03	3.918	5310.	1.1776	.0218
19.650	1555.728	.147E-03	3.943	7229.	1.1809	.0227
26.471	1545.843	.144E-03	4.674	1007.	1.1678	.0209
26.969	1549.513	.145E-03	4.698	2007.	1.1822	.0213
27.356	1558.742	.147E-03	4.779	2993.	1.1582	.0211
26.784	1545.999	.144E-03	4.679	4027.	1.2083	.0209
26.753	1543.536	.143E-03	4.668	5310.	1.1717	.0212
28.218	1561.444	.148E-03	4.802	7229.	1.2246	.0206
38.225	1557.610	.147E-03	5.629	997.	1.1812	.0204
38.312	1560.872	.148E-03	5.652	2013.	1.1867	.0204
38.358	1564.585	.149E-03	5.662	2985.	1.1861	.0203
38.415	1564.138	.149E-03	5.697	4000.	1.1834	.0199
38.507	1561.793	.148E-03	5.661	5263.	1.1911	.0202
38.608	1560.751	.148E-03	5.626	7143.	1.2075	.0203

Table A.4. Operating conditions and parameters, hole-pattern stator 1.

HOLE PATTERN 0.371mm cr. h/cr=2.74 : $\gamma = 0.34$

$Pa - Pb$ (*Bars*)	ρ (Kg/M^3)	μ ($Nsec/M^2$)	$\dot{m}$ (Kg/sec)	CPM (C_{yc}/min)	$1+\varsigma$	λ
4.714	1547.291	.145E-03	2.056	1045.	1.2922	.0241
4.763	1554.031	.146E-03	2.090	1754.	1.2493	.0238
4.763	1548.738	.145E-03	2.062	2614.	1.2534	.0244
5.207	1556.826	.147E-03	2.092	3540.	1.3185	.0264
5.726	1553.071	.146E-03	2.085	5310.	1.3691	.0306
6.988	1566.258	.150E-03	2.143	7186.	1.5652	.0358
10.786	1561.475	.148E-03	3.060	1068.	1.2316	.0229
10.788	1563.553	.149E-03	3.064	1775.	1.2573	.0226
10.846	1564.267	.149E-03	3.068	2667.	1.2467	.0230
10.879	1559.569	.148E-03	3.035	3519.	1.2500	.0238
10.931	1545.707	.144E-03	2.964	5310.	1.2427	.0255
12.075	1557.507	.147E-03	3.017	7186.	1.2606	.0280
16.002	1549.658	.145E-03	3.679	1035.	1.1737	.0226
16.115	1556.862	.147E-03	3.718	1765.	1.1871	.0223
16.266	1558.132	.147E-03	3.717	2643.	1.1930	.0226
16.278	1556.818	.147E-03	3.724	3519.	1.2202	.0223
16.894	1562.960	.148E-03	3.746	5333.	1.1670	.0239
17.286	1546.646	.144E-03	3.660	7186.	1.2249	.0254
22.589	1551.534	.145E-03	4.379	1042.	1.1817	.0219
23.117	1556.542	.147E-03	4.419	1754.	1.1742	.0222
22.623	1550.174	.145E-03	4.380	2620.	1.1649	.0224
23.211	1561.464	.148E-03	4.446	3529.	1.1887	.0222
23.483	1559.200	.147E-03	4.445	5310.	1.1697	.0226
24.515	1562.709	.148E-03	4.462	7229.	1.1506	.0243
33.831	1555.266	.146E-03	5.367	1045.	1.1052	.0218
33.899	1557.991	.147E-03	5.392	1765.	1.1286	.0215
34.030	1559.994	.147E-03	5.409	2632.	1.1231	.0216
34.044	1557.178	.147E-03	5.423	3529.	1.1325	.0214
34.005	1552.602	.145E-03	5.379	5310.	1.1278	.0223
34.379	1561.735	.148E-03	5.363	7186.	1.1043	.0229

Table A.5. Operating conditions and parameters, hole-pattern stator 2.

HOLE PATTERN 0.376mm cr. h/cr=2.92 : $\gamma = 0.34$

$Pa - Pb$ ($Bars$)	ρ (Kg/M^3)	μ ($Nsec/M^2$)	$\dot{m}$ (Kg/sec)	CPM (C_{yo}/min)	$1+\varsigma$	λ
4.660	1558.169	.148E-03	2.102	1045.	1.3423	.0219
4.748	1561.776	.149E-03	2.125	1780.	1.3671	.0216
4.828	1561.442	.148E-03	2.117	2667.	1.3946	.0225
5.036	1558.498	.148E-03	2.106	3529.	1.4181	.0239
5.583	1557.839	.147E-03	2.107	5286.	1.4524	.0276
6.718	1574.453	.152E-03	2.172	7229.	1.5130	.0345
10.634	1571.548	.151E-03	3.109	1075.	1.2670	.0214
10.326	1567.081	.150E-03	3.082	1791.	1.2991	.0209
10.439	1573.888	.151E-03	3.129	2685.	1.2771	.0209
10.469	1566.951	.150E-03	3.085	3582.	1.2804	.0221
10.569	1554.661	.146E-03	3.015	5286.	1.2510	.0241
11.628	1566.615	.150E-03	3.066	7186.	1.2994	.0269
15.775	1561.199	.148E-03	3.747	1068.	1.1688	.0223
15.007	1555.238	.146E-03	3.710	1760.	1.1439	.0214
15.382	1568.791	.150E-03	3.803	2661.	1.1443	.0212
15.385	1559.741	.148E-03	3.749	3540.	1.1934	.0216
15.450	1556.557	.147E-03	3.726	5286.	1.1664	.0229
16.623	1564.028	.149E-03	3.770	7186.	1.2001	.0243
24.122	1565.602	.149E-03	4.616	1075.	1.1456	.0222
24.153	1575.892	.152E-03	4.688	1796.	1.1736	.0212
23.064	1567.634	.150E-03	4.609	2667.	1.1745	.0209
23.315	1567.778	.150E-03	4.629	3571.	1.1749	.0211
23.715	1574.900	.151E-03	4.688	5286.	1.1569	.0217
23.092	1553.818	.146E-03	4.511	7186.	1.1745	.0229
33.968	1564.879	.149E-03	5.455	1060.	1.1203	.0223
34.045	1569.576	.150E-03	5.520	1786.	1.1471	.0213
34.116	1570.399	.150E-03	5.552	2673.	1.1548	.0212
34.123	1571.156	.150E-03	5.608	3582.	1.1589	.0205
34.244	1568.226	.149E-03	5.597	5286.	1.1540	.0209
34.196	1566.095	.149E-03	5.580	7186.	1.1737	.0213

Table A.6. Operating conditions and parameters, hole-pattern stator 3.

HOLE PATTERN 0.379mm cr. h/cr=4.03 : $\gamma = 0.34$

$Pa - Pb$ ($Bars$)	ρ (Kg/M^3)	μ ($Nsec/M^2$)	$\dot{m}$ (Kg/sec)	CPM (C_{yc}/min)	$1+\varsigma$	λ
4.924	1567.033	.150E-03	2.134	1075.	1.6177	.0219
4.923	1565.336	.150E-03	2.133	1775.	1.6261	.0219
4.940	1560.393	.148E-03	2.104	2661.	1.5657	.0236
5.320	1564.715	.149E-03	2.130	3571.	1.5722	.0256
5.725	1558.413	.148E-03	2.102	5310.	1.5634	.0309
6.818	1560.552	.148E-03	2.124	7186.	1.6267	.0389
10.290	1557.791	.147E-03	3.033	1071.	1.4223	.0231
10.124	1560.866	.148E-03	3.058	1770.	1.4327	.0218
10.194	1565.226	.149E-03	3.061	2685.	1.4658	.0218
10.433	1560.641	.148E-03	3.050	3540.	1.4077	.0230
11.016	1558.001	.147E-03	3.032	5310.	1.3974	.0257
11.357	1548.160	.145E-03	2.978	7186.	1.3717	.0298
16.259	1566.385	.149E-03	3.789	1056.	1.4107	.0223
15.892	1561.030	.148E-03	3.750	1770.	1.4140	.0221
15.070	1552.889	.146E-03	3.696	2626.	1.3783	.0218
14.831	1548.747	.145E-03	3.657	3478.	1.3766	.0218
15.500	1546.495	.144E-03	3.659	5333.	1.3367	.0233
16.706	1551.997	.146E-03	3.678	7229.	1.3590	.0260
24.126	1564.363	.149E-03	4.601	1064.	1.3255	.0229
23.179	1555.238	.146E-03	4.508	1760.	1.3777	.0224
23.043	1557.139	.147E-03	4.536	2649.	1.4081	.0214
22.886	1557.452	.147E-03	4.535	3519.	1.3877	.0215
23.423	1554.098	.146E-03	4.515	5286.	1.3490	.0228
23.854	1549.598	.145E-03	4.488	7186.	1.3488	.0239
34.091	1555.355	.146E-03	5.454	1049.	1.3082	.0225
34.049	1554.210	.146E-03	5.463	1744.	1.3368	.0221
33.943	1550.221	.145E-03	5.489	2620.	1.3416	.0215
33.975	1552.595	.145E-03	5.527	3499.	1.3565	.0211
34.211	1557.175	.147E-03	5.537	5310.	1.3520	.0210
34.152	1553.042	.146E-03	5.463	7186.	1.3281	.0221

Table A.7. Operating conditions and parameters, hole-pattern stator 4.

HOLE PATTERN 0.376mm cr. h/cr=2.92 : $\gamma = 0.27$

$Pa - Pb$ $(Bars)$	ρ (Kg/M^3)	μ $(Nsec/M^2)$	$\dot{m}$ (Kg/sec)	CPM (C_{yc}/min)	$1+\varsigma$	λ
4.395	1550.859	.146E-03	2.069	1014.	1.2874	.0236
4.377	1554.413	.147E-03	2.100	2000.	1.1383	.0231
4.717	1558.007	.148E-03	2.113	3008.	1.1603	.0238
4.961	1565.168	.149E-03	2.129	4000.	1.1546	.0236
5.284	1559.128	.148E-03	2.105	5263.	1.2391	.0262
6.338	1557.195	.147E-03	2.098	7186.	1.2093	.0349
9.850	1564.668	.149E-03	3.066	990.	1.1755	.0227
9.664	1561.902	.148E-03	3.057	2000.	1.1411	.0223
9.763	1566.231	.150E-03	3.069	3030.	1.1396	.0222
9.681	1553.422	.146E-03	3.000	3974.	1.1215	.0226
10.137	1554.398	.146E-03	3.024	5286.	1.1291	.0227
10.888	1551.937	.146E-03	3.002	7186.	1.1317	.0249
18.725	1559.992	.148E-03	4.216	1017.	1.1240	.0219
18.796	1562.469	.149E-03	4.231	2007.	1.1495	.0215
18.846	1563.371	.149E-03	4.240	2985.	1.1231	.0215
18.915	1563.430	.149E-03	4.232	4027.	1.1275	.0214
19.078	1560.224	.148E-03	4.224	5263.	1.1226	.0214
20.464	1561.582	.148E-03	4.239	7229.	1.1183	.0225
27.003	1549.781	.145E-03	5.063	1010.	1.1098	.0216
26.951	1554.407	.146E-03	5.096	2000.	1.1173	.0211
26.941	1552.235	.146E-03	5.088	2985.	1.1137	.0208
26.941	1555.507	.147E-03	5.097	4027.	1.1196	.0206
27.522	1554.721	.146E-03	5.109	5286.	1.0898	.0210
29.254	1566.914	.150E-03	5.207	7186.	1.0626	.0217
37.598	1560.925	.148E-03	6.024	990.	1.0655	.0213
37.792	1566.591	.149E-03	6.047	2000.	1.1024	.0208
37.761	1563.286	.148E-03	6.052	2985.	1.1198	.0204
37.729	1557.357	.147E-03	6.018	4013.	1.0961	.0205
37.676	1553.910	.146E-03	6.019	5263.	1.0842	.0205
38.321	1559.369	.147E-03	6.011	7229.	1.0721	.0206

Table A.8. Operating conditions and parameters, hole-pattern stator 5.

HOLE PATTERN 0.381mm cr. h/cr=2.92 : $\gamma = 0.42$

$Pa - Pb$ (*Bars*)	ρ (Kg/M^3)	μ ($Nsec/M^2$)	$\dot{m}$ (Kg/sec)	CPM (C_{po}/min)	$1+\varsigma$	λ
4.504	1545.571	.144E-03	2.062	1010.	.9702	.0305
4.473	1559.087	.148E-03	2.107	2007.	1.0378	.0283
4.564	1560.757	.148E-03	2.110	3015.	1.0682	.0280
4.702	1555.352	.147E-03	2.099	4013.	1.0858	.0286
5.015	1548.224	.145E-03	2.061	5286.	1.1144	.0329
6.335	1564.708	.149E-03	2.125	7186.	1.3123	.0384
11.473	1565.265	.149E-03	3.062	1017.	1.0143	.0331
9.917	1549.575	.145E-03	2.999	2013.	.9772	.0289
9.982	1562.484	.149E-03	3.053	3008.	1.0130	.0279
9.668	1553.489	.146E-03	3.022	4000.	1.0011	.0273
10.373	1566.196	.150E-03	3.086	5333.	1.0675	.0279
11.008	1556.560	.147E-03	3.035	7229.	1.1796	.0287
19.604	1547.498	.144E-03	3.896	997.	.9530	.0337
18.070	1546.795	.144E-03	3.873	2000.	.9654	.0303
16.760	1543.495	.143E-03	3.869	2978.	.9831	.0276
16.874	1553.895	.146E-03	3.931	3987.	1.0085	.0265
16.446	1545.073	.144E-03	3.872	5286.	1.0522	.0262
17.360	1548.756	.145E-03	3.910	7186.	1.1026	.0266
27.290	1547.502	.144E-03	4.574	987.	.9668	.0334
25.379	1548.546	.145E-03	4.583	2007.	.9682	.0305
25.082	1556.816	.147E-03	4.665	3015.	1.0145	.0281
23.854	1552.131	.146E-03	4.621	4000.	1.0131	.0269
24.003	1559.790	.148E-03	4.682	5286.	1.0089	.0261
24.145	1560.984	.148E-03	4.689	7186.	1.0544	.0256
38.092	1555.745	.146E-03	5.405	993.	.9424	.0332
38.030	1561.129	.148E-03	5.528	1993.	.9847	.0306
37.900	1557.599	.147E-03	5.649	2985.	.9818	.0287
37.739	1553.324	.146E-03	5.759	3974.	.9582	.0270
37.664	1557.531	.147E-03	5.818	5286.	.9803	.0260
38.149	1554.008	.146E-03	5.866	7229.	.9823	.0255

Table A.9. Operating conditions and parameters, hole-pattern stator 6.

HELICALLY GROOVED 0.356mm cr. 0 deg.

$Pa - Pb$ (Bars)	ρ (Kg/M^3)	μ ($Nsec/M^2$)	$\dot{m}$ (Kg/sec)	CPM (C_{pc}/min)	$1+\zeta$	λ
4.197	1553.450	.146E-03	2.068	1056.	1.1528	.0259
4.163	1557.953	.148E-03	2.103	1770.	1.0926	.0258
4.213	1556.776	.147E-03	2.092	2649.	1.0937	.0259
4.246	1557.336	.147E-03	2.096	3529.	1.1157	.0262
4.367	1558.469	.148E-03	2.106	5310.	1.1615	.0270
4.724	1566.797	.150E-03	2.130	7186.	1.2931	.0290
9.588	1575.291	.152E-03	3.123	1071.	1.1210	.0247
9.594	1571.375	.151E-03	3.115	1802.	1.1232	.0246
9.612	1570.928	.151E-03	3.108	2703.	1.1366	.0245
9.704	1574.958	.152E-03	3.120	3593.	1.1308	.0245
9.640	1563.657	.149E-03	3.071	5310.	1.1194	.0249
9.708	1559.667	.148E-03	3.038	7229.	1.1652	.0260
15.044	1555.969	.147E-03	3.833	1053.	1.0614	.0249
15.113	1557.530	.147E-03	3.851	1760.	1.0528	.0247
15.151	1559.439	.147E-03	3.865	2661.	1.0750	.0244
15.255	1561.610	.148E-03	3.875	3540.	1.0591	.0244
14.806	1550.267	.145E-03	3.790	5310.	1.0705	.0243
15.234	1555.162	.146E-03	3.825	7186.	1.0801	.0244
22.111	1553.833	.146E-03	4.639	1060.	1.0237	.0248
22.390	1559.126	.147E-03	4.671	1775.	1.0569	.0245
22.482	1561.499	.148E-03	4.677	2655.	1.0666	.0245
22.510	1560.644	.148E-03	4.692	3550.	1.0807	.0241
22.250	1556.452	.147E-03	4.638	5310.	1.0600	.0243
22.934	1567.318	.150E-03	4.733	7186.	1.0855	.0235
33.463	1554.818	.146E-03	5.694	1045.	1.0300	.0243
33.898	1569.314	.150E-03	5.768	1786.	1.0543	.0238
33.714	1559.550	.147E-03	5.732	2643.	1.0413	.0240
33.783	1560.270	.147E-03	5.705	3529.	1.0670	.0241
33.801	1561.336	.148E-03	5.751	5286.	1.0594	.0236
34.004	1562.534	.148E-03	5.779	7229.	1.0483	.0232

Table A.10. Operating conditions and parameters, helically-grooved stator 1, $\alpha = 0°$.

C-2

HELICALLY GROOVED 0.376mm cr. 15 deg.

$Pa - Pb$ ($Bars$)	ρ (Kg/M^3)	μ ($Nsec/M^2$)	$\dot{m}$ (Kg/sec)	CPM (C_{pm}/min)	$1+\zeta$	λ
3.137	1556.534	.147E-03	2.101	993.	.9189	.0218
3.407	1564.188	.149E-03	2.139	2000.	.9255	.0232
4.006	1575.367	.152E-03	2.181	3008.	1.0126	.0257
4.372	1565.137	.149E-03	2.139	4013.	1.1307	.0285
5.116	1575.016	.152E-03	2.177	5286.	1.1131	.0319
6.064	1559.885	.148E-03	2.122	7186.	1.4642	.0415
7.248	1557.945	.148E-03	3.033	1000.	1.0854	.0206
7.444	1561.229	.148E-03	3.043	2000.	1.0830	.0212
7.654	1558.676	.148E-03	3.037	3000.	1.0723	.0220
7.876	1550.444	.145E-03	2.985	4013.	1.1195	.0237
9.134	1563.604	.149E-03	3.068	5310.	1.2267	.0254
10.301	1554.400	.146E-03	3.016	7186.	1.3681	.0298
11.185	1554.387	.146E-03	3.705	997.	1.0941	.0200
10.905	1547.267	.144E-03	3.653	2007.	1.0721	.0203
11.599	1558.690	.147E-03	3.744	3008.	1.0948	.0203
11.987	1554.173	.146E-03	3.714	4027.	1.1524	.0212
12.477	1546.601	.144E-03	3.652	5286.	1.1750	.0234
14.557	1556.032	.147E-03	3.723	7186.	1.2678	.0263
21.079	1547.978	.145E-03	5.045	1000.	1.0902	.0188
21.626	1551.683	.145E-03	5.077	2007.	1.1107	.0189
22.137	1558.825	.147E-03	5.139	3008.	1.1063	.0190
22.165	1556.029	.147E-03	5.108	4013.	1.1191	.0192
23.124	1556.471	.147E-03	5.123	5286.	1.1289	.0202
24.012	1545.796	.144E-03	5.025	7186.	1.2079	.0218
36.112	1560.205	.147E-03	6.626	1003.	1.0829	.0177
36.150	1560.948	.148E-03	6.619	2000.	1.1170	.0176
36.269	1564.404	.149E-03	6.594	3000.	1.1280	.0178
36.276	1561.825	.148E-03	6.560	4000.	1.1371	.0180
36.096	1552.307	.145E-03	6.507	5286.	1.1148	.0185
36.496	1557.543	.147E-03	6.403	7186.	1.1355	.0191

Table A.11. Operating conditions and parameters, helically-grooved stator 2, $\alpha = 15°$.

HELICALLY GROOVED 0.371mm cr. 30 deg.

$Pa - Pb$ (*Bars*)	ρ (Kg/M^3)	μ ($Nsec/M^2$)	$\dot{m}$ (Kg/sec)	CPM (C_{pm}/min)	$1+\zeta$	λ
2.589	1564.512	.149E-03	2.140	1060.	1.0122	.0105
2.779	1567.631	.150E-03	2.132	1791.	1.0457	.0111
2.933	1557.107	.147E-03	2.106	2655.	1.0519	.0121
3.465	1563.747	.149E-03	2.130	3561.	1.0631	.0143
4.354	1561.083	.148E-03	2.113	5286.	1.2007	.0183
5.660	1558.608	.148E-03	2.098	7186.	1.4494	.0248
7.415	1572.073	.151E-03	3.593	1091.	.9378	.0096
7.486	1568.615	.150E-03	3.568	1796.	.9244	.0102
7.816	1569.498	.151E-03	3.579	2685.	.9156	.0106
8.138	1570.740	.151E-03	3.588	3582.	.9385	.0108
9.260	1569.175	.150E-03	3.576	5310.	.9793	.0123
10.464	1562.092	.148E-03	3.535	7229.	.9631	.0156
14.190	1567.838	.150E-03	4.984	1064.	.8507	.0098
13.971	1562.218	.148E-03	4.923	1770.	.8477	.0099
14.321	1561.729	.148E-03	4.922	2643.	.8539	.0101
14.690	1561.772	.148E-03	4.932	3540.	.8588	.0103
15.825	1564.013	.149E-03	4.934	5310.	.8814	.0109
17.029	1553.279	.146E-03	4.861	7186.	.8762	.0126
21.414	1565.972	.149E-03	6.138	1049.	.8342	.0097
21.992	1568.866	.150E-03	6.183	1786.	.8353	.0098
22.108	1566.762	.149E-03	6.158	2655.	.8310	.0099
22.623	1568.625	.150E-03	6.180	3571.	.8411	.0100
23.210	1560.896	.148E-03	6.101	5310.	.8548	.0104
25.037	1567.461	.150E-03	6.162	7186.	.8384	.0115
31.192	1560.187	.147E-03	7.430	1042.	.7944	.0096
31.354	1564.523	.148E-03	7.442	1775.	.8039	.0095
31.482	1565.739	.149E-03	7.380	2667.	.8274	.0097
31.612	1565.901	.149E-03	7.387	3540.	.8121	.0098
31.856	1565.014	.149E-03	7.282	5286.	.8266	.0100
31.992	1559.941	.147E-03	7.133	7186.	.8031	.0109

Table A.12. Operating conditions and parameters, helically-grooved stator 3, $\alpha = 30°$.

HELICALLY GROOVED 0.371mm cr. 30 deg. w/end lands

$Pa - Pb$ (*Bars*)	ρ (Kg/M^3)	μ ($Nsec/M^2$)	$\dot{m}$ (Kg/sec)	CPM (C_{pc}/min)	$1+\zeta$	λ
2.884	1557.492	.148E-03	2.101	1003.	1.7405	.0115
3.194	1562.355	.149E-03	2.130	1993.	1.7409	.0129
3.550	1565.433	.150E-03	2.130	3015.	1.7919	.0151
3.927	1562.513	.149E-03	2.117	3987.	1.8262	.0173
4.495	1558.408	.148E-03	2.097	5310.	1.9182	.0222
5.520	1560.525	.148E-03	2.105	7186.	1.9201	.0313
9.466	1561.482	.148E-03	3.765	993.	1.5608	.0104
9.564	1560.249	.148E-03	3.740	2007.	1.5765	.0109
9.877	1561.217	.148E-03	3.753	3008.	1.5776	.0116
9.979	1555.427	.147E-03	3.710	4000.	1.5470	.0125
10.614	1554.634	.147E-03	3.707	5286.	1.5594	.0139
11.972	1555.427	.147E-03	3.711	7186.	1.5340	.0170
17.886	1561.557	.148E-03	5.154	990.	1.4996	.0099
17.948	1561.073	.148E-03	5.147	2007.	1.4990	.0100
18.033	1558.314	.147E-03	5.136	3000.	1.4792	.0105
18.478	1557.750	.147E-03	5.119	4027.	1.5123	.0111
18.685	1553.930	.146E-03	5.100	5263.	1.4797	.0118
19.817	1547.289	.144E-03	5.041	7229.	1.4939	.0135
24.129	1554.661	.146E-03	6.021	1000.	1.4674	.0098
24.353	1553.151	.146E-03	5.999	2000.	1.5014	.0100
24.888	1559.824	.148E-03	6.078	3023.	1.4852	.0101
25.088	1558.233	.147E-03	6.055	4000.	1.4577	.0107
25.433	1552.664	.146E-03	6.002	5310.	1.4706	.0113
26.084	1545.853	.144E-03	5.942	7186.	1.4271	.0126
35.724	1547.602	.144E-03	7.323	1007.	1.4335	.0096
35.823	1551.275	.145E-03	7.283	2000.	1.4709	.0098
35.886	1550.328	.145E-03	7.229	2993.	1.4846	.0100
35.885	1554.994	.146E-03	7.251	4027.	1.4868	.0101
36.195	1557.505	.147E-03	7.207	5286.	1.4595	.0108
35.973	1552.178	.145E-03	7.083	7186.	1.4319	.0117

Table A.13. Operating conditions and parameters, helically-grooved stator 4, $\alpha = 30°$. End lands are used on this seal.

HELICALLY GROOVED 0.376mm cr. 40 deg.

$Pa - Pb$ ($Bars$)	ρ (Kg/M^3)	μ ($Nsec/M^2$)	$\dot{m}$ (Kg/sec)	CPM (C_{pm}/min)	$1+\zeta$	λ
1.966	1560.438	.148E-03	2.119	993.	.9829	.0055
2.106	1559.418	.148E-03	2.113	2000.	.9339	.0069
2.482	1565.159	.149E-03	2.135	2993.	.9001	.0092
2.882	1563.463	.149E-03	2.119	3987.	.8590	.0114
3.434	1560.321	.148E-03	2.112	5310.	.8257	.0156
4.450	1557.847	.147E-03	2.109	7229.	.7846	.0238
6.573	1566.889	.150E-03	4.026	1000.	.6515	.0068
6.737	1561.603	.148E-03	4.005	2000.	.6768	.0071
6.752	1553.387	.146E-03	3.949	3000.	.6465	.0078
7.154	1555.115	.147E-03	3.948	3987.	.6132	.0087
7.925	1551.697	.146E-03	3.916	5310.	.5923	.0101
9.471	1566.779	.150E-03	4.040	7229.	.5310	.0122
12.218	1553.403	.146E-03	5.544	1017.	.5810	.0071
12.436	1552.861	.146E-03	5.535	2000.	.5755	.0072
13.049	1558.247	.147E-03	5.602	3000.	.5900	.0074
13.050	1551.602	.145E-03	5.519	4013.	.5885	.0078
13.608	1548.468	.145E-03	5.497	5310.	.5458	.0085
16.020	1563.009	.148E-03	5.648	7186.	.5282	.0096
20.413	1552.880	.146E-03	7.143	993.	.5583	.0071
20.405	1549.422	.145E-03	7.104	2007.	.5442	.0071
20.573	1546.417	.144E-03	7.073	3023.	.5573	.0072
20.882	1545.033	.144E-03	7.057	3987.	.5635	.0074
21.526	1544.932	.144E-03	7.065	5310.	.5425	.0079
22.919	1547.398	.144E-03	7.078	7186.	.5220	.0085
30.272	1541.519	.142E-03	8.706	993.	.5320	.0069
30.525	1548.656	.144E-03	8.732	2013.	.5282	.0069
30.796	1557.478	.146E-03	8.736	3015.	.5360	.0069
30.868	1555.964	.146E-03	8.661	3974.	.5315	.0071
31.020	1553.276	.145E-03	8.570	5286.	.5491	.0074
33.159	1554.373	.146E-03	8.730	7186.	.5105	.0080

Table A.14. Operating conditions and parameters, helically-grooved stator 5, $\alpha = 40°$.

HELICALLY GROOVED 0.376mm cr. 50 deg.

$Pa - Pb$ (*Bars*)	ρ (Kg/M^3)	μ ($Nsec/M^2$)	$\dot{m}$ (Kg/sec)	CPM (C_{ps}/min)	$1+\varsigma$	λ
1.368	1568.150	.150E-03	2.152	1079.	.7868	.0047
1.611	1582.430	.154E-03	2.205	1818.	.7940	.0052
1.787	1578.215	.153E-03	2.175	2721.	.8053	.0064
2.106	1578.733	.153E-03	2.191	3636.	.7902	.0076
2.747	1579.728	.153E-03	2.193	5286.	.6702	.0116
3.277	1559.526	.148E-03	2.101	7186.	.6821	.0176
3.273	1588.619	.156E-03	3.206	1107.	.7117	.0047
3.233	1579.413	.153E-03	3.173	1807.	.7048	.0047
3.501	1582.917	.154E-03	3.195	2746.	.7076	.0050
3.556	1569.006	.150E-03	3.097	3571.	.6425	.0059
4.442	1585.610	.155E-03	3.191	5310.	.5922	.0079
5.338	1574.962	.152E-03	3.118	7186.	.5550	.0104
4.523	1570.333	.151E-03	3.812	1087.	.6372	.0047
4.873	1580.322	.153E-03	3.897	1813.	.6478	.0049
5.010	1575.377	.152E-03	3.868	2715.	.6568	.0050
5.366	1582.180	.154E-03	3.905	3625.	.6327	.0053
5.973	1573.749	.152E-03	3.837	5286.	.5956	.0070
6.782	1566.127	.150E-03	3.789	7186.	.5175	.0088
14.503	1582.704	.154E-03	6.811	1087.	.6017	.0043
14.056	1568.160	.150E-03	6.639	1775.	.6006	.0045
14.642	1577.460	.152E-03	6.750	2709.	.6005	.0046
14.967	1577.945	.152E-03	6.760	3604.	.5958	.0047
14.930	1562.085	.148E-03	6.584	5286.	.5824	.0050
15.667	1557.135	.147E-03	6.506	7229.	.5713	.0053
27.816	1558.656	.147E-03	9.448	1060.	.5614	.0039
28.001	1567.862	.149E-03	9.484	1780.	.5686	.0041
27.964	1564.374	.148E-03	9.440	2643.	.5775	.0042
28.003	1559.972	.147E-03	9.387	3519.	.5664	.0044
28.301	1567.224	.149E-03	9.320	5263.	.5687	.0045
29.052	1568.554	.149E-03	9.226	7186.	.5690	.0048

Table A.15. Operating conditions and parameters, helically-grooved stator 6, $\alpha = 50°$.

HELICALLY GROOVED 0.396mm cr. 60 deg.

$Pa - Pb$ (*Bars*)	ρ (Kg/M^3)	μ ($Nsec/M^2$)	$\dot{m}$ (Kg/sec)	CPM (C_{pa}/min)	$1+\zeta$	λ
.894	1560.269	.148E-03	2.116	1053.	.6504	.0079
.857	1552.889	.146E-03	2.072	1754.	.5999	.0091
.978	1551.532	.146E-03	2.077	2620.	.5676	.0101
1.349	1550.445	.146E-03	2.077	3519.	.6594	.0117
1.855	1566.573	.150E-03	2.144	5286.	.7609	.0155
2.598	1565.807	.150E-03	2.128	7229.	1.0859	.0195
2.319	1560.119	.151E-03	3.109	1079.	.6445	.0065
2.343	1561.727	.149E-03	3.065	1775.	.6567	.0068
2.436	1558.888	.148E-03	3.048	2673.	.6554	.0078
2.771	1565.778	.150E-03	3.080	3571.	.6994	.0088
3.391	1566.850	.150E-03	3.082	5310.	.7864	.0101
4.215	1563.361	.149E-03	3.063	7186.	.8779	.0129
3.769	1573.926	.152E-03	3.845	1075.	.6724	.0060
3.896	1574.225	.152E-03	3.847	1796.	.6912	.0060
4.061	1574.883	.152E-03	3.862	2703.	.6879	.0067
4.156	1567.167	.150E-03	3.799	3582.	.6805	.0073
4.974	1572.282	.151E-03	3.846	5286.	.7542	.0089
5.681	1565.560	.150E-03	3.784	7186.	.8015	.0109
12.917	1577.885	.152E-03	6.882	1083.	.6857	.0052
13.016	1576.374	.152E-03	6.866	1807.	.6867	.0054
12.824	1571.146	.151E-03	6.809	2697.	.6800	.0055
12.976	1570.379	.150E-03	6.787	3571.	.6836	.0058
13.633	1571.636	.151E-03	6.812	5286.	.6740	.0065
14.401	1567.852	.150E-03	6.767	7186.	.6851	.0073
27.089	1565.580	.149E-03	9.893	1064.	.6610	.0052
27.287	1571.380	.150E-03	9.885	1775.	.6724	.0051
27.330	1571.835	.150E-03	9.886	2697.	.6731	.0052
27.375	1572.267	.150E-03	9.834	3571.	.6726	.0054
27.485	1572.154	.150E-03	9.794	5265.	.6778	.0056
27.835	1569.942	.150E-03	9.701	7186.	.6714	.0060

Table A.16. Operating conditions and parameters, helically-grooved stator 7, $\alpha = 60°$.

HELICALLY GROOVED 0.379mm cr. 70 deg.

$Pa - Pb$ ($Bars$)	ρ (Kg/M^3)	μ ($Nsec/M^2$)	$\dot{m}$ (Kg/sec)	CPM (C_{pe}/min)	$1+\zeta$	λ
.630	1557.469	.147E-03	2.106	1053.	.5571	.0066
.687	1557.234	.147E-03	2.109	1765.	.5739	.0062
.821	1560.523	.148E-03	2.115	2649.	.6026	.0069
.914	1552.445	.146E-03	2.089	3509.	.6093	.0078
1.410	1555.893	.147E-03	2.068	5286.	.8279	.0102
2.102	1562.933	.149E-03	2.125	7229.	1.0616	.0119
3.925	1572.569	.151E-03	4.312	1083.	.6113	.0043
3.818	1562.901	.149E-03	4.237	1791.	.5839	.0046
3.909	1564.657	.149E-03	4.250	2673.	.5779	.0049
4.230	1569.740	.151E-03	4.295	3582.	.5996	.0050
4.376	1555.417	.147E-03	4.174	5310.	.5802	.0058
5.355	1560.923	.148E-03	4.241	7186.	.6795	.0064
8.744	1569.408	.150E-03	6.432	1064.	.5716	.0043
8.807	1566.436	.150E-03	6.396	1786.	.5753	.0043
8.962	1569.790	.150E-03	6.429	2685.	.5606	.0044
8.792	1559.309	.148E-03	6.303	3540.	.5623	.0045
9.267	1557.047	.147E-03	6.290	5310.	.5697	.0049
10.307	1564.853	.149E-03	6.372	7186.	.5884	.0053
14.510	1561.172	.148E-03	8.203	1049.	.5645	.0041
14.897	1566.127	.149E-03	8.254	1780.	.5719	.0041
14.983	1562.412	.148E-03	8.203	2655.	.5759	.0042
15.126	1562.506	.148E-03	8.218	3540.	.5637	.0043
15.306	1556.446	.147E-03	8.131	5286.	.5711	.0045
16.245	1560.818	.148E-03	8.188	7186.	.5679	.0047
23.039	1552.049	.145E-03	10.279	1060.	.5710	.0040
23.101	1548.719	.144E-03	10.222	1739.	.5700	.0041
23.306	1558.697	.147E-03	10.253	2632.	.5699	.0042
23.438	1560.766	.147E-03	10.224	3519.	.5701	.0042
23.802	1560.427	.147E-03	10.204	5286.	.5643	.0042
24.019	1560.015	.147E-03	10.078	7186.	.5685	.0045

Table A.17. Operating conditions and parameters, helically-grooved stator 8, $\alpha = 70°$.

APPENDIX B.
DYNAMIC TEST DATA

SMOOTH SEAL 0.254mm cr.

Case	R_{ze}	CPM (C_{pe}/min)	F_r/A (MN/M)	dev. (MN/M)	F_θ/A (MN/M)	dev. (MN/M)	$\|F\|$ (KN)
1.	59843.	1007.	-1.430	.1724	1.262	.1937	.1709
2.	59944.	2007.	-1.429	.0977	2.220	.1059	.2349
3.	60338.	3000.	-.695	.0897	3.401	.1092	.3088
4.	59896.	4000.	-.208	.1456	3.420	.1041	.3048
5.	59962.	5310.	.882	.3918	5.234	.2365	.4732
6.	59860.	7186.	1.959	.5947	8.207	.5631	.7518
7.	89821.	987.	-2.879	.3591	1.936	.5161	.3133
8.	90109.	2000.	-5.663	.4047	5.733	.3930	.7174
9.	89673.	3008.	-4.794	.3360	8.695	.3291	.8832
10.	90002.	4013.	-2.391	.3202	9.776	.3153	.8952
11.	90235.	5263.	.356	.2985	8.035	.2817	.7181
12.	90136.	7186.	1.628	.9685	12.370	1.0421	1.1125
13.	129640.	1007.	-5.645	.4560	2.583	.8403	.5579
14.	130273.	2000.	-5.436	.2967	5.274	.3003	.6739
15.	130401.	3000.	-4.210	.3491	7.534	.3231	.7679
16.	129999.	4013.	-3.041	.4155	9.087	.3773	.8525
17.	129930.	5286.	-1.389	.5817	11.576	.4573	1.0378
18.	129619.	7229.	.273	2.5975	16.709	1.4422	1.4995
19.	159784.	1017.	-8.229	.7647	3.008	1.8208	.7977
20.	159654.	2000.	-8.080	.4735	6.611	.4340	.9290
21.	160098.	3000.	-6.715	.3991	9.331	.4106	1.0228
22.	159754.	4000.	-5.360	.5259	11.670	.4751	1.1426
23.	160436.	5286.	-3.374	.6707	14.871	.6590	1.3551
24.	160346.	7186.	-1.678	1.5655	20.310	1.6142	1.8171
25.	190223.	1003.	-10.711	.6921	3.585	1.5614	1.0143
26.	189007.	1993.	-10.491	.6035	8.140	.5737	1.1814
27.	189730.	2978.	-8.898	.5612	11.441	.5286	1.2892
28.	188734.	4027.	-7.476	.7982	13.918	.4296	1.4060
29.	187318.	5263.	-5.076	.8463	17.638	.8407	1.6333
30.	185784.	7143.	-1.946	2.9307	22.758	2.0261	2.0475

Table B.1. Force coefficients (average and standard deviations) and average force magnitudes for a smooth stator; $C_r = 0.254mm$.

SMOOTH SEAL 0.381mm cr.

Case	R_{ee}	CPM (C_{pe}/min)	F_r/A (MN/M)	dev. (MN/M)	F_θ/A (MN/M)	dev. (MN/M)	$\|F\|$ (KN)
1.	89952.	1071.	-.649	.0861	.696	.0828	.0852
2.	90362.	1802.	-.557	.0444	1.003	.0500	.1021
3.	89964.	2703.	-.295	.0499	1.592	.0485	.1440
4.	90345.	3614.	.098	.0793	2.260	.1077	.2012
5.	90219.	5333.	.860	.1518	2.721	.1053	.2540
6.	90006.	7186.	2.404	.1500	3.947	.1799	.4111
7.	149506.	1068.	-1.604	.1596	1.261	.1941	.1825
8.	149710.	1770.	-1.552	.0940	2.038	.0988	.2279
9.	150151.	2673.	-1.104	.1208	2.993	.1466	.2838
10.	149940.	3582.	-.706	.0987	4.051	.1591	.3657
11.	150082.	5333.	.568	.2377	4.971	.1915	.4453
12.	149849.	7186.	2.595	.2713	6.914	.2177	.6569
13.	210420.	1060.	-3.193	.2592	1.782	.4324	.3279
14.	210193.	1780.	-3.163	.1820	3.143	.1693	.3968
15.	210351.	2667.	-2.539	.2032	4.198	.1713	.4364
16.	209897.	3509.	-1.837	.2058	5.540	.2131	.5192
17.	209863.	5333.	-.020	.3167	7.801	.2089	.6941
18.	210372.	7186.	2.265	.3896	10.032	.3793	.9150
19.	269651.	1068.	-5.014	.4320	2.347	.8321	.4989
20.	270058.	1754.	-4.606	.2546	3.921	.2479	.5382
21.	270528.	2643.	-3.967	.3019	5.843	.3217	.6283
22.	269575.	3529.	-3.319	.3129	7.325	.2958	.7154
23.	270539.	5310.	-1.254	.4250	10.442	.4982	.9358
24.	270409.	7186.	1.381	.5004	13.823	.5322	1.2358
25.	341371.	1071.	-7.532	.5091	3.208	.9987	.7340
26.	340874.	1775.	-7.406	.4218	5.262	.3785	.8084
27.	341262.	2667.	-6.732	.4732	7.961	.4593	.9275
28.	341395.	3561.	-5.884	.4283	9.882	.5323	1.0232
29.	339176.	5310.	-3.255	.5439	13.254	.5503	1.2143
30.	344173.	7186.	-.227	.6903	17.464	.5933	1.5538

Table B.2. Force coefficients (average and standard deviations) and average force magnitudes for a smooth stator; $C_r = 0.381mm$.

SMOOTH SEAL 0.508mm cr.

Case	R_{ee}	*CPM* (C_{pe}/*min*)	F_r/A (MN/M)	*dev.* (MN/M)	F_θ/A (MN/M)	*dev.* (MN/M)	$\|F\|$ (KN)
1.	119666.	1000.	-.489	.0785	.506	.0788	.0633
2.	120412.	2000.	-.597	.0453	.902	.0449	.0962
3.	120329.	3008.	-.177	.0610	1.430	.0803	.1282
4.	119703.	4000.	.007	.0771	1.733	.0952	.1542
5.	119621.	5381.	1.169	.1667	2.138	.1331	.2171
6.	120144.	7186.	1.913	.3190	3.637	.3010	.3664
7.	200259.	1000.	-1.419	.1600	.959	.2246	.1540
8.	199706.	2007.	-1.365	.1204	1.710	.1225	.1947
9.	199781.	3023.	-.966	.1610	2.475	.1369	.2366
10.	199826.	4040.	-.355	.2142	3.039	.1287	.2727
11.	200015.	5333.	.982	.1893	4.053	.2129	.3711
12.	200350.	7186.	1.990	.4553	5.975	.4404	.5612
13.	269755.	1007.	-2.444	.2352	1.169	.4601	.2449
14.	270173.	2007.	-2.281	.1874	2.538	.1919	.3037
15.	269841.	3038.	-1.743	.2689	3.615	.2086	.3573
16.	270372.	4027.	-1.370	.2689	4.494	.1409	.4182
17.	270090.	5357.	.734	.3856	5.807	.2468	.5216
18.	270081.	7186.	1.691	.6704	8.476	.7013	.7705
19.	339688.	1003.	-3.634	.3797	1.765	.6852	.3654
20.	340273.	2000.	-3.459	.2236	3.092	.2211	.4115
21.	339765.	3000.	-2.855	.2426	4.847	.2421	.5006
22.	340469.	3987.	-2.354	.3428	5.916	.2401	.5668
23.	340103.	5310.	-.531	.4199	7.565	.3858	.6752
24.	340223.	7186.	.961	.9563	10.823	.8446	.9697
25.	416590.	1014.	-5.474	.5815	2.315	1.1630	.5401
26.	417266.	2007.	-5.384	.3630	4.414	.3930	.6199
27.	420268.	3030.	-4.668	.4601	5.707	.3600	.6562
28.	417642.	3987.	-4.011	.5750	7.689	.4766	.7724
29.	417847.	5333.	-1.746	.5993	9.869	.6030	.8927
30.	419961.	7186.	-.620	.9878	12.898	1.0094	1.1514

Table B.3. Force coefficients (average and standard deviations) and average force magnitudes for a smooth stator; $C_r = 0.508mm$.

HOLE PATTERN 0.376mm cr. Δ/cr=1.00 : γ = 0.34

Case	R_{ee}	CPM (C_{pe}/min)	F_r/A (MN/M)	dev. (MN/M)	F_θ/A (MN/M)	dev. (MN/M)	$\|F\|$ (KN)
1.	90067.	1007.	-.493	.1952	1.141	.1071	.1121
2.	90119.	2013.	-.358	.1655	1.978	.1210	.1793
3.	90484.	3008.	.148	.1654	3.029	.1572	.2700
4.	90030.	4027.	1.037	.1879	3.040	.2058	.2862
5.	89635.	5310.	1.898	.4033	4.287	.2771	.4184
6.	89775.	7186.	4.137	.5935	6.413	.5907	.6808
7.	129612.	997.	-1.149	.2835	1.646	.2286	.1810
8.	129775.	2000.	-1.031	.2252	3.082	.2260	.2896
9.	129773.	3008.	-.270	.2649	4.560	.2569	.4068
10.	129784.	4000.	.671	.3061	4.945	.2679	.4445
11.	130107.	5333.	1.866	.7151	6.651	.4545	.6174
12.	129924.	7186.	4.263	.7976	9.555	.8913	.9327
13.	169892.	997.	-1.781	.3718	2.119	.3401	.2495
14.	170140.	2000.	-1.603	.3026	4.023	.3043	.3858
15.	170186.	3015.	-.898	.3582	5.691	.3633	.5131
16.	170081.	4027.	.619	.4686	6.345	.4175	.5684
17.	170233.	5310.	1.605	.6593	9.077	.5290	.8215
18.	169602.	7229.	4.279	1.8418	12.280	1.0399	1.1682
19.	204984.	1007.	-2.648	.5902	2.557	.6203	.3355
20.	204551.	2007.	-2.376	.4164	5.171	.3840	.5073
21.	204731.	2993.	-1.310	.3868	7 088	.3913	.6417
22.	205054.	4037.	.166	.6565	8.161	.5407	.7279
23.	205488.	5310.	1.013	.8299	10.767	.6613	.9642
24.	204667.	7229.	4.129	2.1990	14.942	1.4011	1.3929
25.	242086.	997.	-3.443	.5988	3.214	.6544	.4251
26.	241792.	2013.	-3.350	.4660	6.225	.4722	.6300
27.	240483.	2985.	-2.193	.5076	8.578	.6283	.7885
28.	242084.	4000.	-.680	.5520	10.564	.6138	.9424
29.	241587.	5263.	1.137	.8201	13.419	.8388	1.1994
30.	240606.	7143.	4.574	2.0594	17.436	1.6561	1.6135

Table B.4. Force coefficients (average and standard deviations) and average force coefficients for hole-pattern stator 1.

HOLE PATTERN 0.371mm cr. h/cr=2.74 : $\gamma = 0.34$

Case	R_{ee}	*CPM* (C_{pe}/min)	F_r/A (MN/M)	*dev.* (MN/M)	F_θ/A (MN/M)	*dev.* (MN/M)	$\|F\|$ (KN)
1.	89746.	1045.	-.773	.1852	1.055	.1357	.1180
2.	90114.	1754.	-.715	.0564	1.702	.0519	.1642
3.	89720.	2614.	-.283	.1005	2.626	.0797	.2350
4.	89755.	3540.	-.213	.0979	3.345	.1001	.2981
5.	90017.	5310.	1.166	.1429	4.357	.1332	.4012
6.	90441.	7186.	3.120	.2376	5.945	.2692	.5973
7.	130362.	1068.	-1.499	.2348	1.686	.2123	.2024
8.	130080.	1775.	-1.696	.1050	2.787	.0979	.2901
9.	130085.	2667.	-1.288	.1585	3.997	.1145	.3735
10.	129772.	3519.	-.718	.1063	4.943	.1240	.4442
11.	129892.	5310.	.872	.2110	6.688	.2101	.5999
12.	129463.	7186.	2.856	.3752	9.206	.4090	.8575
13.	160315.	1035.	-2.222	.2840	1.862	.3290	.2604
14.	159960.	1765.	-2.398	.1616	3.351	.1615	.3666
15.	159587.	2643.	-1.841	.1633	4.680	.1813	.4474
16.	160169.	3519.	-1.368	.1841	6.324	.2513	.5753
17.	159529.	5333.	.312	.6138	8.728	.3314	.7783
18.	160326.	7186.	2.625	.5501	11.658	.4379	1.0635
19.	190171.	1042.	-2.899	.3871	2.359	.4897	.3366
20.	190209.	1754.	-3.198	.1919	3.983	.1934	.4544
21.	190321.	2620.	-2.569	.2164	5.513	.2344	.5410
22.	189692.	3529.	-1.957	.1802	7.440	.1689	.6841
23.	190408.	5310.	-.235	.3410	10.471	.3478	.9316
24.	189995.	7229.	2.557	1.8748	13.924	.7476	1.2699
25.	232087.	1045.	-4.439	.4416	2.751	.6897	.4696
26.	231959.	1765.	-4.579	.2112	5.019	.2096	.6043
27.	231905.	2632.	-4.055	.2525	7.002	.2787	.7197
28.	233606.	3529.	-3.811	.3865	9.562	.2964	.9158
29.	233561.	5310.	-1.193	.6576	12.988	.4132	1.1611
30.	229257.	7186.	1.436	.8100	17.172	.7606	1.5335

Table B.5. Force coefficients (average and standard deviations) and average force coefficients for hole-pattern stator 2.

HOLE PATTERN 0.376mm cr. h/cr=2.92 : $\gamma = 0.34$

Case	R_{ee}	*CPM* (C_{ee}/min)	F_r/A (MN/M)	*dev.* (MN/M)	F_θ/A (MN/M)	*dev.* (MN/M)	$\|F\|$ (KN)
1.	89934.	1045.	-.768	.1250	.969	.1039	.1108
2.	90353.	1780.	-.641	.0752	1.832	.0629	.1726
3.	90089.	2667.	-.500	.0600	2.405	.0741	.2185
4.	90079.	3529.	-.037	.0607	2.965	.0925	.2637
5.	90247.	5286.	1.208	.2039	3.990	.1793	.3710
6.	90398.	7229.	3.160	.7338	5.873	.5079	.5973
7.	130167.	1075.	-1.596	.2188	1.446	.2372	.1935
8.	129982.	1791.	-1.398	.1193	2.758	.1314	.2751
9.	130464.	2685.	-1.166	.1248	3.737	.1255	.3482
10.	130201.	3582.	-.832	.1214	4.562	.0997	.4124
11.	130007.	5286.	.994	.3831	6.242	.2257	.5629
12.	129510.	7186.	2.937	.4673	9.089	.4773	.8500
13.	159968.	1068.	-2.372	.2791	1.684	.3546	.2614
14.	159990.	1760.	-2.147	.1219	3.050	.1252	.3318
15.	160198.	2661.	-1.613	.1966	4.570	.1467	.4311
16.	160438.	3540.	-1.482	.1683	5.956	.2160	.5459
17.	160348.	5286.	.503	.3256	7.859	.2727	.7008
18.	160185.	7186.	2.678	.6022	11.477	.6203	1.0489
19.	195467.	1075.	-3.632	.3545	2.216	.5370	.3822
20.	195079.	1796.	-3.331	.2132	4.381	.2371	.4897
21.	194528.	2667.	-3.166	.2697	5.694	.2749	.5796
22.	195318.	3571.	-2.366	.2930	7.445	.2496	.6950
23.	195399.	5286.	-.307	.4147	10.190	.4419	.9069
24.	195021.	7186.	1.936	.7894	13.723	.8013	1.2340
25.	231851.	1060.	-5.002	.4316	2.519	.7592	.5034
26.	232754.	1786.	-4.420	.2733	5.021	.2688	.5950
27.	233802.	2673.	-5.030	.3117	6.817	.3049	.7537
28.	235871.	3582.	-3.833	.3981	8.619	.2977	.8393
29.	236533.	5286.	-1.273	.6920	12.203	.5483	1.0926
30.	236627.	7186.	1.085	1.2456	16.665	1.0108	1.4887

Table B.6. Force coefficients (average and standard deviations) and average force coefficients for hole-pattern stator 3.

HOLE PATTERN 0.370mm cr. h/cr=4.03 : $\gamma = 0.34$

Case	R_{ee}	*CPM* (C_{pe}/*min*)	F_r/A (*MN/M*)	*dev.* (*MN/M*)	F_θ/A (*MN/M*)	*dev.* (*MN/M*)	$\|F\|$ (*KN*)
1.	89901.	1075.	-.776	.1367	1.085	.1040	.1195
2.	90097.	1775.	-.971	.0996	1.967	.1030	.1952
3.	89839.	2661.	-.709	.1137	2.499	.1002	.2312
4.	90046.	3571.	.053	.1194	3.384	.1583	.3011
5.	89827.	5310.	.684	.1676	3.939	.1904	.3558
6.	90498.	7186.	2.716	.2545	4.859	.2476	.4953
7.	129968.	1071.	-1.619	.1771	1.568	.1766	.2015
8.	130360.	1770.	-1.717	.1560	3.031	.1517	.3100
9.	129519.	2685.	-1.565	.2040	3.941	.2234	.3774
10.	130141.	3540.	-.760	.1576	4.948	.1928	.4453
11.	129968.	5310.	.218	.2685	6.657	.2702	.5926
12.	129956.	7186.	1.859	.4001	8.860	.4461	.8055
13.	160315.	1056.	-2.276	.3042	2.014	.3548	.2733
14.	160111.	1770.	-2.647	.1485	3.890	.1568	.4185
15.	160106.	2626.	-2.446	.1818	4.679	.1672	.4697
16.	159653.	3478.	-1.347	.1741	6.076	.2354	.5534
17.	160363.	5333.	-.278	.4156	8.395	.3380	.7477
18.	159592.	7229.	1.467	1.4641	11.407	.5691	1.0307
19.	195284.	1064.	-3.243	.2734	2.027	.4062	.3425
20.	194498.	1760.	-3.738	.2618	4.327	.2644	.5088
21.	195025.	2649.	-3.510	.3601	5.531	.2962	.5831
22.	194893.	3519.	-2.691	.2069	7.611	.2157	.7179
23.	195169.	5286.	-1.211	.5685	10.673	.5491	.9564
24.	195549.	7186.	.875	.7461	14.602	.7149	1.3022
25.	235839.	1049.	-4.162	.4493	2.729	.7053	.4483
26.	236690.	1744.	-4.539	.3543	5.611	.3616	.6423
27.	239523.	2620.	-4.357	.3410	6.736	.2796	.7137
28.	240212.	3499.	-3.830	.5139	10.017	.4865	.9545
29.	238612.	5310.	-2.771	.7564	13.052	.7128	1.1882
30.	237121.	7186.	-.158	.9996	17.490	.8224	1.5574

Table B.7. Force coefficients (average and standard deviations) and average force coefficients for hole-pattern stator 4.

HOLE PATTERN 0.570mm cr. h/cr=2.92 : $\gamma = 0.27$

Case	R_{ce}	*CPM* (C_{pc}/*min*)	F_r/A (*MN/M*)	*dev.* (*MN/M*)	F_θ/A (*MN/M*)	*dev.* (*MN/M*)	$\|F\|$ (*KN*)
1.	89844.	1014.	-.740	.2100	.945	.1646	.1091
2.	90872.	2000.	-.696	.0980	1.750	.0793	.1666
3.	90452.	3008.	-.288	.1324	2.815	.1439	.2518
4.	89922.	4000.	.974	.1494	3.023	.1270	.2692
5.	89920.	5263.	1.226	.2113	3.829	.1930	.3579
6.	89968.	7186.	3.550	.3250	5.107	.2715	.5538
7.	129778.	990.	-1.545	.2729	1.491	.3133	.1941
8.	130035.	2000.	-1.477	.1833	2.811	.2001	.2828
9.	129526.	3030.	-.832	.2432	4.092	.2238	.3718
10.	129552.	3974.	-.393	.2399	4.432	.2457	.3961
11.	130408.	5286.	1.193	.4272	6.132	.3537	.5566
12.	129974.	7186.	3.125	.5549	8.106	.4394	.7737
13.	179960.	1017.	-3.064	.4072	1.836	.5666	.3230
14.	179825.	2007.	-2.789	.3257	3.912	.3114	.4281
15.	179979.	2985.	-1.977	.3409	5.729	.3270	.5397
16.	179558.	4027.	-1.496	.4560	6.693	.3039	.6108
17.	180235.	5263.	.257	.5687	9.230	.6115	.8224
18.	180442.	7229.	3.064	1.6814	11.577	.8547	1.0759
19.	220300.	1010.	-4.324	.5943	2.486	.9420	.4535
20.	219962.	2000.	-3.823	.4021	5.149	.4082	.5712
21.	220450.	2985.	-3.035	.4114	6.793	.4468	.6625
22.	219631.	4027.	-2.043	.7367	8.074	.4590	.7429
23.	220393.	5286.	-.474	.7317	11.202	.7550	.9989
24.	219799.	7186.	2.838	.9846	14.684	1.0625	1.3326
25.	257877.	990.	-5.567	.5776	3.333	.8429	.5830
26.	258941.	2000.	-5.052	.5089	6.185	.4834	.7113
27.	257681.	2985.	-4.048	.4482	7.574	.4911	.7645
28.	259013.	4013.	-3.006	.6977	10.582	.6502	.9801
29.	260582.	5263.	-.928	.7752	13.463	.8083	1.2016
30.	257684.	7229.	1.957	2.4960	16.878	1.1434	1.5265

Table B.8. Force coefficients (average and standard deviations) and average force coefficients for hole-pattern stator 5.

HOLE PATTERN 0.381mm cr. h/cr=2.92 : $\gamma = 0.42$

Case	R_{ee}	*CPM* (C_{pe}/*min*)	F_r/A (MN/M^2)	*dev.* (MN/M^2)	F_θ/A (MN/M^2)	*dev.* (MN/M^2)	$\|F\|$ (KN)
1.	90857.	1010.	-1.106	.1466	.602	.2154	.1141
2.	90152.	2007.	-.880	.1064	1.206	.0980	.1325
3.	90027.	3015.	-.405	.1127	2.206	.1167	.2064
4.	90304.	4013.	.932	.1793	2.670	.1743	.2519
5.	89675.	5286.	1.254	.2020	3.496	.1938	.3306
6.	89863.	7186.	2.851	.3467	4.886	.4263	.5040
7.	129501.	1017.	-2.200	.2814	1.020	.5029	.2211
8.	130410.	2013.	-2.123	.1768	1.751	.1732	.2451
9.	129701.	3006.	-1.392	.1720	2.968	.2018	.2919
10.	130432.	4000.	-.120	.1924	3.789	.1710	.3374
11.	130197.	5333.	.307	.6890	5.470	.3536	.4909
12.	130312.	7229.	1.963	1.1405	7.437	.5327	.6914
13.	170303.	997.	-3.206	.3247	1.520	.5157	.3192
14.	169506.	2000.	-3.534	.3186	2.726	.3339	.3978
15.	170295.	2978.	-2.745	.3451	3.920	.3122	.4263
16.	169874.	3987.	-1.268	.2688	4.630	.2855	.4274
17.	169967.	5286.	-.396	.5326	6.422	.4373	.5740
18.	170479.	7186.	1.274	.8083	10.031	.7746	.9016
19.	199875.	987.	-3.865	.4556	2.004	.7295	.3936
20.	199820.	2007.	-4.470	.4631	3.656	.4417	.5151
21.	200[illegible]7.	3015.	-4.209	.4666	4.299	.3708	.5358
22.	200155.	4000.	-2.341	.4502	5.523	.3780	.5348
23.	200059.	5286.	-1.223	.5031	7.645	.5983	.6898
24.	199992.	7186.	.711	.9754	11.185	.7944	1.0000
25.	233288.	993.	-5.175	.4801	2.292	.8689	.5099
26.	236353.	1993.	-5.467	.4881	5.317	.4675	.6794
27.	243082.	2985.	-5.300	.4722	5.917	.4930	.7072
28.	249676.	3974.	-4.462	.6032	7.756	.5449	.7970
29.	250329.	5286.	-3.482	.7271	9.469	.7019	.8991
30.	253967.	7229.	-1.764	1.8798	12.928	.9151	1.1721

Table B.9. Force coefficients (average and standard deviations) and average force coefficients for hole-pattern stator 6.

HELICALLY GROOVED 0.356mm cr. 0 deg.

Case	R_{ee}	*CPM* (C_{pe}/*min*)	F_r/A (*MN/M*)	*dev.* (*MN/M*)	F_θ/A (*MN/M*)	*dev.* (*MN/M*)	$\|F\|$ (*KN*)
1.	90113.	1056.	-.396	.0925	.720	.0566	.0736
2.	90016.	1770.	-.231	.0529	1.134	.0392	.1030
3.	89748.	2649.	-.064	.0484	1.643	.0560	.1462
4.	89802.	3529.	.244	.0511	1.858	.0396	.1667
5.	90086.	5310.	1.339	.1764	2.883	.1336	.2831
6.	89758.	7186.	2.347	.2334	4.142	.2426	.4236
7.	129842.	1071.	-.919	.1405	1.033	.1286	.1240
8.	130357.	1802.	-.768	.0806	1.964	.0754	.1876
9.	130140.	2703.	-.418	.1529	2.573	.1197	.2321
10.	129749.	3593.	.073	.0962	3.373	.0782	.3000
11.	130218.	5310.	1.422	.2036	4.439	.1736	.4149
12.	129778.	7229.	2.890	.7728	5.922	.4852	.5906
13.	165159.	1053.	-1.280	.1754	1.133	.2019	.1537
14.	165472.	1760.	-1.316	.1045	2.448	.0971	.2473
15.	165486.	2661.	-1.066	.1435	3.095	.1223	.2912
16.	165307.	3540.	-.137	.1362	4.019	.1753	.3577
17.	164891.	5310.	1.217	.2441	5.550	.2303	.5056
18.	164978.	7186.	2.994	.4365	7.860	.4226	.7487
19.	200538.	1060.	-2.043	.2451	1.260	.3730	.2169
20.	200093.	1775.	-1.957	.1815	3.378	.1811	.3475
21.	199514.	2655.	-2.012	.1965	4.081	.1995	.4050
22.	200452.	3550.	-1.190	.2446	5.094	.2321	.4656
23.	199579.	5310.	.762	.3030	7.113	.2958	.6386
24.	199924.	7186.	2.997	.5540	9.618	.5226	.8969
25.	246398.	1045.	-3.094	.3401	1.737	.5965	.3210
26.	243244.	1786.	-2.707	.2167	4.170	.2138	.4425
27.	246006.	2643.	-2.874	.2378	4.296	.2118	.4600
28.	244530.	3529.	-1.025	.2724	6.517	.2083	.5871
29.	246030.	5286.	.567	.3674	8.902	.3605	.7937
30.	246669.	7229.	2.583	1.4855	11.384	.6469	1.0463

Table B.10. Operating conditions and parameters, helically-grooved stator 1, $\alpha = 0°$.

HELICALLY GROOVED 0.376mm cr. 15 deg.

Case	R_{ec}	*CPM* (C_{pc}/min)	F_r/A (MN/M)	*dev.* (MN/M)	F_θ/A (MN/M)	*dev.* (MN/M)	$\|F\|$ (KN)
1.	90121.	993.	-.130	.0988	.769	.0403	.0699
2.	90492.	2000.	.118	.0551	1.297	.0468	.1158
3.	90483.	3008.	.330	.1067	2.106	.0979	.1898
4.	90310.	4013.	.874	.0764	2.103	.0962	.2026
5.	90357.	5286.	1.678	.1447	3.390	.1579	.3365
6.	90496.	7186.	2.825	.4937	5.571	.4699	.5568
7.	129627.	1000.	-.257	.1668	1.164	.0631	.1071
8.	129545.	2000.	-.142	.0881	2.108	.0699	.1880
9.	129623.	3000.	.511	.1056	2.988	.1443	.2696
10.	129584.	4013.	1.208	.1473	3.199	.1289	.3043
11.	130126.	5310.	2.021	.2640	4.852	.2367	.4679
12.	130012.	7186.	3.438	.6796	7.447	.6560	.7316
13.	159649.	997.	-.358	.2011	1.412	.0731	.1308
14.	159666.	2007.	-.202	.0956	2.372	.0796	.2118
15.	160255.	3008.	.416	.1288	3.719	.1414	.3328
16.	160218.	4027.	.958	.2068	4.038	.1950	.3695
17.	159777.	5286.	2.345	.2513	5.862	.2649	.5618
18.	160211.	7186.	3.863	.8166	8.760	.8385	.8543
19.	220299.	1000.	-.734	.2771	2.000	.1422	.1912
20.	220342.	2007.	-.785	.1802	3.585	.1292	.3267
21.	220184.	3008.	.113	.1684	5.249	.2488	.4669
22.	219907.	4013.	.800	.3150	5.720	.2582	.5143
23.	220381.	5286.	2.569	.3502	8.435	.3812	.7846
24.	220279.	7186.	4.094	1.0204	11.712	1.0734	1.1068
25.	283797.	1003.	-1.209	.4593	2.809	.2190	.2755
26.	282999.	2000.	-1.179	.1802	5.129	.1714	.4681
27.	280333.	3000.	.201	.1724	6.312	.2583	.5617
28.	280050.	4000.	.895	.3650	8.416	.3735	.7532
29.	282518.	5286.	2.587	.5744	10.774	.3635	.9864
30.	275515.	7186.	4.144	1.3858	14.248	1.2596	1.3247

Table B.11. Operating conditions and parameters, helically-grooved stator 2, $\alpha = 15°$.

HELICALLY GROOVED 0.371mm cr. 30 deg.

Case	R_{ee}	*CPM* (C_{pe}/min)	F_r/A (MN/M)	*dev.* (MN/M)	F_θ/A (MN/M)	*dev.* (MN/M)	$\|F\|$ (KN)
1.	99801.	1080.	-.120	.1020	.702	.0383	.0640
2.	99719.	1791.	-.104	.0418	1.077	.0504	.0963
3.	99869.	2655.	.428	.0539	1.402	.0547	.1306
4.	99940.	3561.	.596	.0674	1.981	.0973	.1840
5.	99962.	5306.	1.657	.1150	2.427	.1263	.2615
6.	99723.	7186.	3.272	.2879	3.808	.2327	.4511
7.	150154.	1091.	-.159	.2070	1.132	.0532	.1033
8.	149881.	1796.	-.040	.0842	2.037	.0977	.1804
9.	150152.	2685.	.268	.1002	2.804	.1153	.2240
10.	150233.	3582.	.810	.1353	3.322	.1619	.3042
11.	150190.	5310.	2.041	.2860	4.805	.2253	.4405
12.	150383.	7229.	3.912	.8809	6.014	.6121	.6441
13.	210131.	1064.	-.462	.2135	1.655	.0895	.1540
14.	209886.	1770.	-.260	.1261	2.929	.1402	.2616
15.	209815.	2343.	.597	.1402	3.791	.1539	.3415
16.	210226.	3540.	.957	.1237	4.482	.1674	.4076
17.	209542.	5310.	2.242	.3687	6.344	.3009	.5990
18.	210491.	7186.	4.430	.5701	8.944	.5955	.8886
19.	259771.	1049.	-.636	.2934	2.116	.1279	.1963
20.	260343.	1786.	-.453	.1770	3.814	.1869	.3418
21.	260214.	2655.	-.082	.2201	4.427	.2268	.3941
22.	260294.	3571.	1.019	.1461	5.614	.1914	.5074
23.	260419.	5310.	2.446	.5540	8.132	.3936	.7565
24.	259977.	7186.	5.333	.6446	10.934	.6978	1.0830
25.	318528.	1042.	-1.240	.3827	2.458	.2435	.2477
26.	316498.	1775.	-.654	.1962	4.625	.2314	.4157
27.	313302.	2667.	-.188	.2196	5.558	.2175	.4948
28.	313573.	3540.	1.121	.1798	7.310	.1237	.6577
29.	309585.	5286.	2.873	.7164	9.725	.4399	.9038
30.	305991.	7186.	5.083	.7937	12.477	.7544	1.2000

Table B.12. Operating conditions and parameters, helically-grooved stator 3, $\alpha = 30°$.

HELICALLY GROOVED 0.371mm cr. 30 deg. w/end lands

Case	R_{es}	CPM (C_{ps}/min)	F_r/A (MN/M)	dev. (MN/M)	F_θ/A (MN/M)	dev. (MN/M)	$\|F\|$ (KN)
1.	89876.	1003.	-.422	.1259	.843	.0772	.0847
2.	90417.	1993.	-.306	.0761	1.388	.0618	.1266
3.	89909.	3015.	.189	.0947	2.102	.1000	.1878
4.	89885.	3987.	.490	.1006	2.387	.1156	.2168
5.	89866.	5310.	1.216	.1594	2.642	.1562	.2589
6.	89836.	7186.	2.215	.3216	3.725	.3834	.3865
7.	160257.	993.	-1.049	.2904	1.681	.2007	.1786
8.	159528.	2007.	-1.064	.1435	2.426	.1496	.2358
9.	159812.	3008.	-.371	.1685	3.707	.1789	.3316
10.	159821.	4000.	.234	.2130	4.532	.2307	.4039
11.	159732.	5286.	1.428	.2633	5.257	.3046	.4848
12.	159797.	7186.	2.573	.6260	7.057	.4800	.6699
13.	219552.	990.	-1.947	.3872	2.408	.3277	.2786
14.	219551.	2007.	-1.623	.2481	3.903	.2524	.3764
15.	220073.	3000.	-.609	.2646	5.288	.2887	.4737
16.	219552.	4027.	-.252	.2907	6.622	.3220	.5898
17.	220403.	5263.	1.196	.3327	7.733	.3163	.6961
18.	220390.	7229.	2.462	1.4939	10.006	.8535	.9255
19.	259030.	1000.	-2.678	.4404	3.155	.4021	.3712
20.	259565.	2000.	-2.150	.2324	4.868	.2489	.4734
21.	259006.	3023.	-1.660	.2522	6.420	.2741	.5899
22.	259599.	4000.	-.640	.3918	8.209	.3883	.7328
23.	259034.	5310.	.515	.9963	9.495	.3983	.8499
24.	260458.	7186.	2.503	1.1102	12.006	.8779	1.0948
25.	320917.	1007.	-3.653	.7493	4.043	.6788	.4918
26.	317029.	2000.	-3.005	.4076	6.236	.4214	.6165
27.	315161.	2993.	-1.940	.4387	8.216	.4576	.7515
28.	313461.	4027.	-1.355	.5189	9.870	.4752	.8868
29.	310062.	5286.	.460	.9486	11.647	.6364	1.0395
30.	307853.	7186.	2.616	1.2138	13.614	1.4366	1.2374

Table B.13. Operating conditions and parameters, helically-grooved stator 4, $\alpha = 30°$. End lands are used on this seal.

HELICALLY GROOVED 0.376mm cr. 40 deg.

Case	R_{ge}	*CPM* (C_{ge}/*min*)	F_r/A (MN/M)	*dev.* (MN/M)	F_θ/A (MN/M)	*dev.* (MN/M)	$\|F\|$ (KN)
1.	90240.	993.	-.097	.0648	.490	.0346	.0451
2.	90156.	2000.	-.054	.0436	.799	.0480	.0713
3.	90178.	2993.	.379	.0706	1.269	.0776	.1179
4.	89740.	3987.	.783	.0912	1.462	.1190	.1478
5.	89958.	5310.	1.462	.1378	1.819	.1357	.2079
6.	90314.	7229.	2.392	.4140	2.753	.3769	.3273
7.	169688.	1000.	-.387	.1756	1.180	.0906	.1116
8.	170412.	2000.	-.218	.1092	1.799	.1160	.1614
9.	170458.	3000.	.306	.1335	2.469	.1644	.2215
10.	169916.	3987.	.991	.1819	3.027	.2233	.2837
11.	169618.	5310.	1.871	.2413	3.695	.2419	.3689
12.	170424.	7229.	3.117	.7687	5.244	.5925	.5479
13.	239809.	1017.	-.724	.3862	1.663	.1910	.1654
14.	239692.	2000.	-.311	.1621	2.564	.1528	.2300
15.	240256.	3000.	.316	.2185	3.844	.2547	.3434
16.	239525.	4013.	1.044	.2866	4.441	.2119	.4064
17.	239069.	5310.	2.080	.3328	5.366	.3254	.5124
18.	240398.	7186.	3.271	.5818	7.726	.5078	.7478
19.	309571.	993.	-1.340	.4237	2.500	.2802	.2556
20.	309730.	2007.	-.763	.2239	3.734	.2258	.3394
21.	310067.	3023.	-.032	.2816	5.023	.2927	.4473
22.	310128.	3987.	.975	.3614	6.326	.4184	.5700
23.	310482.	5310.	2.078	.4659	7.695	.4628	.7098
24.	309535.	7186.	2.759	.7263	9.100	.5902	.8477
25.	386503.	993.	-2.012	.6456	3.319	.4370	.3514
26.	382493.	2013.	-1.532	.3327	4.897	.3327	.4571
27.	376516.	3015.	-.982	.3058	6.302	.3145	.5677
28.	374224.	3974.	.725	.4855	7.928	.4552	.7092
29.	372000.	5286.	2.108	.5863	9.326	.5476	.8516
30.	378158.	7186.	3.839	.9633	11.558	1.0640	1.0858

Table B.14. Operating conditions and parameters, helically-grooved stator 5, $\alpha = 40°$.

HELICALLY GROOVED 0.370mm cr. 50 deg.

Case	R_{ee}	*CPM* (C_{pm}/*min*)	F_r/A (*MN/M*)	*dev.* (*MN/M*)	F_θ/A (*MN/M*)	*dev.* (*MN/M*)	$\|F\|$ (*KN*)
1.	90423.	1079.	-.188	.0518	.429	.0285	.0417
2.	90827.	1818.	.012	.0229	.710	.0208	.0632
3.	89718.	2721.	.080	.0845	1.041	.0321	.0929
4.	90830.	3636.	.536	.0944	1.094	.0286	.1084
5.	90258.	5386.	1.563	.0833	1.357	.0801	.1841
6.	89613.	7186.	2.796	.1609	2.375	.1682	.3266
7.	130006.	1107.	-.489	.1142	.765	.0785	.0816
8.	130662.	1807.	-.244	.0440	1.199	.0545	.1088
9.	130792.	2746.	.067	.0610	1.532	.0477	.1365
10.	129962.	3571.	.481	.0416	1.658	.0550	.1535
11.	130060.	5310.	1.508	.1468	2.332	.1172	.2517
12.	129541.	7186.	3.173	.2322	3.534	.2392	.4228
13.	159561.	1087.	-.632	.1273	.876	.0930	.0970
14.	160361.	1813.	-.406	.0502	1.483	.0629	.1367
15.	160549.	2715.	-.050	.0871	1.970	.0823	.1753
16.	160206.	3625.	.263	.0894	2.492	.1066	.2230
17.	159728.	5286.	1.768	.1214	2.981	.1199	.3083
18.	159929.	7186.	3.175	.2790	4.408	.2401	.4836
19.	280034.	1087.	-1.874	.2912	1.981	.2800	.2448
20.	279735.	1775.	-1.482	.1111	2.728	.1027	.2762
21.	279964.	2709.	-.917	.1555	3.610	.1209	.3313
22.	280175.	3604.	-.238	.1387	4.624	.1639	.4118
23.	280500.	5286.	1.686	.2625	6.083	.2335	.5617
24.	279722.	7229.	3.142	1.2323	8.312	.6316	.7963
25.	406328.	1080.	-3.329	.4474	3.119	.4805	.4093
26.	401388.	1780.	-2.757	.1941	4.478	.1890	.4678
27.	401805.	2643.	-2.208	.2517	6.053	.2800	.5732
28.	402699.	3519.	-1.018	.1732	6.659	.1379	.5991
29.	394829.	5263.	.878	.4324	9.111	.3276	.8146
30.	390012.	7186.	3.026	.7936	11.670	.7649	1.0742

Table B.15. Operating conditions and parameters, helically-grooved stator 6, $\alpha = 50°$.

HELICALLY GROOVED 0.336mm cr. 60 deg.

Case	R_{ee}	*CPM* (C_{pe}/*min*)	F_r/A (*MN/M*)	*dev.* (*MN/M*)	F_θ/A (*MN/M*)	*dev.* (*MN/M*)	$\|F\|$ (*KN*)
1.	90211.	1053.	-.233	.0606	.412	.0368	.0425
2.	89638.	1754.	-.183	.0210	.550	.0247	.0516
3.	89914.	2620.	.189	.0235	.802	.0299	.0733
4.	90080.	3519.	.161	.0344	1.007	.0284	.0907
5.	90319.	5286.	1.295	.0815	1.292	.0780	.1628
6.	89730.	7229.	2.407	.2698	1.986	.3022	.2795
7.	130365.	1079.	-.412	.0872	.636	.0616	.0681
8.	130241.	1775.	-.182	.0319	.866	.0415	.0787
9.	130156.	2673.	-.071	.0508	1.335	.0446	.1189
10.	129945.	3571.	.183	.0498	1.482	.0422	.1328
11.	129738.	5310.	1.265	.1237	2.091	.1113	.2177
12.	129794.	7186.	2.630	.1761	2.950	.1302	.3516
13.	159895.	1075.	-.722	.1108	.860	.0961	.1006
14.	159712.	1796.	-.704	.0556	1.299	.0626	.1314
15.	160393.	2703.	.007	.0513	1.711	.0852	.1521
16.	159849.	3582.	.093	.0588	1.868	.0659	.1664
17.	160451.	5286.	1.273	.1649	2.802	.1119	.2740
18.	159755.	7186.	2.739	.2129	3.742	.1781	.4127
19.	285145.	1083.	-2.247	.1942	1.768	.2251	.2553
20.	285202.	1807.	-1.942	.1259	2.671	.1212	.2938
21.	285366.	2697.	-1.299	.1496	3.593	.1184	.3400
22.	284808.	3571.	-.986	.0945	4.276	.1181	.3902
23.	285300.	5286.	.782	.3153	5.870	.2027	.5272
24.	285373.	7186.	2.788	.3728	7.417	.3006	.7053
25.	420328.	1064.	-4.769	.3435	2.316	.6316	.4753
26.	415849.	1775.	-3.806	.2445	4.349	.2380	.5141
27.	415546.	2697.	-3.972	.3690	5.423	.2783	.5983
28.	413059.	3571.	-2.301	.2420	6.876	.2574	.6448
29.	411381.	5263.	-.774	.3408	8.753	.3332	.7818
30.	409047.	7186.	1.554	.5430	11.241	.5804	1.0098

Table B.16. Operating conditions and parameters, helically-grooved stator 7, $\alpha = 60°$.

HELICALLY GROOVED 0.379mm cr. 70 deg.

Case	R_{ee}	*CPM* (C_{pe}/*min*)	F_r/A (MN/M)	*dev.* (MN/M)	F_θ/A (MN/M)	*dev.* (MN/M)	$\|F\|$ (KN)
1.	90227.	1053.	-.195	.0310	.265	.0238	.0294
2.	90429.	1765.	-.053	.0242	.611	.0206	.0546
3.	90115.	2649.	.057	.0220	.615	.0276	.0550
4.	90305.	3509.	.223	.0252	.757	.0338	.0702
5.	89610.	5286.	1.332	.0542	.914	.0526	.1436
6.	90164.	7229.	2.027	.1658	1.173	.2449	.2097
7.	179763.	1083.	-.697	.0930	.772	.0858	.0931
8.	179688.	1791.	-.599	.0543	1.239	.0576	.1225
9.	179657.	2673.	-.307	.0509	1.494	.0528	.1356
10.	180017.	3582.	-.315	.0741	2.048	.0892	.1843
11.	179409.	5310.	.971	.1332	2.274	.0891	.2201
12.	180545.	7186.	2.017	.1615	3.056	.1597	.3258
13.	270266.	1064.	-1.666	.1277	1.096	.1775	.1782
14.	270212.	1786.	-1.487	.1055	1.968	.1051	.2195
15.	269959.	2685.	-1.220	.1023	2.344	.0898	.2351
16.	269519.	3540.	-.812	.1060	3.019	.0884	.2781
17.	270072.	5310.	.500	.3201	3.895	.1693	.3503
18.	269987.	7186.	1.751	.2383	5.282	.2403	.4951
19.	350380.	1049.	-2.784	.2215	1.746	.3208	.2940
20.	349557.	1780.	-2.407	.1254	2.325	.1162	.2977
21.	349620.	2655.	-1.786	.1413	3.535	.1319	.3523
22.	350154.	3540.	-1.607	.1240	4.071	.1086	.3893
23.	350152.	5286.	-.117	.2042	5.541	.2409	.4930
24.	349794.	7186.	1.284	.3936	7.500	.2918	.6772
25.	447883.	1060.	-4.537	.5268	2.545	.8112	.4700
26.	448158.	1739.	-3.850	.2162	3.454	.1994	.4603
27.	441521.	2632.	-2.641	.2397	4.722	.2519	.4815
28.	438643.	3519.	-2.408	.1793	5.573	.1370	.5400
29.	438024.	5286.	-.822	.3219	7.306	.3528	.6543
30.	432888.	7186.	.578	.4648	9.474	.4672	.8449

Table B.17. Operating conditions and parameters, helically-grooved stator 8, $\alpha = 70°$.